Department of Physics
Indian Institute of Technology Guwahati
Ph.D. Thesis

A Theoretical Study of Rabi Oscillations in Graphene

Enamullah

Supervisor:
Dr. Girish S. Setlur
(Associate Professor)

A Theoretical Study of Rabi Oscillations in Graphene

A thesis submitted by

Enamullah

to

Indian Institute of Technology Guwahati
in partial fulfillment of the requirements
for the award of the degree of
Doctor of Philosophy in Physics

Department of Physics
Indian Institute of Technology Guwahati
Guwahati - 781039, Assam, India

Statement

The contained work in this thesis entitled "*A Theoretical Study of Rabi Oscillations in Graphene*" has been carried out by me under the supervision of Dr. Girish S Setlur, Associate Professor, Department of Physics, Indian Institute of Technology Guwahati. Neither has this work been submitted elsewhere for the award of any degree nor any other qualification.

(Enamullah)
Department of Physics
Indian Institute of Technology Guwahati
Guwahati - 781039

March, 2014

Certificate

It is certified that the work contained in this thesis entitled "*A Theoretical Study of Rabi Oscillations in Graphene*" by Mr. Enamullah, a Ph.D. student of the Department of Physics, Indian Institute of Technology Guwahati for the award of Doctor of Philosophy has been carried out under my supervision and guidance. This work has not been submitted elsewhere for the award of any degree.

Dr. Girish S Setlur
(Associate Professor)
Department of Physics
Indian Institute of Technology Guwahati
Guwahati - 781039

March, 2014

To my family

.....my source of inspiration

Acknowledgements

I consider Indian Institute of Technology Guwahati as my second home and my supervisor Dr. Girish S Setlur and his wife Dr. Uma Dutta Setlur as parent. I am indebted to both of them for their excellent guidance, valuable suggestions, inspiration towards research and support throughout my research work. My experience as a Ph.D. student under him is excellent. I am very fortunate and thankful to God that He selected Dr. Setlur as my guide. I can not explain his beauty in to words but I must say, he is wonderful, as a human being, as a philosopher, as a thinker and as a guide. Due to unique teaching style and way of explaining the subjects, he is one of the best teacher in IIT Guwahati.

But a teacher also angry with his students. In our case whenever he become angry, he did not say anything in-front of us but he express his anger through an email. The way of expressing his anger is also unique similar to his distinguishable way of teaching.

I wish to thank my doctoral committee members, Dr. T. N. Dey, Dr. P. Poulose and Dr. R. K. Sinha for their valuable suggestions and critical comments during my progress seminars. I am grateful to have a fruitful discussion with the chairman of my doctoral committee, Dr. T. N. Dey and Dr. Amrendra Kumar Sarma. My hearty thanks to all other faculty members of Physics department. My special thanks to Prof. Saurabh Basu and Prof. S. Ravi for their timely help and support. I am also grateful to Prof. K. Thayagrajan from IIT Delhi and Prof. J. H. Eberly for their fruitful discussion and suggestions.

I am thankful to department of Physics, IIT Guwahati, for providing me the facilities for my research. I thank all the technical staff of the department for their assistance in various ways during my research period.

I am thankful to Prof. Stephen Wolfram, the chief designer of Mathematica software by which I have plotted all the graphs contained in this thesis.

I am very fortunate that I had found Dr. Meera V. as senior, as a mentor, as an elder sister, who motivated me towards graphene research field. She is one of the punctual research scholar, highly dedicated towards research, used to come to lab at 7:30 am and stayed up to 7:30 pm, such type of dedication I have never seen. Similar to her characteristic, Dr. Jahir Abbas Ahmed is one, who is also highly dedicated towards his research work. I have learnt a lot of research techniques from both of them. They treated me as younger brother due to which they often scolded me also but only for my betterment. I am hearty thankful to both of them.

I am thankful to Dr. D. N. Patel at IIT Kanpur for the initial motivation towards research and his helping nature, to whom I met during my struggling period after my master degree.

I am grateful to IIT Guwahati for the financial support.

As I mention that IIT Guwahati is my second home, all credit goes to my loving batch-met friends, Swarnadeep Acharyya, to whom I met first time when I joined my Ph.D. here; Akhilesh, Mukesh, Satendra, Suresh, Onkar, Padam Rajender, Santosh, Munindhar, Shyni, Tribedi, Paulami, Md. Hassan, Jitender and my loving juniors; Rohit Singh, Obaidulla and all others. To all of them I would like to give my hearty thanks. My batch-met usually called me 'junior Setlur'.

I am indebted to my loving friend, Ramizuddin Ahmed and his family, who has given me extra encouragement towards research. His family did not let me realize that I was away from home.

I am thankful to my loving juniors, Vipin Kumar and Upendra Kumar for their constant support and fruitful discussion about research.

I would like to give my hearty thanks to my childhood friend; Mohammad Shameem Asharfi, school friends; Istkhar Ali, Kamal Kishor Gupta and Amit Jaiswal.

I am hearty thankful to my school teachers; Mr. Manzoor Hassan Khan, Mr. Amarnath Chaubey, Mr. A. K. Singh, Mr. K. C. Gupta and all other teachers.

I am deeply indebted to my Father (Mr. Hafiz Ahsanullah Khan), my mother (Mrs. Raheemun Nisha), my grand mother, younger brothers (Abdurrehman and Habiburrehman) and sisters (Roshan Fatima, Mufleha, Jannat, Ishrat and Shaba) for their unlimited support and love. Without their support I would not be able to achieve anything. They were always supported me whenever I felt low. Special thanks to my nephew; Imran and my niece; Iram who make me forget all my problems when I am with them.

Finally I would like to hearty thanks to most beneficent and merciful "ALLAH".

Enamullah

Abstract

The nonlinear optical response of graphene has been studied by the newly developed technique which is an alternative to rotating wave approximation (RWA). This is referred to as asymptotic RWA (ARWA). "Graphene" is a single layer of graphite material possessing a degree of freedom known as pseudospin. It is a bridge between condensed matter and relativistic electrodynamics, since the low energy spectrum of graphene near some particular points called Dirac points is linear in momentum. The interaction between the charge carrier and the periodic potential of graphene leads to quasiparticles which obey the Dirac relativistic equation. At the Dirac points, the conduction band just touches the valance band due to which it is also called zero band gap semiconductor. These peculiar properties of graphene are the motivation behind our work and are studied using optical means, specifically through nonlinear optical response. As the title of the thesis itself suggests, this work is the study of the well-known coherent optical phenomenon in nonlinear optics viz. Rabi oscillation - a periodic exchange of energy between a two level system in case of atoms and two band system in case of semiconductors and the applied optical field. It is the oscillation in the population and polarization of carries (with a given wave-vector in case of a band) with a frequency ω_R determined by the intensity of the externally applied optical field. This frequency ω_R is typically much smaller than the optical frequency ω itself. This phenomenon is well described in various textbooks on quantum optics. The same phenomenon manifests itself in semiconductors, which have bands instead of energy levels. It is therefore appropriate to investigate the same effects in graphene where the bands are linear instead of parabolic and the system is two dimensional instead of three and there is pseudospin character. The phenomenon of Rabi oscillations in graphene has been studied by Mishchenko among others, near the particle-hole resonance using the well known rotating wave approximation (RWA). Our main contribution has been to show that graphene exhibits a second 'anomalous' Rabi oscillation that occurs far from resonance

when the applied frequency is much larger than the particle-hole energy. To study these new oscillations we have had to invoke a method we refer to as asymptotic rotating wave appoximation or ARWA for short. This alternative approach is able to show that for systems with pseudospin such as graphene, the current density in the frequency domain exhibits a crossover from one type of singular behavior close to the normal Rabi frequency to another type of singular behavior close to the (typically even smaller) 'anomalous' Rabi frequency. A comparison with an exactly solvable model identical to graphene in all respects except lacking in pseudospin shows that the anomalous Rabi frequency is peculiar to models with pseudospin.

The natural question that now arises is how to detect this kind of anomalous Rabi oscillations in graphene? The method which we have suggested is pump-probe spectroscopy, where our analysis shows that varying pump probe delay or pump duration with all else being fixed is the key to the detection of anomalous Rabi oscillations. Pump-probe spectroscopy is typically used to study the relaxation dynamics of nonequilibrium photoexcited band electrons. Using this technique we have shown the probe susceptibility depends upon the area of the pump field and it has oscillatory behavior as a function of pump duration. The frequency of these oscillations is just the anomalous Rabi frequency. This oscillatory behavior is robust since it is present even when the system has decaying terms. The theoretical prediction of anomalous Rabi oscillations is experimentally verified by the available data (details are given in chapter 3).

Till now we have treated the electromagnetic field as purely classical, but what would happen if the field is treated quantum mechanically? It is well known that in this case, Rabi oscillations collapse and revive due to the discrete nature of the Fock states of the coherent photon field described by Poisson statistics. In our case, collapse and revival extends to anomalous Rabi oscillations as well. From a semiclassical perspective, an atom in an excited state cannot make a transition to a lower level in the absence of an external field whereas in the quantum case, this transition is possible even in a vacuum because of spontaneous emission (zero point quantum fluctuations of radiation). A solvable model of quantum radiation interacting with a two-level system has been given by Jaynes and Cummings. The most interesting phenomena in this model are the collapse and revival oscillations that occur when the electromagnetic (EM) field is in a coherent state. These phenomena may be intuitively understood as follows. The population density consists of a sum of oscillating terms, each corresponding to a well-defined photon number n and each term oscillates with a particular Rabi frequency

proportional to $\sqrt{n+1}$. In this case, one may see that even without any relaxation, the distribution of Rabi frequencies produces an initial dephasing ('collapse') in the sinusoidal Rabi oscillations. The basic reason is, if two neighboring terms oscillate 180° out of phase, they destructively interfere whereas if they are in phase, there is constructive interference. In case of collapse, the various contributions destructively interfere thereby producing the effect of decay or dephasing. Revival is purely a quantum phenomenon, however. Revival refers to the resurrection of previously extinguished oscillations due to destructive interference gradually diminishing, revealing the original oscillations. It depends not only upon the coherent state of photons but also on the statistical distribution of photon numbers. A continuous photon distribution would give a collapse just like a classical field, but no revivals. The interaction between a two level atom and a quantized electromagnetic field viz. the phenomenon of collapse and revival of Rabi oscillations have been observed in experiments such as cavity quantum electrodynamics (CQED), performed with circular Rydberg atoms (atoms excited to highly quantum number state) and also center-of-mass motion of a trapped ion. It remains to be seen if these phenomena will be seen in graphene as well.

Contents

List of Figures

Chapter 1

Introduction

Carbon, the stuff of life, is one of the most abundant elements found on earth after hydrogen, helium and oxygen. In its pure form, it is found in nature in two completely different allotropic forms - diamond and graphite. They have very different properties, even though they differ only in the arrangement of carbon atoms. A suitable arrangement of carbon atoms leads to diamond which is insulating and very hard while graphite is conducting and lubricative. Carbon by itself is responsible for a branch of chemistry known as organic chemistry. The first artificial pure carbon material known as fullerene[1] was found in 1985. Thereafter, an intense research effort on other allotropic forms of carbon was set in motion. In 1991, the one-dimensional carbon nanotube[2] was produced. By that time, the known allotropes of carbon had swelled to, diamond, graphite, fullerene and carbon nanotubes. The final addition to this family was graphene. The humble element, carbon, was the star of a Nobel prize winning discovery of this real two dimensional material[3,4]. Graphene, a single sheet of carbon atoms arranged in a honeycomb pattern was first synthesised by the group of physicists at Manchester, Andre Geim and Konstantin Novoselov in 2004. However the literature shows ultathin graphite (but not one atomic thick) was already reported[5–9] in the early 1960's. The invention of graphene started a new field of research in nanomaterials due to its amazing properties that had never been observed before.

After the synthesis of graphene, the Nobel prize committee of the Royal Swedish Academy said, "*Carbon - the basis of all known life on the earth, has surprised us once again*".

Graphene, a wonder discovery of 21^{st} century, is the building block of all graphite-related materials. It can be wrapped up into zero dimension (0D) called fullerene, one

Figure 1.1: The Nobel laureates(from the right) A. K. Geim and K. S. Novoselov during the press conference in 2010 (picture has been taken from the Wikipedia-page of graphene)

dimension (1D) as carbon nanotube, 2D graphene sheet or it can be stacked into three dimension known as graphite given by the following figure,

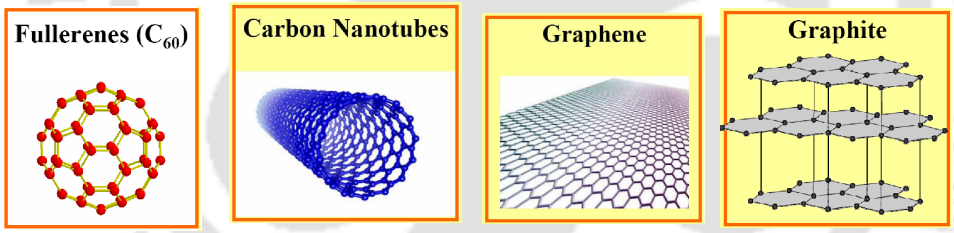

Figure 1.2: Three different carbon allotropes (picture has been taken from PPT presented in summer conference by Korea Magnetic Society 2008).

Graphene[3,4] is the bridge between condensed matter and relativistic electrodynamics[10], since the low energy dispersion spectrum (energy vs momentum relation) of graphene near some particular points called Dirac points[4] is linear. The linear energy spectrum leads to the term 'massless Dirac fermions' since the charge carriers obey Dirac relativistic equation[11–16]. At the Dirac points, the conduction band just touches the valence band, due to that it is also called zero band gap semiconductor. The most relevant difference between conventional semiconductor and graphene is that, in case of graphene, the charge carriers obey the relativistic Dirac equation near the Dirac point, and have a pseudo spin degree of freedom[4], while in the case of conventional semicon-

ductors, the charged particles obey a parabolic dispersion relation ($\frac{p^2}{2m}$) and lack pseudo spin. The motivation behind our work is based upon attempting to elucidate these peculiar properties of graphene using optical means, specifically through nonlinear optical response.

1.1 Definition

Graphene[3,4] is a one atom thick, single layer of graphite material completely made of carbon atoms arranged in a honeycomb crystal lattice. The honeycomb crystal lattice can be split in to two triangular sub-lattices which are generally labeled by 'A' and 'B' sublattices.

1.2 Graphene: 2 dimensional or NOT !

The famous Mermin-Wagner[17] theorem, states that it is impossible to have a long range crystalline order in two dimension because of large thermodynamic fluctuations which prevent a strictly 2D crystalline structure, consequently dislocations appear in two dimensional crystals at any finite temperature. This theory is supported by Landau and Peierls that strictly two dimensional crystals could not exist in nature due to the same reason. The natural doubt to come to mind is that since graphene is a one atomic thick layer of graphite, and the atom is three dimensional then how would it be two dimensional? The reason why it is a 2D is that the electron in the graphene lattice confined in the two dimensional plane. In other words, its dynamics is governed by a Hamiltonian in two spatial dimensions. The 2D-electron behavior is experimentally verified by De Heer and his collaborators[9].

1.3 Peculiar properties of graphene

The low energy spectrum of graphene is conical which distinguishes it from conventional semiconductors where the energy bands are parabolic. Neither the conduction and valence band are separated by the energy gap nor they do overlap due to which it is also called 'gapless' semiconductor or semi-metal. The conduction and valence band intersect at two inequivalent point generally called Dirac points 'K' and 'K'' in first

Brillouin zone. In case of undoped graphene, the Fermi energy level lies exactly at the intersection points. The other distinguishing property of graphene is the unique nature of its charge carriers. Usually in condensed matter physics, the electronic behavior is governed by the usual Schrodinger equation while in case of graphene the charge carriers obey the massless Dirac relativistic equation [11–16,18–20]. The relativistic equation obeyed by the charge carriers does not mean that the velocity of electrons in the honeycomb lattice is relativistic but the interaction with a periodic two dimensional potential leads to the new quasi-particles, due to which the low energy spectrum becomes linearly in the momentum, accurately described by the Dirac relativistic equation with the effective speed approximately equal to the $\frac{1}{300}$ of the speed of light in vacuum. These quasi-particles are generally known as "massless Dirac fermions". The literature survey shows the study of graphene has branched out into different areas such as electronic properties [4], transport properties [21], optical properties [22–27] and also in other graphene based systems [28–31].

Let us move on to the description of atomic and band structure of graphene as follows,

1.3.1 Atomic or crystal structure

As we have described above, graphene is a monolayer of carbon atoms with honeycomb crystal lattice. Each carbon atom has four electrons in its outer shell called valence electrons, sharing three electrons with its neighboring carbon atoms. In terms of bond theory its atomic structure can be described by the two type of carbon-carbon bonds known as sigma (σ) and pi (π) bonds. An isolated carbon atom possesses the valence orbital configuration $2s^2$, $2p^2$. The energy difference between $2s^2$, $2p^2$ orbital is much smaller than the binding energy of neighboring carbon atoms, hence the wavefunction of electrons mixed up easily by the process called hybridization [32]. Therefore each carbon atom has sp^2 hybridized orbital (orbital formed from one s and two p orbitals). In sp^2 hybridization the $2s$, $2p_x$ and $2p_y$ orbitals mix to form the 'σ' bond that lies in the x-y plane with 120° as the angle between two neighboring chemical bonds. The remaining one electron with $2p_z$ orbital forms a 'π' bond aligned in a 'z' direction. These 'π-orbital' electrons are free and responsible for the conduction and transport process in graphene. The hybridization in graphene i.e. sp^2 leads to a trigonal planar structure. Graphene can be thought of as the interpenetration of two trigonal planar structures referred to

as A and B sublattices. The graphene lattice has two atoms per unit cell and the A type of atoms are connected with B type of atoms with time reversal symmetry. The nearest carbon-carbon distance is 1.42 $\mathring{A}$. The figure (1.3) shows the ideal monolayer

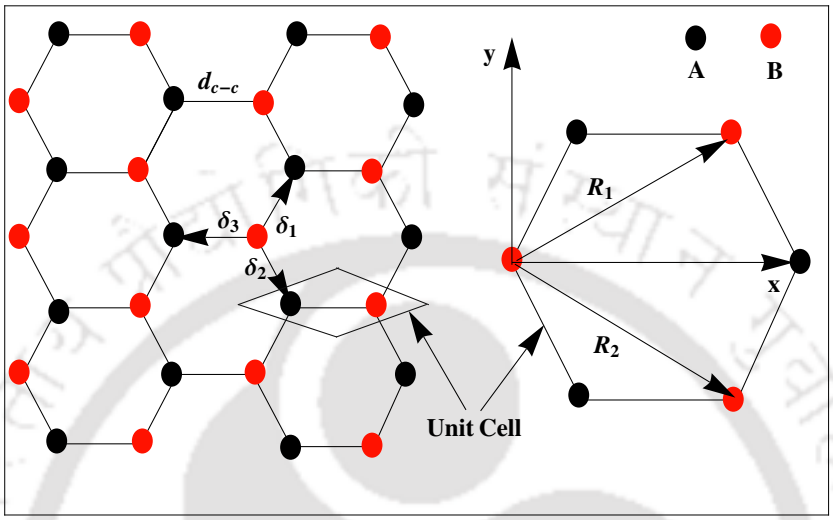

Figure 1.3: The figure depicts the ideal 2D graphene honeycomb lattice made by the interpenetration of two triangular sublattices labeled 'A' and 'B' type of atoms. The unit cell of graphene lattice contain 2 atoms (shown in the figure). The figure on the right can be taken as the unit cell since it effectively contains two atoms.

graphene with the direct lattice vector $\vec{R}_1$ and $\vec{R}_2$ and the nearest neighbor vector $\vec{\delta}_i$ (i= 1,2 and 3) in real space. The direct lattice vectors are given by,

$$\vec{R}_1 = \frac{3}{2}d_{c-c}\,\hat{x} + \frac{\sqrt{3}}{2}d_{c-c}\,\hat{y}, \quad \vec{R}_2 = \frac{3}{2}d_{c-c}\,\hat{x} - \frac{\sqrt{3}}{2}d_{c-c}\,\hat{y}, \tag{1.1}$$

where, d_{c-c} is the carbon-carbon distance ($\approx$ 1.42 $\mathring{A}$), $|\vec{R}_1| = |\vec{R}_2| = \sqrt{3}d_{c-c}$ is the lattice constant and $\hat{x}$ and $\hat{y}$ are the unit vectors. The vector form of nearest neighbor distances can be expressed as,

$$\vec{\delta}_1 = \frac{1}{2}d_{c-c}\,\hat{x} + \frac{\sqrt{3}}{2}d_{c-c}\,\hat{y}, \quad \vec{\delta}_2 = \frac{1}{2}d_{c-c}\,\hat{x} - \frac{\sqrt{3}}{2}d_{c-c}\,\hat{y}, \quad \vec{\delta}_3 = -d_{c-c}\,\hat{x} \tag{1.2}$$

From this basis we may construct the reciprocal lattice as points $\vec{G}$. The first Brillouin zone is a volume in reciprocal lattice space (Fig.(1.4)). It is the minimum volume enclosed by planes that bisect the nearest neighbors in reciprocal space. The reciprocal lattice of graphene is tilted through 90° with respect to the graphene direct lattice

as shown in the following figure, The center of the first Brillouin zone is denoted by

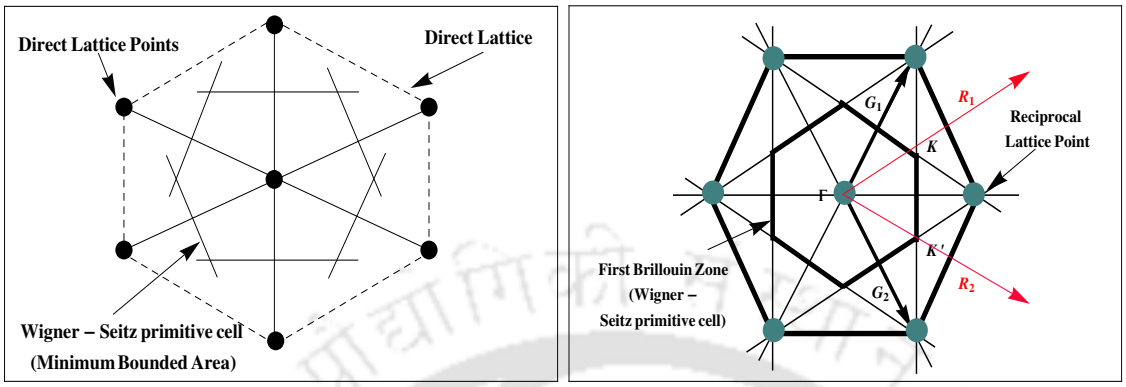

Figure 1.4: In the plot, the left figure shows generally how to prepare the Wigner-Seitz primitive cell from the direct lattice of graphene. The second figure shows the reciprocal lattice of graphene, tilted through 90° from the direct lattice with reciprocal lattice vector G_1 and G_2, this figure also depicts the formation of Wigner-Seitz primitive cell (first Brillouin zone) from the reciprocal lattice point. Γ is the center point and 'K', 'K'' are the edges of the first Brillouin zone made by the reciprocal lattice of graphene.

Γ, corners points by K and K'. These corner points are generally known as Dirac points. They are of special interest because at these points the conduction and valence band touch. These Dirac points have very high degree of symmetry related through time reversal symmetry[4]. The reciprocal lattice vector $\vec{G}_1$ and $\vec{G}_2$ can be calculated through the following relation,

$$\vec{R}_i \cdot \vec{G}_j = 2\pi\delta_{i,j},$$

or,

$$\vec{R}_1 \cdot \vec{G}_1 = 2\pi, \quad \vec{R}_2 \cdot \vec{G}_1 = 0$$

where, $\delta_{i,j}$ is the Kronecker delta. The reciprocal lattice vectors are,

$$\vec{G}_1 = \frac{2\pi}{3d_{c-c}}\,\hat{x} + \frac{2\pi}{\sqrt{3}d_{c-c}}\,\hat{y}, \quad \vec{G}_2 = \frac{2\pi}{3d_{c-c}}\,\hat{x} - \frac{2\pi}{\sqrt{3}d_{c-c}}\,\hat{y} \tag{1.3}$$

The first Brillouin zone in momentum space has two sets of inequivalent Dirac points (K and K') and each set contains three equivalent Dirac points. The vector representation of these Dirac points in momentum space is given by,

$$\vec{K} = \frac{2\pi}{3d_{c-c}}\,\hat{x} + \frac{2\pi}{3\sqrt{3}d_{c-c}}\,\hat{y}, \quad \vec{K'} = \frac{2\pi}{3d_{c-c}}\,\hat{x} - \frac{2\pi}{3\sqrt{3}d_{c-c}}\,\hat{y} \tag{1.4}$$

1.3.2 Electronic band structure: Tight binding approach

The tight binding (TB) method is one of the standard methods to calculate the electronic band structure in condensed matter systems. It is based upon the linear combination of atomic orbitals (LCAO), explained in various text books[33,34]. In the TB approximation, localized orbitals are associated with each atomic site. The wavefunction of the system is assumed to be a linear combination of these basis eigenfunctions. After solving the eigenvalue equation, we get an energy dispersion relation which describes the band structure of the given condensed matter system.

In 1947, Wallace[35] calculated the electronic band structure of graphite on the basis of hopping of electrons within nearest and next nearest neighboring atoms using the tight binding approximation. This led to further developments on tight binding study of graphene[36–38].

For the sake of simplicity, we take only the nearest neighbor hopping[4,35,39], in order to calculate the band structure of graphene. We start with the following hopping based Hamiltonian,

$$\hat{H} = -t \sum_{\langle i,j\rangle,\sigma} \left(\hat{a}^{\dagger}_{\sigma i}\, \hat{b}_{\sigma j} + h.c. \right), \tag{1.5}$$

where, $\hat{a}^{\dagger}_{\sigma i}(\hat{b}_{\sigma i})$ creates(annihilate) one electron with spin σ at $i^{th}(j^{th})$ site of A (B) sublattice called creation (annihilation) operator, $\langle i, j\rangle$ stand for nearest neighbor hopping, 't' denotes the hopping parameter with hopping value approximately of the order of 2.8 eV and h.c. stands for the Hermitian conjugate.

The eigenfunction of graphene is represented by the two component spinor wave functions described in the section (1.3.4). Hence in the TB approximation, it is better to write the eigenfunctions in terms of the spinor denoted by $\begin{pmatrix} \psi_A(\vec{k}) \\ \psi_B(\vec{k}) \end{pmatrix}$, where each component of the spinor labeled by A and B represent the amplitude of A and B type of atoms respectively within a unit cell labeled by the reference point $\vec{R}^0_i$. From our convention, we choose the B atom separated by a A atom by distance $\vec{\delta}_1$ provided A atom is taken as a reference point $\vec{R}^0_i$. In this case the eigenfunction becomes[39](suppressing the spin index),

$$\begin{pmatrix} \psi_A(\vec{k}) \\ \psi_B(\vec{k}) \end{pmatrix} = \sum_i e^{i\vec{k}\cdot\vec{R}^0_i} \begin{pmatrix} a^{\dagger}_i e^{-i\vec{k}\cdot\vec{\delta}_1/2} \\ b^{\dagger}_i e^{i\vec{k}\cdot\vec{\delta}_1/2} \end{pmatrix}.$$

Hence the Hamiltonian becomes off-diagonal, represented in momentum space as,

$$\hat{H} = \begin{pmatrix} 0 & \Delta_\mu \\ \Delta_\mu^* & 0 \end{pmatrix}$$

where, the component Δ_μ is given in terms of direct lattice vector as,

$$\Delta_\mu = -t\left(e^{-i\vec{k}\cdot\vec{R}_1} + e^{-i\vec{k}\cdot\vec{R}_2} + 1\right) \tag{1.6}$$

The eigenvalues of Hamiltonian $\hat{H}$ are given by,

$$\epsilon(k) = \pm|\Delta_\mu| = \pm t\sqrt{3 + 2\cos(\sqrt{3}k_y d_{c-c}) + 4\cos(\frac{\sqrt{3}}{2}k_y d_{c-c})\cos(\frac{3}{2}k_x d_{c-c})}. \tag{1.7}$$

From the above expression, one can easily generate the band structure of graphene shown below, It is interesting to know where the energy eigenvalue vanishes i.e. the point where the conduction and valence band touch each other. It can be easily seen from Eq. (1.7) that there are two choices,

$$\frac{3}{2}k_x d_{c-c} = 2n\pi, \qquad \cos(\frac{3}{2}k_x d_{c-c}) = -\frac{1}{2}$$

or,

$$\frac{3}{2}k_x d_{c-c} = (2n+1)\pi, \qquad \cos(\frac{3}{2}k_x d_{c-c}) = \frac{1}{2},$$

where, n is an integer. The first choice is not possible since the component k_y is lies out side the first Brillouin zone since $k_y = \frac{2\pi}{3\sqrt{3}d_{c-c}}$. The second choice is best because it lies exactly at the corner points of the first Brillouin zone denoted by 'K' and 'K'' known as Dirac points. Now we move on to the calculation of low energy graphene Hamiltonian from the TB approximation. To calculate the low energy dispersion relation, use the Taylor series expansion of the Eq. (1.6) near one of the Dirac points i.e. at $\vec{k} = \vec{K} + \vec{q}$, where q is the small wave vector[39], we have,

$$\begin{aligned} \Delta_{\mu,K}(\vec{q}) &= 2e^{-iK_x d_{c-c}}\vec{q}\cdot\vec{\nabla}_1\left(e^{3ik_x d_{c-c}/2}\cos(\frac{\sqrt{3}}{2}k_y d_{c-c})\right)_{k=K} \\ &= -\frac{3t}{2d_{c-c}}\, e^{-iK_x d_{c-c}}\,(iq_x - q_y) \end{aligned} \tag{1.8}$$

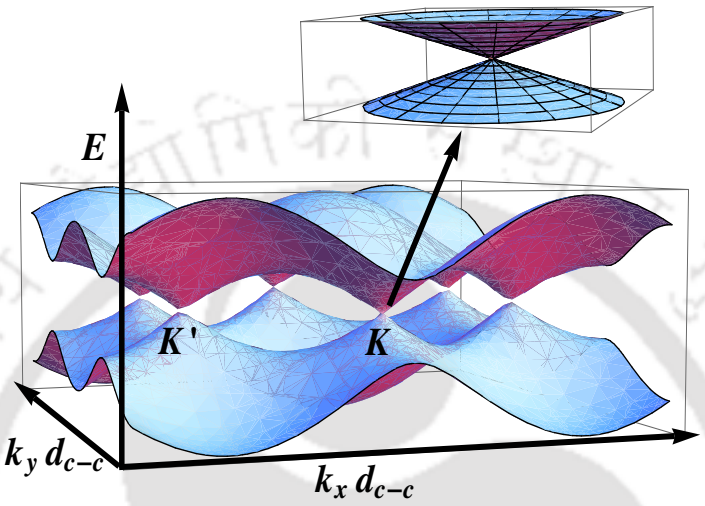

Figure 1.5: 3D reciprocal lattice of graphene band structure, shows the conduction band and valence band vanishes at the particular (Dirac) points where the energy momentum relation is linear (shown in inset).

The constant factor $e^{-iK_x d_{c-c}}$ does not affect the result. Hence the low energy Hamiltonian can be written as,

$$\Delta_{\mu,K}(\mathbf{q}) = \hbar v_F(q_x + iq_y) + O(q/K)^2 \tag{1.9}$$

where $v_F = \frac{3t}{2d_{c-c}} \cong 10^6 m/sec$. If we expand the same Eq. (1.6) close to another Dirac point 'K'', we obtain,

$$\Delta_{\mu,K'}(\mathbf{q}) = \hbar v_F(q_x - iq_y) = \Delta^*_{\mu,K}(\vec{q}).$$

Therefore the low energy Hamiltonian can be finally written as,

$$H \equiv \hbar v_F \begin{pmatrix} 0 & q_x + iq_y \\ q_x - iq_y & 0 \end{pmatrix} \equiv \hbar v_F\ (\vec{\sigma} \cdot \vec{q}) \tag{1.10}$$

Therefore the energy eigenvalue is $E(q) = \pm\hbar v_F|q|$ where $\hat{\sigma}$ are the Pauli spin matrices. We can see that the eigenvalues are functions only of the magnitude of $\mathbf{q}$ and not on the direction. Comparison with Eq. (1.7) shows that equation (1.10) is the Hamiltonian for mass-less relativistic particle of spin 1/2 with velocity of light c replaced by the Fermi velocity v_F which is 300 times smaller than velocity of light[39]. The reciprocal lattice of honeycomb graphene lattice is also in hexagonal shape shown by the figure (1.6).

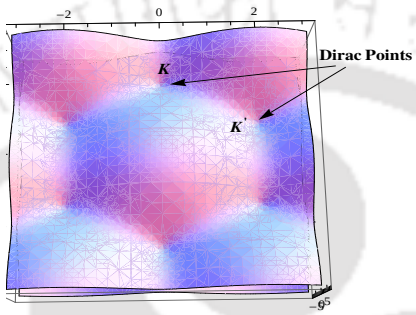

Figure 1.6: The 3D reciprocal lattice of graphene clearly shows the hexagonal shape with six number of edges, coupled in to two sets labeled by K and K' related to time reversal symmetry.

1.3.3 Alternative approach to graphene band structure

The energy spectrum can also be calculated by the much simpler way[40]. From the TB method the graphene Hamiltonian can be written as,

$$\hat{H} = t \sum_{i,\delta,\sigma} \left(\hat{a}^{\dagger}_{i,\sigma} \hat{b}_{i+\delta,\sigma} + \hat{b}^{\dagger}_{i+\delta,\sigma} \hat{a}_{i,\sigma} \right)$$

where, δ is the nearest neighbor distances, individually it is δ_1, δ_2 and δ_3. Define the following Fourier transformation equations,

$$\hat{a}_{i,\sigma} = \frac{1}{\sqrt{N}} \sum_{k} e^{-i\vec{k}\cdot\vec{R}^0_i}\, \hat{a}_{k,\sigma}, \quad \hat{b}_{i+\delta,\sigma} = \frac{1}{\sqrt{N}} \sum_{k} e^{-i\vec{k}\cdot(\vec{R}^0_i+\vec{\delta})}\, \hat{b}_{k,\sigma},$$

where, N is the number of atomic sites and $\vec{R}^0_i$ is the initial vector of atom 'A' (or 'B').

After substitution the Hamiltonian become,

$$\hat{H} = t\frac{1}{N}\sum_{k,\delta,\sigma}\left(e^{-i\vec{k}\cdot\delta}\hat{a}^{\dagger}_{k,\sigma}\hat{b}_{k,\sigma} + e^{i\vec{k}\cdot\delta}\hat{b}^{\dagger}_{k,\sigma}\hat{a}_{k,\sigma}\right)$$

or, in matrix form,

$$\hat{H} = \frac{1}{N}t\sum_{k,\delta,\sigma}\begin{pmatrix}\hat{b}^{\dagger}_{k,\sigma} & \hat{a}^{\dagger}_{k,\sigma}\end{pmatrix}\begin{pmatrix}0 & \sum_{\delta}e^{i\vec{k}\cdot\vec{\delta}}\\ \sum_{\delta}e^{-i\vec{k}\cdot\vec{\delta}} & 0\end{pmatrix}\begin{pmatrix}\hat{b}_{k,\sigma}\\ \hat{a}_{k,\sigma}\end{pmatrix}$$

The energy spectrum can be calculated through the following matrix,

$$H = t\begin{pmatrix}0 & \sum_{\delta}e^{i\vec{k}\cdot\vec{\delta}}\\ \sum_{\delta}e^{-i\vec{k}\cdot\vec{\delta}} & 0\end{pmatrix} \tag{1.11}$$

The eigenvalue of the above matrix,

$$\epsilon(k) = \pm t\sum_{\delta}|e^{i\vec{k}\cdot\vec{\delta}}| = \pm t|e^{i\vec{k}\cdot\vec{\delta}_1} + e^{i\vec{k}\cdot\vec{\delta}_2} + e^{i\vec{k}\cdot\vec{\delta}_3}|$$

After substituting the value of nearest neighbor vectors from Eq. (1.2) we get the desired energy spectrum of graphene given by,

$$\begin{aligned}\epsilon(k) &= \pm t\sqrt{1 + 4\cos^2(\frac{\sqrt{3}}{2}k_y d_{c-c}) + 4\cos(\frac{\sqrt{3}}{2}k_y d_{c-c})\cos(\frac{3}{2}k_x d_{c-c})}\\ &= \pm t\sqrt{3 + 2\cos(\sqrt{3}k_y d_{c-c}) + 4\cos(\frac{\sqrt{3}}{2}k_y d_{c-c})\cos(\frac{3}{2}k_x d_{c-c})}\end{aligned} \tag{1.12}$$

which is nothing but the band structure derived in previous section matches with Eq.(1.7).

To calculate the low energy dispersion relation, start with the following eigenvalue matrix (1.7) at one of the Dirac point K,

$$H_K = t\begin{pmatrix}0 & \sum_{\delta}e^{i\vec{k}\cdot\vec{\delta}}\\ \sum_{\delta}e^{-i\vec{k}\cdot\vec{\delta}} & 0\end{pmatrix}$$

Near the Dirac point we can write the wave vector '$\vec{k}$' as,

$$\vec{k} = \vec{K} + \vec{q}, \quad |\vec{K}| \gg |\vec{q}|.$$

Applying the Taylor series expansion rule in the following expression near one of the Dirac point 'K' we have,

$$\sum_{\delta} e^{i\vec{k}\cdot\vec{\delta}} = \sum_{\delta} e^{i(\vec{K}+\vec{q})\cdot\vec{\delta}} = \sum_{\delta} e^{i\vec{K}\cdot\vec{\delta}} \left(1 + i\vec{q}\cdot\vec{\delta}\right) = \frac{3t}{2} d_{c-c} \left(q_x - iq_y\right)$$

The final expression for the low energy spectrum of the Hamiltonian is given by,

$$H_K = \frac{3t}{2} d_{c-c} \begin{pmatrix} 0 & q_x - iq_y \\ q_x + iq_y & 0 \end{pmatrix} = \frac{3t}{2} d_{c-c} \left(\vec{\sigma}\cdot\vec{q}\right) \tag{1.13}$$

where, $\sigma = (\sigma_x, \sigma_y)$ is the set pseudo-spin pauli matrices. The eigenvalue of above Hamiltonian can simply be written as,

$$E(k = K + q) = \frac{3t}{2} d_{c-c} \sqrt{q_x^2 + q_y^2} = v_F \, |\vec{q}|,$$

where, $v_F (= \frac{3t}{2} d_{c-c})$ defined as the Fermi velocity.

Similarly, if we expand the low energy at spectrum near the other Dirac point 'K'', we get the following expression for the Hamiltonian,

$$H_{K'} = v_F \begin{pmatrix} 0 & q_x + iq_y \\ q_x - iq_y & 0 \end{pmatrix} = v_F \left(\vec{\sigma}^* \cdot \vec{q}\right) \tag{1.14}$$

where, $\sigma^* = (\sigma_x, -\sigma_y)$. Thus we see that the Hamiltonian (1.13) and (1.14) are linear dependant on momentum and they are related to each other by time reversal symmetry[4].

1.3.4 'Pseudospin' property: An additional degree of freedom

Graphene is formed by the interpenetration of two triangular sublattice labeled by 'A' and 'B'. This interpenetration gives us an additional degree of freedom known as pseudospin[4], not present in conventional 2D systems, which leads to the exceptional electronic properties[4]. In graphene, the eigenvalue equation near one of the Dirac

point 'K' with wave function $\psi(\mathbf{k})$ describing the two component spinor function and the Hamiltonian (1.10) may be written as,

$$\hat{H}_K\ \psi(\vec{k}) = E\ \psi(\vec{k}), \quad \hat{H}_K = v_F(\vec{\sigma}\cdot\vec{p}),$$

where, v_F is the group velocity or Fermi velocity near the Dirac point 'K', E defines the eigenvalue and 'σ' is 2D pseudospin matrix describes the two sublattices of honeycomb lattice. The expression for $\psi(\mathbf{k})$ can be written as,

$$\psi(\vec{k}) = \begin{pmatrix} \psi_A(\vec{k}) \\ \psi_B(\vec{k}) \end{pmatrix}.$$

Hence the above eigenvalue equation changes to,

$$\hbar v_F \begin{pmatrix} 0 & k_x - ik_y \\ k_x + ik_y & 0 \end{pmatrix} \begin{pmatrix} \psi_A(\vec{k}) \\ \psi_B(\vec{k}) \end{pmatrix} = E \begin{pmatrix} \psi_A(\vec{k}) \\ \psi_B(\vec{k}) \end{pmatrix}.$$

After solving the two component spinor wave function and energy eigenvalue can be written as,

$$\psi_{\pm,K}(\vec{k}) = \frac{1}{\sqrt{2}} \begin{pmatrix} e^{-i\theta_k/2} \\ \pm e^{i\theta_k/2} \end{pmatrix}, \quad E = \pm\hbar v_F \sqrt{k_x^2 + k_y^2},$$

where, θ_k is the phase factor (or the angle between between the wave vector 'k' and to the x-axis) and the $\pm$ sign denotes the conduction band (or π bond) and valence band (or π^* bond) respectively.

Similarly one can find the wave function around the other Dirac point ($K^{'}$) given as,

$$\psi_{\pm,K'}(\vec{k}) = \frac{1}{\sqrt{2}} \begin{pmatrix} e^{i\theta_k/2} \\ \pm e^{-i\theta_k/2} \end{pmatrix}.$$

It is easy to find from above wave functions that if the phase factor θ_k is rotated by 2π then the wave function changes its sign indicating a phase of π, this change in the phase is generally known as *Berry phase*. The property is usually the characteristic property of a spinor wave function due to which the wave function of graphene is the two component spinor. The projection of pseudospin along the direction of momentum

defines *helicity* or *chirality* of electron define through the following operator,

$$\hat{O}_{hel} = \frac{1}{\sqrt{p_x^2 + p_y^2}} (\vec{\sigma} \cdot \vec{p}) .$$

From the above equation it is clear that the two component spinor wave function $\psi_K(\vec{k})$ is the eigenfunction of the helicity operator which leads to the conclusion that electron and holes in graphene have definite helicity. The wave functions associated with the Dirac points have time reversal symmetry if we choose the origin exactly at the mid point of the line joining to the Dirac points K and K' in momentum space. In this case, the time reversal become equivalent by the reflection along k_x axis $(k_x, k_y \rightarrow k_x, -k_y)$.

We have tried to emphasize here that the linear spectrum near the Dirac points is not the only essential feature of the band structure. The electronic state near the 'K' and 'K'' are composed of states belonging to different sublattices leading to two component wave functions (spinors) which requires an index to indicate sublattice 'A' and sublattice 'B' which is very much similar to the spin index in quantum electrodynamics referred to as 'psudospin'.

1.3.5 Electronic and transport properties

Undoped graphene is either a semi-metal or zero band gap semiconductor. The energy spectrum of graphene Hamiltonian obtained from tight binding approximation expanded near Dirac points leads to the energy relation: $E = \hbar v_F |k|$, where 'k' is the wave number. This linear spectrum of graphene leads to many interesting properties and also links with relativistic phenomena. The obtained energy dispersion relation for a relativistic charged particle from the Dirac relativistic equation leads to the graphene energy dispersion relation if we set mass equal to zero in that equation where the Fermi velocity plays the same role as the velocity of light $E = \hbar c|k|$. Experimentally the transport properties of graphene shows a very high electron mobility more than 15000 $cm^2V^{-1}s^{-1}$ under ambient conditions[3,41–43]. Recent experimental study of ballistic transport properties of graphene nanoribbons[44] shows the electronic resistance changes like step function following quantum mechanical rules. The graphene nanoribbons act like optical wave guide which allow the electrons flow smoothly along the edges of the material whereas in conventional conductors like copper, nickel, the electrical resistance increases in proportion to the length as the electrons encounter with more

impurities while moving through it. The resistance of the graphene nanoribbons does not depend on temperature, also it does not depend upon the amount current putting through it. These properties are a great incentive for experimental and theoretical studies on graphene.

1.3.6 Optical properties

Apart from these properties, optical properties of graphene lead to the most remarkable phenomena that are described in various textbooks[45–49] and original literature[22–31]. These works indicate the importance attached by the community to the study of interaction of graphene with light from both experimental as well as theoretical perspectives.

1.3.6.1 Theoretical study

In 1947 Wallace[35] conducted the first theoretical study of graphite with the calculation of electronic band structure which was followed by optical studies of graphite by others[28–31] all of which pointed to graphene as the building block. Although the theoretical background for graphene was known 60 years ago, the two dimensional material actually came into existence after Geim and Novoselov synthesised it in 2004. After the experimental realization of graphene, the research on graphene as branched out in many directions including in quantum optics. Optics related issues that have been studied in the context of graphene are, optical conductivity, optical Stark effect[46] and Rabi oscillations[45–47,49]. Minimum quantum conductivity of graphene has been experimentally observed with the finite value[42] ($\frac{e^2}{h}$), where, h is the plank constant. A lot of theory[13,14,16,19,21,50–52] also discuss the minimum conductivity of graphene near the vanishing density of states and zero field for the linear 2D spectrum. Optical conductivity of graphene and graphene based systems are also studied in various regions of the electromagnetic spectrum such as visible, far infrared region etc. Coming back to the issue of Rabi oscillations, defined as the periodic oscillation of energy between the two level systems and the applied optical field which can be understood by the following pictorial diagram.

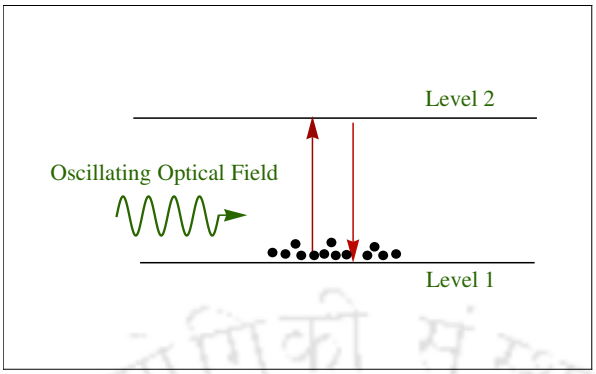

Figure 1.7: A schematic diagram of atomic oscillations (Rabi oscillations) between two level systems in presence of applied optical field.

In order to understand the phenomena of Rabi oscillations in two level system, consider the hydrogen atom interacting with light field leads to the following Schrodinger equation [46],

$$i\hbar\frac{\partial}{\partial t}\,\psi(\vec{r},t) = [H_0 + H_I(t)]\,\psi(\vec{r},t), \tag{1.15}$$

where, $H_0 = -\frac{\hbar^2\nabla^2}{2m_0} - \frac{e^2}{r}$ is defined as the unperturbed Hamiltonian for the hydrogen atom, $H_I(t) = -\vec{d}\cdot\vec{E}(t)$ is the interacting Hamiltonian in which 'd' represents dipole moment operator, $\vec{E}(t) = \vec{E}(\omega_{in})\ \ (e^{i\omega_{in}t} + c.c.)$ monochromatic incident electric field and $\psi(\vec{r},t)$ is the time dependent wave function, which can be further written in terms of stationary eigenfunctions as follows,

$$\psi(\vec{r},t) = \sum_n b_n(t)e^{-i\omega_n t}\,\psi_n(t),$$

where, b_n is related to probability amplitude, ϵ_n is the eigen value and $\psi_n(t)$ is the eigen function of the unperturbed Hamiltonian H_0.

With the help of Eqn.(1.15) one can write the equation of motion for the probability amplitude 'b_m' as,

$$i\hbar\frac{\partial}{\partial t}\,b_m = -E(t)\,\sum_n e^{-i\omega_{nm}t}\,\langle m|d|n\rangle\,b_n,$$

where, $\omega_{nm} = \omega_n - \omega_m$ is the frequency difference and $\langle m|d|n\rangle = \int d^3r\psi_m^* d\psi_n \equiv d_{mn}$ is defined as the dipole matrix element. The equation of motion for the probability

coefficients 'b_1' and 'b_2' is given by,

$$i\hbar\frac{\partial}{\partial t}\, b_1 = -E(t)e^{-i\omega_{21}t}\, \langle 1|d|2\rangle\, b_2,$$

and,

$$i\hbar\frac{\partial}{\partial t}\, b_m = -E(t)\, e^{-i\omega_{21}t}\, \langle 1|d|2\rangle\, b_1,$$

or,

$$i\hbar\frac{\partial}{\partial t}\, b_1 = -d_{12}\, \frac{E(\omega_{in})}{2}\left(e^{-i(\omega_{in}+\omega_{21})t} + e^{-i(\omega_{in}-\omega_{21})t}\right)\, b_2,$$

and,

$$i\hbar\frac{\partial}{\partial t}\, b_2 = -d_{21}\, \frac{E(\omega_{in})}{2}\left(e^{-i(\omega_{in}-\omega_{21})t} + e^{i(\omega_{in}+\omega_{21})t}\right)\, b_1,$$

These equations are generally called the optical Bloch equations. If the light interact with the hydrogen atom nearly around the resonance i.e. $\omega_{in} - \omega_{12}$ then one can see that the exponential factor $e^{i(\omega_{in}-\omega_{12})}$ is almost time independent, whereas the other exponential, $e^{i(\omega_{in}+\omega_{12})}$ oscillates very fast almost double of the incident frequency. Within the reasonable time interval the average contribution of the fast oscillating term will nearly vanish. In quantum optics this approximation has a specific name called 'rotating wave approximation' (RWA). Within this approximation the above equation reduces as,

$$i\hbar\frac{\partial}{\partial t}\, b_1 = -d_{12}\, \frac{E(\omega_{in})}{2}\, e^{-i(\omega_{in}-\omega_{21})t}\, b_2,$$

and,

$$i\hbar\frac{\partial}{\partial t}\, b_2 = -d_{21}\, \frac{E(\omega_{in})}{2}\, e^{-i(\omega_{in}-\omega_{21})t}\, b_1,$$

At exact resonance, both coupled equation reduces as,

$$\frac{d^2}{dt^2}b_2 = i\frac{d_{12}E(\omega_{in})}{2\hbar}\, \frac{b_1}{dt} = -|\frac{d_{12}E(\omega_{12})}{2\hbar}|\, b_2 = -\frac{\omega_R^2}{4}\, b_2.$$

The solution of above equation reflect the oscillatory behavior of the probability amplitude factor with a certain frequency, $\omega_R = \frac{|\vec{d}_{21}\cdot\vec{E}(\omega_{in})|}{\hbar}$, known as the Rabi frequency. The frequency (ω_R) depends only upon the intensity of the applied optical field and is independent to the applied frequency. In most of the cases, Rabi frequency (ω_R) is always less than the frequency of incident applied optical field.

Even though these phenomena in two level systems were predicted theoretically a

along time ago, they have been observed in conventional semiconductors (bands instead of levels) only in the 1980's. Recently one of the coherent optical properties, Rabi oscillations has also been studied in case graphene in presence of classical[53–55] and quantum fields[56] in the various regimes with various approximations[53]. In presence of a quantum EM field, the observed Rabi oscillations[56] are quite different from those observed in presence of a classical field[53]. Other than coherent effects such as Rabi oscillations, incoherent effects too have been studied, such as optical dephasing and relaxation of band electrons (intra-band as well as inter-band)[57,58].

1.3.6.2 Experimental study

Since graphene single layer can not be seen with bare eyes it can only be realized experimentally. The first experiment based upon interference effect[3] has been used to detect the single layer graphene on silicon dioxide substrate. After that a lot of experimental techniques have been developed for the experimental verification of single layer graphene[59]. Raman spectroscopy is one of them which detect not only the single layer but also differentiate between the single layer, bilayer and multilayer samples[22–27]. Thickness of graphene layers can also be done with the contrast spectroscopy[60]. Recently a lot of literature survey based on the optical properties which can be further classified as coherent optical properties such as optical Stark effect[46], optical conductivity, Rabi oscillations[45–47,49], universal optical conductance[13,14,16,19,21,42,50–52], measurement of fine structure constant[61], four wave mixing[49] and incoherent optical properties like optical dephasing[46], relaxation of charge carriers, both inter-band and intra-band in graphene and graphene based systems on various substrate has been reported experimentally by pump-probe technique[57,58,62–66]. One of the important phenomena that is worth addressing is how the charge carriers relax after excitation in conventional semiconductors[46] as well as in graphene[57,58,62–66]. This is traditionally investigated using pump-probe spectroscopy where two successive laser pulses are used with a variable time delay. The earlier pulse called the pump is much stronger than the later one which is called the probe. The differential transmission coefficient viz. the change in transmission coefficient of the probe with and without the pump is plotted and the relaxation times are then inferred from this plot.

1.3.7 Other interesting properties

The peculiar effect shown by the graphene is not limited to the ones we have described so far. Many of its properties like zitterbewegung[14,67], Klein paradox[15,68] etc. can be explained by relativistic electrodynamics. Other important properties such as electric field effect[3,69], Aharonov Bohm effect[70,71], integer quantum Hall effect[43,72–76], universal conductivity[77,78], minimum conductivity[79,80] etc. are seen in single layer graphene.

1.4 Method of obtaining graphene

Experimentally, graphene can be obtained by the following methods,

1.4.1 Mechanical method: Scotch tape

The scotch tape method Fig.(1.8) or drawing method was used by the Manchester group of Andre Geim and K. S. Novoselov to obtain a single layer of graphene from graphite material for the first time. This method is based upon the splitting of weakly bonded layers of graphite coupled to each other by Van der Waals force. For instance, one could employ the following approach - initially a flake of graphite material is put on the scotch tape and then the tape is rubbed against itself many times thereby causing the graphite flake to spread over the surface of the tape[81]. On this surface, there will be some spot that is one atomic layer thick exhibiting the properties of graphene. This way of producing graphene is easiest for research purposes but not for large scale production. For industrial use, graphene with reasonable dimensions is required. After obtaining a two dimensional spot of graphene over the tape, one may transfer it onto a SiO_2 substrate to make it visible. This is possible due to the visual appearance of colors caused by light interference compared to bare substrate.

1.4.2 Epitaxial growth on various substrate

Epitaxial growth means the deposition of a material in crystalline order on a crystalline substrate with a concomitant weak coupling between the layers. In this method, graphene layers are grown on a three dimensional substrate where the fluctuations are suppressed by substrate material. By an appropriate chemical method, the substrate

Figure 1.8: Scotch tape method for the mechanical exfoliation of graphene (picture has been taken from the Wikipedia-page of graphene)

can be removed and one can recover the graphene layers only. Silicon carbide (SiC) is used as a major substrate material for the epitaxial growth of graphene because this material produces insulating environment[82] automatically. Graphene layers can also be grown on metallic substrate such as Rubedium, Platinum and Iridium via chemical method deposition (CVD) method[83] within high temperature environment. High quality graphene layers can be obtained by chemical vapor deposition method in which deposition takes place on thin nickel film and methane used as a carbon source, then these layers can be transferred to various substrate leading to the numerous electronic applications[84,85]. But these methods are very costly due to the requirement of high temperature and very high vacuum.

1.5 Recent experimental study on graphene based systems

Researchers at the University of Maryland reported that bilayer graphene, a two atomic thick layer of graphene, can be used to make a very sensitive photodetector known as a "hot electron bolometer" [86]. Due to the unique properties of graphene, the detector is expected to be very sensitive to a broad range of light energies from infrared to visible range.

Recent experimental studies on ballistic transport properties of graphene nanoribbons show unusual characteristics[44], which can be used as an optical waveguide. In this regard, Prof. Walt A. de Heer said, "due to an unusual ballistic transport prop-

erty, this material could result a new class of coherent electronic devices based on room temperature, such devices would be very different from what we make today in silicon."

Scientists at the University of Vienna reported that calcium doped graphene is a superconducting material[87], but they are still trying to estimate the superconducting critical temperature. They performed angle-resolved photoemission spectroscopy (ARPES) to find an electron donor for graphene that is capable of inducing strong electron-phonon coupling and superconductivity. However, phonon mediated superconductivity has already been observed in graphene by lithium deposition[88].

1.6 Graphene dreams: Applications

Graphene is not only of immense interest to physicists due to its unique electronic and other properties but it has important applications as well. It presents an opportunity for enabling new classes of electronics, optoelectronics and electromechanical devices. However, for industrial applications, efficient and cheap methods of large scale production is yet to achieved. From an application point of view, graphene can be used in to the field of electronics, sensors, data storage devices. The experimental result shows that the transistors made from graphene nanoribbons make efficient magnetic field sensors[89]. It has also been reported that the carbon nanotube is an excellent material for the solid state gas sensors[90]. A finite band gap in graphene is obtained in a strained sample[91] which may be used to make switchable devices. It can also be used as spin valve and superconducting field effect transistors as the recent report describing magneto-resistance[92] and substantial bipolar supercurrents[93]. Bilayer graphene may also be used to make a sensitive detector of infrared light[86] with applications including remote detection of chemical and biochemical weapons. Experiments on graphene nanoribbons show unusual ballistic transport properties[44]. This property can be exploited in the construction of optical waveguides and quantum dots.

Chapter 2

Coherent Rabi oscillations in graphene

2.1 Introduction

The study of interaction of light with matter has always led to novel outcomes. One of the most well-studied coherent phenomenon in nonlinear optics is the phenomenon of Rabi oscillations[94]. A coherent periodic exchange of energy between a two level system and the applied optical field is known as Rabi oscillation. This represents the oscillations in the population and polarization of carries (with a given wave-vector in case of a band) with a frequency ω_R determined by the intensity of the externally applied optical field. This frequency ω_R is typically much smaller than the optical frequency ω itself. This phenomenon is most easily understood in two level systems studied in atomic physics[45,94]. The same phenomenon manifests itself in semiconductors, which have bands instead of energy levels and where there is a mixing of these energies due to long-range Coulomb interactions. This leads to, among other effects, the phenomenon of excitonic quantum beats and excitonic optical Stark effect[46]. It is therefore, appropriate to investigate the same effects in graphene where the bands are linear instead of parabolic and the system is two dimensional instead of three and there is pseudospin character. A recurring theme in the subject of nonlinear optics of semiconductors has been the comparison between nonlinear optical processes that occur in two-level atoms[45] and conventional semiconductors as described in the extensive literature on the subject[46,95–104]. With the advent of graphene, the comparison is now between conventional semiconductors and graphene. This comparative effort is well underway as may be seen from the emergence of several papers on the subject[54,55,104–111]. It is

our intention therefore, to contribute to this growing literature and the present investigation being a modest start. Nonlinear optics of graphene is a nascent field judging by the small number of papers in the field to date[110,111]. Indeed Romanets et.al.[110] even make a remark to the effect that there are very few works either experimental or theoretical in the field of nonlinear optics of graphene in the introduction to their paper. Mischenko[54] has studied the nonlinear response of graphene and investigated saturation effects in the current due to relaxation (at the single photon level). These works have studied detailed many body effects including relaxation processes when new physics at the level of coherent phenomena are still unexplored. Hendry et.al.[105] and Mikhailov et.al.[106–108] have stressed the importance of including higher harmonics in the evaluation of nonlinear optical response in graphene. It is the purpose of this chapter to highlight simple yet important new phenomena at the level of coherent mean-field approximations. We also find new phenomena upon inclusion of higher harmonics. Non-resonant/nonlinear optical response of graphene in the time domain has been investigated by Ishikawa[55]. The resonant nonlinear dynamics of establishment of electron-hole coherent superpositions states in graphene by multi-photon resonant excitation of inter- band transitions in laser fields with corresponding Rabi oscillations of Fermi-Dirac sea has been considered by Avetissian et al.[109]. These works are closest in spirit to the present work although our methods are considerably different.

The main advancement reported here is the use of an alternative to the rotating wave approximation (RWA) (which we have called 'asymptotic rotating wave approximation') used in the context of two-level systems. This alternative approach is able to show that for systems with the pseudospin such as graphene, a second anomalous Rabi frequency is present, and the current density exhibits a crossover from one type of singular behavior close to the normal Rabi frequency to another type of singular behavior close to the (typically smaller) 'anomalous' Rabi frequency. A comparison with an exactly solvable model identical to graphene in all respects except lacking in pseudospin shows that the anomalous Rabi frequency is peculiar to models with pseudospin. This exactly solvable model also validates the new technique we refer to as asymptotic rotating wave approximation (ARWA) (the ARWA on this model agrees with the appropriate limit of the exact solution). Lastly, we introduce an analytical technique that interpolates between these two regimes (RWA and ARWA) and express the nonlinear current in a closed form. The numerically exact solution of coherent Bloch equations also reconfirm these findings.

2.2 Problem formulation

In this chapter, we present a theoretical description of one of the better known optical properties - Rabi oscillations. We study this phenomenon in the presence of both a high intensity continuous optical field and a high intensity optical pulse. At resonance, when the frequency of incident optical field is comparable to the frequency corresponding to particle hole energy, Rabi oscillations have been analyzed by Mishchenko[54] using the well known rotating wave approximation (RWA). The main original contribution of the present work is to show that in addition to conventional Rabi oscillations, a new kind of slow oscillation in population and polarization densities is present only in graphene-like systems that is seen far from conventional resonance. This phenomenon has been studied using an alternate technique to RWA which we refer to as asymptotic rotating wave approximation (ARWA) which is also an original contribution. We provide an interpolation scheme between RWA and ARWA regime in order to complete the description and place these ideas in their proper context.
This chapter starts with the study of coherent Rabi oscillations in the presence of a classical EM field studied in the velocity gauge (and later with the length gauge as well) in two different regimes - RWA and ARWA. Interpolation between these two different regimes is done both analytically and by a numerical simulation of coherent Bloch equations. This is followed by the Result and Discussion section that analyses the results with the help of various plots.

2.3 Bloch equations of graphene in presence of continuous optical pump field

In the tight binding approach, graphene is modeled using a lattice Hamiltonian with hopping and interaction terms. The low energy part of the Hamiltonian is expressible in terms of creation and annihilation operators. We also include coupling to a gauge field using the radiation gauge. In what follows, we treat the radiation classically and the matter fields as quantum. With these assumptions, the low energy dispersion relation near the Dirac points can be expressed as[4,35](for the derivation, refer to (A.1) of Appendix-A),

$$\hat{H} = \sum_{\alpha,\beta} v_F \ \vec{\sigma}_{\alpha,\beta} \cdot (\vec{p} - \frac{e}{c}\vec{A}(t)) \ \hat{c}^{\dagger}_{p,\alpha}\hat{c}_{p,\beta} \tag{2.1}$$

where the Greek indices stand for either sublattice A or sublattice B of the honeycomb lattice and $\hat{c}_p^\dagger$ ($\hat{c}_p$) is the creation (annihilation) operators, $\vec{\sigma}$ are the three set of pseudo spin Pauli matrices, $\vec{p}$ is momentum and in addition to sublattice index the fermions also carry a spin index and a valley index. If we take these indices in to account, the full form of $\hat{c}$ would be $\hat{c}_{\vec{p},\alpha,\sigma,\lambda}$ where $\alpha = A, B$ and $\sigma \in \{\uparrow, \downarrow\}$ and $\lambda \in \{1, 2\}$, where, λ stands for valley indices. In the remainder of this chapter, we suppress the spin and valley indices since they are important only when Coulomb terms are studied or when magnetic impurities are present since these situations involve valley to valley scattering and/or flipping of spins. We shall make these terms more explicit in future publications that deal with excitonic effects.

With the help of Heisenberg's equation ($i\hbar\frac{\partial}{\partial t}\langle\hat{O}\rangle = \langle[\hat{H}, \hat{O}]\rangle$) followed by anti-commutation relations ($\{\hat{x}, \hat{y}\} = \hat{x}\hat{y} + \hat{y}\hat{x}$), we have derived the equation of motion for the following physical quantities,

$$n_{diff}(\vec{k}, t) = n_A(\vec{k}, t) - n_B(\vec{k}, t) = \langle c_{k,A}^\dagger(t) c_{k,A}(t)\rangle - \langle c_{k,B}^\dagger(t) c_{k,B}(t)\rangle$$

and

$$p(\vec{k}, t) = \langle c_{k,A}^\dagger(t) c_{k,B}(t)\rangle$$

where, $n_{diff}(\vec{k}, t)$ is the population excess between sublattice 'A' and sublattice 'B', and $p(\vec{k}, t)$ is defined as polarization. The equations are (setting $\hbar = 1$),

$$\frac{\partial}{\partial t} n_{diff}(\vec{k}, t) = 4\ Im\left(v_F\ \vec{\sigma}_{AB} \cdot (\vec{k} - \frac{e}{c}\vec{A}^*(t)) p(\vec{k}, t)\right) \tag{2.2}$$

and,

$$i\frac{\partial}{\partial t} p(\vec{k}, t) = v_F \vec{\sigma}_{BA} \cdot (\vec{k} - \frac{e}{c}\vec{A}(t)) n_{diff}(\vec{k}, t) \tag{2.3}$$

In keeping with custom, when dealing with sinusoidal fields, we choose to regard the vector potential as complex and write $\vec{A}(t) = \vec{A}(0)e^{-i\omega t}$ and $\vec{A}^*(t) = \vec{A}^*(0)e^{i\omega t}$. However, one may derive the equations below assuming $\vec{A}(t)$ is purely real (e.g. $A_x(t) = C_x cos(\omega t + \delta_x)$ and $A_y(t) = C_y cos(\omega t + \delta_y)$) and then promote them to complex quantities (e.g. $A_x(t) = C_x e^{-i(\omega t + \delta_x)}$ and $A_y(t) = C_y e^{-i(\omega t + \delta_y)}$) consistent with the requirement that n_{diff} is purely real and slow oscillations of n_{diff} at the Dirac points are due to one branch of p only that oscillates with frequency $e^{-i\omega t}$. The difference between treating $\vec{A}(t)$ real and complex only appears in the explicit formulas relating say, Rabi frequen-

cies and the components of the fields. The phenomenon of anomalous Rabi oscillations can also be obtained by treating the vector potential as purely real (see the appendix). In this chapter we only care about establishing the phenomenon of anomalous Rabi oscillations and comparing this frequency with that of resonant Rabi oscillations for which any approach will suffice.

The above equations are also called coherent Bloch equations for graphene because of the absence of a relaxation term. The relaxation terms lead to incoherent or dissipative processes. These equations may be solved close to resonance using the well-known rotating wave approximation. Far from resonance, a new version of RWA namely ARWA has been employed. In the next two sections, we study these Bloch equations in the regime where the frequency of incident optical field is much higher than the frequency corresponding to the particle hole energy. We refer to this regime as the 'ARWA regime'. Whereas in the second section, we study these equations in the RWA regime, the regime where the frequency of incident optical field is nearly equal to the frequency corresponding to the particle hole energy and compare and contrast the results obtained in these two cases.

2.4 Rabi oscillations in graphene

When a system of two level atoms interact with the externally applied optical field, oscillation of atoms between the levels take place viz. a periodic exchange of energy between the two level atoms and the applied optical field. This oscillation is known as Rabi oscillation[94] and the frequency of such periodic oscillations is known as the Rabi frequency. The frequency of these oscillations (the Rabi frequency) depends upon the strength of applied field rather than its frequency. The sinusoidal oscillations have a maximum amplitude at resonance. Since Rabi oscillations are associated with the two level system, it is conceivable that a study the same phenomenon in case of graphene where the levels are replaced by bands and possess a pseudospin degree of freedom, may lead to some interesting novel phenomena.

2.4.1 Conventional Rabi oscillations using rotating wave approximation

In this subsection, we derive the equations of motion of the population excess and polarization (also known as density matrix equations) (2.2) and (2.3) in the RWA regime. Traditionally[94], RWA refers to an approximation where the driving frequency is close to one of the excitation or resonant frequencies of the system and the time dependence of the dynamical quantities are factored into 'fast' and 'slow' variables: fast being the external frequency, and slow referring to the difference between the external frequency and the resonant frequency - characteristic of the two-level/two-band system. The basic idea behind this approximation is that when we compute the time average of the rapidly varying terms contained in density matrix equation over any a time interval long compared to the rather small period of these rapidly varying terms, the result may be expected to be very small. Hence we may therefore, neglect the rapidly varying terms. This justification of RWA is not perfect, since it is just an approximation. In 1940 Bloch and Siegert showed that the terms which RWA neglects gives rise to a shift in the true resonance frequency of the dipoles[45,112].

The Bloch equation (2.2) and (2.3) can be written in matrix form as,

$$i\,\partial_t \begin{pmatrix} n_{diff}(\vec{k},t) \\ p(\vec{k},t) \\ p^*(\vec{k},t) \end{pmatrix} = \begin{pmatrix} 0 & 2z_k & -2z_k^* \\ z_k^* & 0 & 0 \\ -z_k & 0 & 0 \end{pmatrix} \begin{pmatrix} n_{diff}(\vec{k},t) \\ p(\vec{k},t) \\ p^*(\vec{k},t) \end{pmatrix}$$
$$+ \begin{pmatrix} 0 & -2z_A^* & 2z_A \\ -z_A & 0 & 0 \\ z_A^* & 0 & 0 \end{pmatrix} \begin{pmatrix} n_{diff}(\vec{k},t) \\ p(\vec{k},t) \\ p^*(\vec{k},t) \end{pmatrix}$$

where, $z_k = v_F\,(\vec{\sigma}_{AB}\cdot\vec{k})$ and $z_A = v_F\,(\vec{\sigma}_{BA}\cdot\frac{e}{c}\vec{A}(t))$ and ∂_t is stand for $\frac{\partial}{\partial t}$. Diagonalize the unperturbed Hamiltonian and make the following substitution,

$$\begin{pmatrix} n_{diff}(\vec{k},t) \\ p(\vec{k},t) \\ p^*(\vec{k},t) \end{pmatrix} = \begin{pmatrix} 0 & 2\sqrt{\frac{z_k^*}{z_k}} & -2\sqrt{\frac{z_k^*}{z_k}} \\ \frac{z_k^*}{z_k} & -\frac{z_k^*}{z_k} & -\frac{z_k^*}{z_k} \\ 1 & 1 & 1 \end{pmatrix} \begin{pmatrix} \tilde{n}_{diff}(\vec{k},t) \\ \tilde{p}(\vec{k},t) \\ \tilde{p}'(\vec{k},t) \end{pmatrix}$$

After substituting we get a set of equations followed by the further substitutions

$\tilde{p}(\vec{k},t) = e^{2iv_F|k|}\ P(\vec{k},t),\ \tilde{p}'(\vec{k},t) = e^{-2iv_F|k|}\ P'(\vec{k},t)$ and applying RWA we have,

$$
\begin{aligned}
i\partial_t\tilde{n}_{diff}(\vec{k},t) &= -e^{-i\Delta t}\frac{z_R z_k}{v_F|k|}P(\vec{k},t) - \frac{z_R^* z_k^*}{v_F|k|}e^{i\Delta t}P'(\vec{k},t)\\
i\partial_t P(\vec{k},t) &= -e^{i\Delta t}\frac{z_R^* z_k^*}{2v_F|k|}\tilde{n}_{diff}(\vec{k},t)\\
i\partial_t P'(\vec{k},t) &= -e^{-i\Delta t}\frac{z_R z_k}{2v_F|k|}\tilde{n}_{diff}(\vec{k},t)
\end{aligned}
$$

where, $\Delta = \omega - 2v_F|k|$ defined as small detuning.

Upon solving these equations, we may write the solution for $n_{diff}(\vec{k},t)$ and $p(\vec{k},t)$ as (for detailed calculation see the Appendix-A),

$$
\begin{aligned}
n_{diff}(\vec{k},t) \;=\; & \frac{1}{2i\ (v_F|k|)\ \Omega_B}(z_k^* z_R^*\ e^{i\omega t} - z_k z_R\ e^{-i\omega t})\ \sin(\Omega_B\ t)\\
& -\frac{\Delta}{2(v_F|k|)\ \Omega_B^2}(z_k^* z_R^*\ e^{i\omega t} + z_k z_R\ e^{-i\omega t})\ (1-\cos(\Omega_B\ t))
\end{aligned}
$$

and,

$$
\begin{aligned}
p(\vec{k},t) \;=\; & \left(\frac{-(v_F|k|)\ \Delta^2}{2z_k\ \Omega_B^2} + \frac{z_k^* z_R^*\ \Delta}{4z_k\ \Omega_B^2}\ e^{i\omega t} - \frac{z_R\ \Delta}{4\Omega_B^2}e^{-i\omega t}\right) - \left(\frac{z_k^* z_R^*}{4iz_k\Omega_B}e^{i\omega t} + \frac{z_R}{4i\ \Omega_B}e^{-i\omega t}\right)\\
& \sin(\Omega_B\ t) - \left(\frac{(v_F|k|){\omega_R}^2}{2z_k\ \Omega_B^2} + \frac{z_k^* z_R^*\ \Delta}{4z_k\ \Omega_B^2}e^{i\omega t} - \frac{z_R\ \Delta}{4\Omega_B^2}e^{-i\omega t}\right)\cos(\Omega_B\ t),
\end{aligned}
$$

and the expression for the generalized Rabi frequency (in RWA regime) is given by,

$$\Omega_B = \sqrt{\Delta^2 + \omega_R^2} \tag{2.4}$$

and $\Delta = \omega - 2v_F|k|$ is defined as small detuning.

Mischenko and Ishikawa use the following formulas to evaluate the current density (for detailed calculation of current density see the Appendix-A)

$$\vec{J}(t) = 4\sum_{\vec{k}}\vec{j}_{\vec{k}} = 4ev_F\sum_{\vec{k}}p^*(k,t)\vec{\sigma}_{BA} + 4ev_F\sum_{\vec{k}}p(\vec{k},t)\vec{\sigma}_{AB}$$

where the prefactor $4 = 2\times 2$ is for spin and valley degeneracy. For the small detuning

case the expression for the $p(\vec{k},t)$ becomes (see for example the textbook by Haug),

$$p(\vec{k},t) \sim -\frac{z_R}{4i\Omega_B}\sin(\Omega_B t)\ e^{-i\omega t}$$

If one presumes that this expression is valid for all $|k|$ then one may extract the slowly varying part of the current density and use the Fourier transform in the frequency domain one obtains,

$$\vec{j}_{slow,B}(\omega^{'}) = -4ev_F\vec{\sigma}_{AB}\ \sum_k \frac{z_R}{4i\Omega_B}\ \int_{-\infty}^{+\infty} dt\ \sin(\Omega_B\ t)\ e^{-i\omega^{'}t}$$

This means for $\omega^{'} > \omega_R$,

$$\vec{j}_{slow,B}(\omega^{'}) = -ev_F\vec{\sigma}_{AB}\frac{z_R}{\omega_R}A\frac{\omega}{4v_F}\ \frac{\omega^{'}}{v_F\sqrt{\omega^{'2}-\omega_R^2}} \tag{2.5}$$

and $\vec{j}_{slow,B}(\omega^{'}) = 0$ for $\omega^{'} < \omega_R$. In real time domain the expression for currents density is given by (the physical current is the real part of this expressions),

$$\vec{J}_B(t) = ev_F\vec{\sigma}_{AB}\ z_R A\frac{i\omega}{8v_F^2}Y_1(\omega_R|t|)\ Sign(t)\ e^{-i\omega t} \tag{2.6}$$

where, Y_1 is the Bessel function of first kind.

2.4.2 Anomalous Rabi oscillations using asymptotic rotating wave approximation

In the earlier section we described the conventional approach of obtaining an approximate solution of the Bloch equations (2.2) and (2.3), viz. the RWA, but this is valid only close to conventional resonance. The main contribution of this thesis is the observation that in graphene pseudospin affords other resonances not probed by RWA. In order to probe resonances that are solely due to pseudospin new approximations have to be introduced. One such approximation goes by the name of asymptotic rotating wave approximation (ARWA) which is the alternative to rotating wave approximation (RWA). The RWA interpretation is valid close to (conventional) resonance whereas ARWA is valid when the driving frequency is much larger than any of the resonant frequencies of the system i.e. extreme non-resonance case. The basic idea behind the

ARWA interpretation is that the unknowns in the problem namely the number density and polarization density are expressible as a harmonic series involving the largest of the frequencies. The coefficients are assumed to be slowly varying on the scale of the largest of frequencies. The equations for these coefficients are then solved by retaining only the leading harmonics (see Results and Discussion section for a justification). In what follows we postulate that the largest frequency is ω which is the frequency of the external field. One assumes that the external driving frequency ω is always much larger than the conventional Rabi frequency ω_R which in turn we assume is much larger than the 'resonant' frequency for the creation of particle hole pairs namely $2v_F|k|$ ($\omega \gg \omega_R$ and $\omega \gg 2v_F|k|$). This is in contrast to the usual condition (RWA) namely $|\omega - 2v_F|k|| \ll \omega$. The main purpose of this work is to provide a contrast between the predictions made using these two very different assumptions. In light of the observations just made, we may write,

$$n_{diff}(\vec{k},t) = n_s(\vec{k},t) + n_f(\vec{k},t)\ e^{-i\omega t} + n_f^*(\vec{k},t)\ e^{i\omega t}$$

and

$$p(\vec{k},t) = p_s(\vec{k},t) + p_+(\vec{k},t)\ e^{-i\omega t} + p_-(\vec{k},t)\ e^{i\omega t}$$

where, $n_s(\vec{k},t)$ and $p_s(\vec{k},t)$ are the slow variables and $n_f(\vec{k},t)$, $p_+(\vec{k},t)$, $p_-(\vec{k},t)$ are the fast variable along with $e^{\pm i\omega t}$ and '*' appear at superscript position stand for the complex conjugate. Substituting these values in to the equations (2.2) and (2.3) and comparing the coefficients, the slowly varying parts obey the equations below,

$$\partial_t n_s(\vec{k},t) = 4\ Im\left(z_k\ p_s(\vec{k},t)\right) + 4\ Im\left(z_R\ p_+^*(\vec{k},t)\right)$$

and

$$i\partial_t p_s(\vec{k},t) = z_k^*\ n_s(\vec{k},t) - z_R\ n_f^*(\vec{k},t)$$

whereas the rapidly varying parts obey the equations given by,

$$i\partial_t p_+(\vec{k},t) + \omega\ p_+(\vec{k},t) = -z_R\ n_s(\vec{k},t) + z_k^*\ n_f(\vec{k},t),$$

$$i\partial_t p_-(\vec{k},t) - \omega\ p_-(\vec{k},t) = z_k^*\ n_f^*(\vec{k},t)$$

and,

$$i\partial_t n_f(\vec{k},t) + \omega\ n_f(\vec{k},t) = 2z_k\ p_+(\vec{k},t) + 2z_R\ p_s^*(\vec{k},t) - 2z_k^*\ p_-^*(\vec{k},t)$$

where we define $z_k \equiv v_F\ (\vec{\sigma}_{AB} \cdot \vec{k})$, $z_k^* \equiv v_F\ (\vec{\sigma}_{BA} \cdot \vec{k})$, $z_R = v_F(\vec{\sigma}_{BA} \cdot \frac{e}{c}\vec{A}(0))$, $z_R^* = v_F(\vec{\sigma}_{AB} \cdot \frac{e}{c}\vec{A}^*(0))$ and ∂_t as partial time derivative. In the remainder of this section, we focus on the case when mutual interactions between the particles are absent ($V_q = 0$). In other words we postpone the discussion of excitonic effects such as Excitonic Optical Stark effect, dephasing and other incoherent effects brought about by carrier-phonon scattering and carrier-carrier scattering to future works. Now we turn to the solutions of above equations in ARWA regime.

The above set of equations may be solved analytically using an ansatz of the form, $X(\vec{k},t) = X(\vec{k},0)\ \cos(\Omega t) + \frac{1}{\Omega}\dot{X}(\vec{k},0)\ \sin(\Omega t)$ where $X = n_s, n_f, p_+,\ p_-, p_s$. From the set of all possible solutions we may extract the effective Rabi frequencies Ω that are relevant in the various limits under consideration. In general, one finds that Ω is one of several possible solutions to a polynomial equation of a high degree. Further approximations are needed to extract the frequencies in interesting limits. From Mishchenko's[54] work, we may infer that the Rabi frequency (for the Fermi bilinears) is $\Omega \approx (\omega_R^2 + (\omega - 2v_F|k|)^2)^{\frac{1}{2}}$ valid in the limit $|\omega - 2v_F|k|| \ll \omega_R \ll \omega$ where $\omega_R = v_F|\frac{e}{c}\vec{\sigma}_{BA} \cdot \vec{A}(0)|$. The main disadvantage of this limit is that for a fixed external frequency ω, the results for polarization and population are available only for momenta such that $|k| \sim \frac{\omega}{2v_F}$. Upon including Coulomb interaction, the various momenta get mixed up and this solution becomes rather less useful. Hence we wish to focus on a more general case. In particular we choose the limit $\omega \gg \omega_R$ and $\omega \gg v_F|k|$. In this limit we find that $|\frac{dX}{dt}| \ll \omega|X|$ hence terms such $\frac{dX}{dt}$ may be ignored in comparison with ωX. This leads to the following solution for the slow and fast components of the occupation and polarization.

$$n_f(\vec{k},t) \approx \frac{2z_R}{\omega}\ p_s^*(\vec{k},t);\ \ n_f^*(\vec{k},t) \approx \frac{2z_R^*}{\omega}\ p_s(\vec{k},t)$$

and

$$p_+(\vec{k},t) \approx -\frac{z_R}{\omega}n_s(\vec{k},t);\ \ p_-(\vec{k},t) \approx -\frac{2z_R^* z_k^*}{\omega^2}\ p_s(\vec{k},t)$$

Therefore, equation for the slowly varying coefficient is given by,

$$i\partial_t p_s(\vec{k},t) = z_k^*\ n_s(\vec{k},t) - \frac{2z_R^* z_R}{\omega}\ p_s(\vec{k},t)$$

and

$$\partial_t n_s(\vec{k},t) = 4\ Im\left(z_k\ p_s(\vec{k},t)\right)$$

The solution above coupled equations may be written down as,

$$n_s(\vec{k},t) = n_s(\vec{k},0)\ \cos(\Omega_R t)$$

$$p_s(\vec{k},t) = \frac{\Omega_R z_k^* n_s(\vec{k},0)}{4i(v_F k)^2}\ \left(\sin(\Omega_R t) - i\frac{2\omega_R^2}{\Omega_R \omega}\ \cos(\Omega_R t)\right) \tag{2.7}$$

where, Ω_R appear in the above equations is defined as the generalized Rabi frequency given by the following expression,

$$\Omega_R = 2\frac{\sqrt{\omega_R^4 + (v_F|k|)^2\omega^2}}{\omega} \tag{2.8}$$

and $\omega_R = v_F|\vec{\sigma}_{BA}\cdot\frac{e}{c}\vec{A}(0)|$ is the conventional Rabi frequency and $n_s(\vec{k},0) = \frac{\omega(v_F|k|)}{\omega_R^2}$, $p_0(\vec{k}) = -\frac{k_x+ik_y}{2|k|}$ is the value of polarization at t = 0 (for detailed calculation see the Appendix-A). To calculate the equilibrium value of polarization we have considered an undoped graphene system. Note that since we are operating in the limit $\omega_R \ll \omega$ and $v_F|k| \ll \omega$ it is quite possible that $(v_F|k|)\omega \sim \omega_R^2$ hence both these terms are retained in the formula for Ω_R.

To evaluate the current density in ARWA regime we use the same formula (2.4.1) as in earlier section. Considering that one has to sum over all possible values of $\vec{k}$ and the results obtained in earlier section (RWA regime) are valid only for $|k| \sim \frac{\omega}{2v_F}$ it seems more appropriate that we use our results which is valid for all $|k| \ll \frac{\omega}{2v_F}$ and $\omega_R \ll \omega$. We have to use the polarization formula given below,

$$p(\vec{k},t) \approx p_s(\vec{k},t) - \frac{z_R(v_F|k|)}{\omega_R^2}\ \cos(\Omega_R t)e^{-i\omega t}.$$

The slowly varying part p_s drops out upon summing over $\vec{k}$ leaving a term that oscillates with the same frequency and in phase with the external field as we may have expected. Thus the total current is,

$$\vec{J}(t) = -4ev_F\vec{\sigma}_{AB}\ \sum_k \frac{z_R(v_F|k|)}{\omega_R^2}\ \cos(\Omega_R t)\ e^{-i\omega t}.$$

The experimentalist should extract the amplitude of the current that is oscillating with frequency ω, Fourier transform it and plot it as a function of frequency. The Fourier

transform of the slowly varying part of the current is,

$$\begin{aligned}\vec{j}_{slow}(t) &= -4ev_F\vec{\sigma}_{AB}\sum_k \frac{z_R(v_F|k|)}{\omega_R^2}\cos(\Omega_R t) \\ &= \int_{-\infty}^{+\infty}\frac{d\omega^{'}}{2\pi}\, e^{i\omega^{'}t}\,\vec{j}_{slow}(\omega^{'})\end{aligned}$$

therefore,

$$\vec{j}_{slow}(\omega^{'}) = -2e\vec{\sigma}_{AB}\; A\;\frac{z_R}{\omega_R^2}\left(\frac{\omega^{'2}}{4}-\frac{\omega_R^4}{\omega^2}\right)^{\frac{1}{2}}\;\frac{|\omega^{'}|}{4v_F} \tag{2.9}$$

where, $\frac{\omega^{'2}}{4} > \frac{\omega_R^4}{\omega^2}$ and $\vec{j}_{slow}(\omega^{'}) = 0$ otherwise. The slowly varying part of the net current density in the system exhibits a threshold behavior in frequency domain with threshold frequency equal to $\frac{2\omega_R^2}{\omega}$. This is one of the main predictions of the present work. In real time domain the current density is($t \neq 0$ and $\omega_{R*} = \frac{2\omega_R^2}{\omega}$),

$$\vec{J}_R(t) = -ev_F\vec{\sigma}_{AB}\; A\;\frac{z_R}{8v_F^2\omega_R^2}\;\frac{\omega_{R*}^2 J_2(\omega_{R*}t)}{|t|}\;e^{-i\omega t} \tag{2.10}$$

where J_2 is the Bessel function of second kind.

2.4.2.1 Solution of Bloch equations

In this section we justify why we are taking only upto first harmonics in ARWA analysis. At the outset it is clear that if one includes only the slowly varying terms and drops all the rapidly oscillating terms, the conventional Rabi resonance is lost. Therefore it is important to include at least the first harmonic. Higher harmonics are important at stronger field strengths where strong nonlinearity leads to effects such as the Bloch Siegert shift [45,112] and so forth. But for graphene something more interesting is seen far from resonance where a new form of Rabi oscillation attributable to pseudospin emerges with a Rabi frequency small compared to the conventional Rabi frequency. Inclusion of higher harmonics leads to newer anomalous resonances unlike in conventional Rabi oscillations where inclusion of higher harmonics merely causes a shift in the conventional resonance frequency. There is one special situation where the Bloch equations (2.2) and (2.3) may be solved analytically. That special point is at the tip of the Dirac cones : $\vec{k} = 0$. Exactly at the Dirac point, the Bloch equations become (where the momentum

vanish),

$$i\partial_t\ n_{diff}(\vec{0},t) = -2z_R^*\ e^{i\omega t}p(\vec{0},t) + 2z_R\ e^{-i\omega t}p^*(\vec{0},t)$$

and

$$i\partial_t\ p(\vec{0},t) = -z_R\ e^{-i\omega t}n_{diff}(\vec{0},t)$$

The following substitution turns these equations into ODEs with constant coefficients that may be solved analytically. Set $p(\vec{0},t) = e^{-i\omega t}\tilde{p}(\vec{0},t)$ to obtain,

$$i\ \partial_t\ n_{diff}(\vec{0},t) = 2\ z_R\ \tilde{p}^*(\vec{0},t) - 2\ z_R^*\ \tilde{p}(\vec{0},t)$$

and

$$\omega\ \tilde{p}(\vec{0},t) + i\ \partial_t\ \tilde{p}(\vec{0},t) = -z_R\ n_{diff}(\vec{0},t)$$

which leads to the solution $\tilde{p}(\vec{0},t) \sim e^{\pm\ i\sqrt{\omega^2+4\omega_R^2}\ t}\ \tilde{p}(\vec{0},0)$. After back substitution we may see that the slowly varying part of the polarization density for $\omega \gg \omega_R$ oscillates with the anomalous Rabi frequency $\frac{2\omega_R^2}{\omega}$.

2.4.3 Difference between conventional RWA and ARWA

In RWA limit, the applied optical frequency is comparable to the transition frequency of the system i.e. the detuning ($\Delta = \omega - \omega_0$) is small compared to ω whereas in the ARWA case, the applied optical frequency is much larger than the transition frequency. Mathematically, the RWA is effected by keeping the detuning (difference between ω and ω_0) fixed while taking the $\omega \to \infty$ limit, whereas it the product of ω and ω_0 that is fixed in ARWA.

2.4.4 Comparison between the results obtained in RWA and ARWA regimes

Above analysis shows two important conclusions - one is the crossover phenomenon from anomalous to conventional Rabi oscillation as a function of the wave number of the electron bands when the external frequency is kept fixed and the other is the threshold behavior exhibited by the current density in the two different regimes. The expression for the generalized Rabi frequencies Ω_R (Eq.(2.8)) obtained in ARWA regime and Ω_B (Eq.(2.4)) inferred from the RWA reveals the crossover phenomenon. Fig.(2.1)

which is the central result of our work describes this cross-over pictorially. A more detailed description of this figure will be given later. The other significant observation

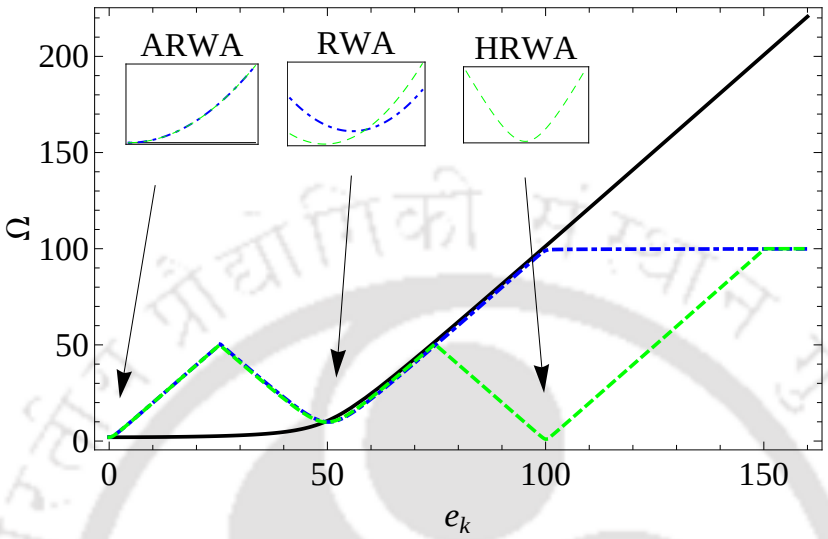

Figure 2.1: This is the central result of our work. It depicts the dependence of the effective or generalized Rabi frequency on the band energy $e_k = v_F|k|$ for a fixed value of external frequency ($\omega = 100$) and Rabi frequency for zero detuning ($\omega_R = 10$) in generalized unit ($\hbar = 1$). The solid black line ignore all harmonics in external frequency, The blue dot-dash line line includes first harmonic and ignore second and higher harmonics. The green dashed line includes upto second harmonic in the external frequency. The second inset figure shows the small shift in minima which is nothing but the Bloch-Siegert shift.

is the two quite different threshold behaviors in frequency domain, in case of ARWA Eq.(2.9) shows that the current approaches zero as a power law with threshold frequency equal to $\frac{2\omega_R^2}{\omega}$ whereas in case of conventional resonance (RWA), Eq.(2.5) shows that the current diverges as a power law with the threshold frequency being the simple Rabi frequency ω_R. In real time, the distinction is less obvious. For the sake of comparison, the two currents in the frequency domain and time domain are given in Fig.(2.2) and Fig.(2.3).

Our results are valid when $v_F\frac{2\pi}{a} \gg \omega \gg \omega_R$ where a is the lattice spacing, so that the Dirac cone approximation is still valid.

Till now we have discussed the Rabi oscillations and obtained the results using the velocity gauge. For the sake of highlighting the nature of gauge choices, the next section is totally devoted to the length gauge. This exercise is also meant to highlight the gauge invariance of experimentally measurable quantities.

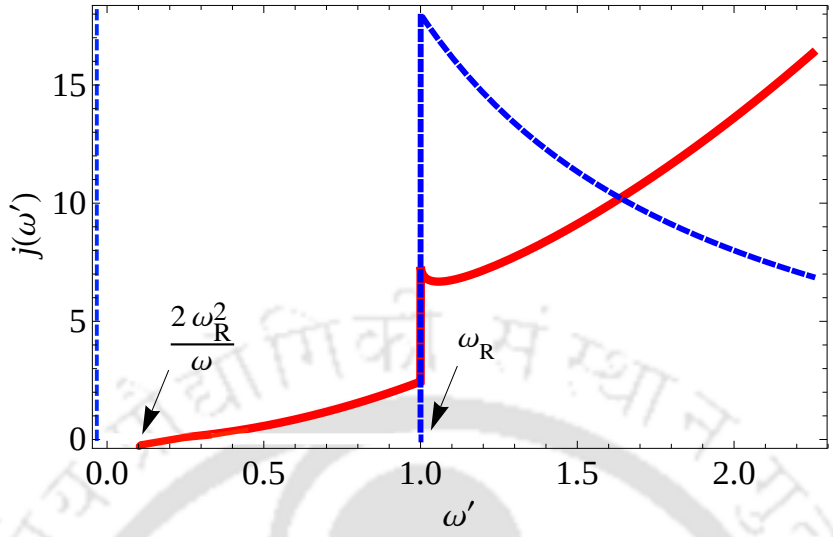

Figure 2.2: This plots shows the dependence of the slow part of the current density on frequency. We have chosen $\omega_R = 4Z^*Z = 1$. The red solid curve is for graphene and blue dotted one is for the exactly solvable model. In case of graphene there are two thresholds, the smaller one is at $\frac{2\omega_R^2}{\omega}$ (anomalous Rabi frequency) below which there is no current

2.5 Analysis under length gauge: The question of gauge invariance

Here we wish to address the important question as to whether the results obtained so far, especially the notion of anomalous Rabi frequency and cross-over, are gauge invariant notions. This is important since only gauge invariant quantities are experimentally accessible. In the earlier sections we have computed the current density which is gauge invariant. In this section we investigate this issue in greater depth.

In earlier sections we have employed the so-called velocity gauge (only vector potential is present but no scalar potential). We now wish to show that the same results are obtained with the other extreme choice namely - the length gauge (vice versa). This transformation is well known and a good description may be found in this reference[113]. The required transformation is given in Eq.(10) of this paper. We wish to apply this transformation to the Bloch equations (2.2) and (2.3) that uses the velocity gauge. We can rewrite these equations in real space as,

$$i\,\partial_t N_{diff}(\vec{r},t) = 2v_F\left(\vec{\sigma}_{AB}\cdot(i\nabla - \frac{e}{c}\vec{A}^*(t))P(\vec{r},t) - \vec{\sigma}_{BA}\cdot(i\nabla - \frac{e}{c}\vec{A}(t))P^*(-\vec{r},t)\right),$$

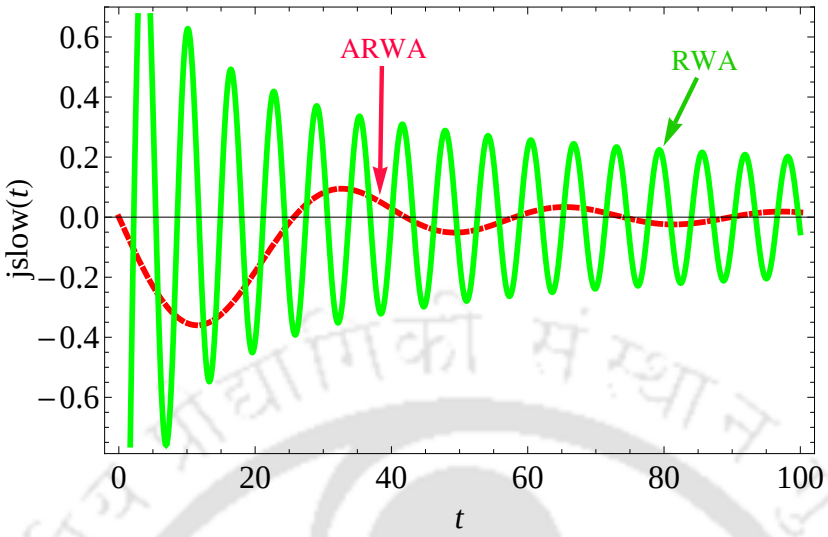

Figure 2.3: Here we see the slowly varying part of the current density with time of graphene only. The dotted red curve is ARWA whereas solid green curve is RWA. The frequency associated with the red curve is the anomalous Rabi frequency $\frac{2\omega_R^2}{\omega}$. The frequency with the simple green curve is conventional Rabi frequency ω_R

$$i\,\partial_t P(\vec{r},t) = v_F \vec{\sigma}_{BA}\cdot(i\nabla - \frac{e}{c}\vec{A}(t))N_{diff}(\vec{r},t),$$

where we have used the following definition to write $N_{diff}(\vec{k},t)$ and $p(\vec{k},t)$ in real space,

$$\psi(\vec{r},t) = \frac{1}{\sqrt{A}}\,e^{i\vec{k}\cdot\vec{r}}\,c_k(t), \quad \psi^\dagger(\vec{r},t) = \frac{1}{\sqrt{A}}\,e^{-i\vec{k}\cdot\vec{r}}\,c_k^\dagger(t).$$

Hence,

$$\begin{aligned} N_{diff}(\vec{r}-\vec{r'},t) &\equiv \langle\psi_A^\dagger(\vec{r},t)\psi_A(\vec{r'},t)\rangle - \langle\psi_B^\dagger(\vec{r},t)\psi_B(\vec{r'},t)\rangle \\ &= \frac{1}{A}\sum_{\vec{k}} e^{-i\vec{k}.(\vec{r}-\vec{r'})}\,n_{diff}(\vec{k},t), \end{aligned}$$

$$P(\vec{r}-\vec{r'},t) \equiv \langle\psi_A^\dagger(\vec{r},t)\psi_B(\vec{r'},t)\rangle = \frac{1}{A}\sum_{\vec{k}} e^{-i\vec{k}.(\vec{r}-\vec{r'})}\,p(\vec{k},t),$$

Setting $\vec{r'} = 0$ the above equation becomes,

$$\begin{aligned} N_{diff}(\vec{r},t) &\equiv \langle\psi_A^\dagger(\vec{r},t)\psi_A(\vec{0},t)\rangle - \langle\psi_B^\dagger(\vec{r},t)\psi_B(\vec{0},t)\rangle \\ &= \frac{1}{A}\sum_{\vec{k}} e^{-i\vec{k}.(\vec{r})}\ n_{diff}(\vec{k},t), \end{aligned}$$

$$P(\vec{r},t) \equiv \langle\psi_A^\dagger(\vec{r},t)\psi_B(\vec{0},t)\rangle = \frac{1}{A}\sum_{\vec{k}} e^{-i\vec{k}.(\vec{r})}\ p(\vec{k},t).$$

Note that due to translational symmetry of the propagators, $N^*_{diff}(\vec{r},t) = N_{diff}(-\vec{r},t)$. These equations are written in a specific gauge namely the velocity gauge where the scalar potential is zero. In order to demonstrate gauge invariance we have to restore the scalar potential and study the general equations. The presence of the scalar potential alters the Hamiltonian by the addition of a piece $\int d^2r\ e(\phi(\vec{r},t)-\phi(\vec{0},t))\ (\psi_A^\dagger(\vec{r},t)\psi_A(\vec{r},t)+\psi_B^\dagger(\vec{r},t)\psi_B(\vec{r},t))$.

$$\begin{aligned} i\ \partial_t N_{diff}(\vec{r},t) = 2v_F\ \vec{\sigma}_{AB}\cdot(i\nabla - \frac{e}{c}\vec{A}^*(t))P(\vec{r},t) - 2v_F\ \vec{\sigma}_{BA}\cdot(i\nabla - \frac{e}{c}\vec{A}(t))P^*(-\vec{r},t) \\ -e\phi(\vec{r},t)N_{diff}(\vec{r},t) \end{aligned} \tag{2.11}$$

$$i\ \partial_t P(\vec{r},t) = v_F\vec{\sigma}_{BA}\cdot(i\nabla - \frac{e}{c}\vec{A}(t))N_{diff}(\vec{r},t) - e\phi(\vec{r},t)P(\vec{r},t) \tag{2.12}$$

Now we wish to effect a gauge transformation. This means we have to change the field variables $\tilde{\psi}_{A,B}(\vec{r},t) = e^{-ie\chi(\vec{r},t)}\psi_{A,B}(\vec{r},t)$ by a local phase factor and simultaneously shift the vector and scalar potentials by some amount that is going to be related to this $\chi(\vec{r},t)$. We set,

$$\vec{\tilde{A}}(t) = \vec{A}(t) - \nabla c\chi(\vec{r},t), \quad \tilde{\phi}(\vec{r},t) = \phi(\vec{r},t) + \frac{\partial}{\partial t}\chi(\vec{r},t).$$

We assert that the same equations hold for the new fields. We substitute these into the equations to get,

$$\tilde{X}(\vec{r},t) = e^{ie\chi(\vec{r},t)}\ X(\vec{r},t)$$

for $X = N_{diff}, P$. Thus the equations (2.11) and (2.12) are *gauge invariant under the gauge transformations defined above* . Now we consider two different possibilities,

first is the velocity gauge of the previous section. In this case, $\phi = 0$ but $\vec{A} \neq 0$. Its antithesis is the length gauge wherein $\tilde{\phi} \neq 0$ but $\vec{\tilde{A}} = 0$. Since we have just established the relation between these two we may write,

$$\tilde{\phi}(\vec{r},t) = \phi(\vec{r},t) + \frac{\partial}{\partial t}\chi(\vec{r},t) = 0 + \frac{\partial}{\partial t}\chi(\vec{r},t),$$
$$0 = \vec{\tilde{A}}(t) = \vec{A}(t) - \nabla c\chi(\vec{r},t),$$

from this it follows that,

$$\chi(\vec{r},t) = \frac{1}{c}\ \vec{r}\cdot\vec{A}(t).$$

Thus in the length gauge we have to couple the equations to a scalar potential given by $\tilde{\phi}(\vec{r},t) = \frac{1}{c}\ \vec{r}\cdot\frac{\partial}{\partial t}\vec{A}(t) = -\vec{r}\cdot\vec{E}(t)$ where $\vec{E}(t)$ is the applied electric field whereas the vector potential is zero $\vec{\tilde{A}} = 0$. Thus in the length gauge the Bloch equations read as follows,

$$\begin{aligned} i\ \partial_t \tilde{N}_{diff}(\vec{r},t) &= 2v_F\ \vec{\sigma}_{AB}\cdot i\nabla\tilde{P}(\vec{r},t) - 2v_F\ \vec{\sigma}_{BA}\cdot i\nabla\tilde{P}^*(-\vec{r},t) \\ &\quad + e\vec{r}\cdot\vec{E}(t)\tilde{N}_{diff}(\vec{r},t) \end{aligned} \tag{2.13}$$

$$i\ \partial_t\tilde{P}(\vec{r},t) = v_F\vec{\sigma}_{BA}\cdot i\nabla\tilde{N}_{diff}(\vec{r},t) + e\vec{r}\cdot\vec{E}(t)\tilde{P}(\vec{r},t) \tag{2.14}$$

Note that here $\vec{E}(t)$ is taken to be real. Now we wish to show that these equations also lead to the anomalous Rabi frequency, thereby establishing the gauge invariance of the concept of cross-over of Rabi oscillations. We note at the outset that the results for the Rabi frequencies depend crucially on what we precisely mean by Rabi frequency. In the cited works they refer to slow oscillations of *wavefunctions* relative to a predesignated fast frequency. In this case, the results of the length gauge are not guaranteed to agree with those obtained using the velocity gauge since wavefunctions are not gauge invariant. Indeed it is well known that the Rabi frequency associated with the wavefunction (rather than its bilinears) is given in the velocity gauge as[54].

$$\omega_{Rabi,VG} = |sin(\theta_p)|\frac{eEv_F}{\hbar\omega} \tag{2.15}$$

whereas in the length gauge it is[109],

$$\omega_{Rabi,LG} = |sin(\theta_p)|\frac{eE}{2p} \tag{2.16}$$

where $tan(\theta_p) = \frac{p_y}{p_x}$. An accidental equality emerges at exact resonance $2pv_F = \hbar\omega$. We have to focus on quantities that are gauge invariant in order to extract Rabi frequencies that are independent of choice of gauge. The gauge invariant quantities are naturally - densities and currents. In case of graphene, the current is already gauge invariant without the need to introduce a vector potential: $\mathbf{J}(\vec{r},t) = ev_F\psi^\dagger(\vec{r})\vec{\sigma}\psi(\vec{r})$. Solving Eq.(2.13) and Eq.(2.14) in real space directly using the analytical methods of previous section seems not feasible.

To see this let us rewrite these equations in a form reminiscent of the time-dependent Schrodinger equation (in the present context, 'Dirac equation' would be a better term).

$$X(\vec{r},t) = \begin{pmatrix} \tilde{P}^*(-\vec{r},t) \\ \tilde{N}_{diff}(\vec{r},t) \\ \tilde{P}(\vec{r},t) \end{pmatrix} \tag{2.17}$$

$$H_0(-i\nabla) \equiv \begin{pmatrix} 0 & -v_F\vec{\sigma}_{AB}\cdot i\nabla & 0 \\ -2v_F\vec{\sigma}_{BA}\cdot i\nabla & 0 & 2v_F\vec{\sigma}_{AB}\cdot i\nabla \\ 0 & v_F\ \vec{\sigma}_{BA}\cdot i\nabla & 0 \end{pmatrix} \tag{2.18}$$

$$i\partial_t X(\vec{r},t) = (H_0(-i\nabla) + \vec{r}\cdot e\vec{E}(t))X(\vec{r},t) \tag{2.19}$$

We now wish to diagonalize the full Hamiltonian to find a set of basis functions.

$$(H_0(-i\nabla) + \vec{r}\cdot e\vec{E}(t))\varphi(\vec{r},t) = \lambda(t)\varphi(\vec{r},t)$$

Thus we are compelled to find solutions to the following eigenvalue problem $\varphi \equiv (\varphi_{-1},\varphi_0,\varphi_1)^T$.

$$-v_F\vec{\sigma}_{AB}\cdot i\nabla\varphi_0(\vec{r},t) = (\lambda(t) - \vec{r}\cdot e\vec{E}(t))\varphi_{-1}(\vec{r},t)$$

$$-2v_F\vec{\sigma}_{BA}\cdot i\nabla\varphi_{-1}(\vec{r},t) + 2v_F\vec{\sigma}_{AB}\cdot i\nabla\varphi_1(\vec{r},t) = (\lambda(t) - \vec{r}\cdot e\vec{E}(t))\varphi_0(\vec{r},t)$$

$$v_F\ \vec{\sigma}_{BA}\cdot i\nabla\varphi_0(\vec{r},t)=(\lambda(t)-\vec{r}\cdot e\vec{E}(t))\varphi_1(\vec{r},t).$$

This is difficult to do. The simpler route is to transform away the potential part via a unitary transformation which will lead us back to the velocity gauge where a simple solution is possible as we have already shown in earlier section.

Thus showing that our results are recovered also in the length gauge amounts to first transforming the equations to the length gauge, realizing that the two formalisms are equivalent, also realizing that explicit analytical results are hard to obtain systematically due to the combined presence of a position vector and gradient operator, transforming back to the velocity gauge and showing that the equations are solvable analytically due to the absence of gradients and position vectors and so on. The reason why Ishikawa, Avetissian et al. are able work with the length gauge is because they deal with wavefunctions and single out one special direction namely the direction of the electric field and when the external momentum is parallel to this field the equation for the wavefunctions (the Dirac equation) becomes analytically soluble. However we deal with equations for the bilinears that do not appear to have any such feature. We feel our approach is natural as it is similar to much of the discussion on optical properties of semiconductors as discussed in the book by Haug and Koch[46].

2.5.1 Computations of gauge invariant quantities

The preceding discussion makes it clear that in the present context, the notion of a Rabi frequency is not particularly meaningful as it is tied to a specific choice of gauge. Thus in order to give universal meaning to this notion we have to focus on gauge invariant quantities. From the earlier section it is clear that the quantities $P(\vec{r},t), N_{diff}(\vec{r},t)$ are in general not gauge invariant. However $P(\vec{0},t)=\langle\psi_A^\dagger(\vec{0},t)\psi_B(\vec{0},t)\rangle$ and $N_{diff}(\vec{0},t)=\langle\psi_A^\dagger(\vec{0},t)\psi_A(\vec{0},t)\rangle-\langle\psi_B^\dagger(\vec{0},t)\psi_B(\vec{0},t)\rangle$ are in fact gauge invariant. Thus we have to somehow solve for these quantities and then examine whether they exhibit oscillations that may be characterized as Rabi oscillations. To this end we rewrite Eq.(2.13) and Eq.(2.14) as a time dependent Schrodinger (Dirac) equation (we work in the velocity gauge $\phi\equiv 0$ as we have just argued that this is the ideal gauge when dealing with bilinears of the fields).

$$i\ \partial_t P^*(-\vec{r},t)=-v_F\vec{\sigma}_{AB}\cdot(i\nabla-\frac{e}{c}\vec{A}^*(t))N_{diff}(\vec{r},t) \tag{2.20}$$

$$i\,\partial_t N_{diff}(\vec{r},t) = 2v_F\left(\vec{\sigma}_{AB}\cdot(i\nabla-\frac{e}{c}\vec{A}^*(t))P(\vec{r},t) - \vec{\sigma}_{BA}\cdot(i\nabla-\frac{e}{c}\vec{A}(t))P^*(-\vec{r},t)\right) \tag{2.21}$$

$$i\,\partial_t P(\vec{r},t) = v_F\vec{\sigma}_{BA}\cdot(i\nabla-\frac{e}{c}\vec{A}(t))N_{diff}(\vec{r},t) \tag{2.22}$$

Define X as,

$$X(\vec{r},t) = \begin{pmatrix} \tilde{P}^*(-\vec{r},t) \\ \tilde{N}_{diff}(\vec{r},t) \\ \tilde{P}(\vec{r},t) \end{pmatrix} \tag{2.23}$$

also,

$$\hat{V}(t) \equiv \begin{pmatrix} 0 & v_F\vec{\sigma}_{AB}\cdot\frac{e}{c}\vec{A}^*(t) & 0 \\ 2v_F\vec{\sigma}_{BA}\cdot\frac{e}{c}\vec{A}(t) & 0 & -2v_F\vec{\sigma}_{AB}\cdot\frac{e}{c}\vec{A}^*(t) \\ 0 & -v_F\ \vec{\sigma}_{BA}\cdot\frac{e}{c}\vec{A}(t) & 0 \end{pmatrix} \tag{2.24}$$

In momentum space,

$$X(\vec{r},t) = \frac{1}{A}\sum_{\vec{k}} e^{-i\vec{k}\cdot\vec{r}}x(\vec{k},t)$$

If,

$$H_0 \equiv \begin{pmatrix} 0 & -v_F\vec{\sigma}_{AB}\cdot\vec{k} & 0 \\ -2v_F\vec{\sigma}_{BA}\cdot\vec{k} & 0 & 2v_F\vec{\sigma}_{AB}\cdot\vec{k} \\ 0 & v_F\ \vec{\sigma}_{BA}\cdot\vec{k} & 0 \end{pmatrix} \tag{2.25}$$

then,

$$i\partial_t x(\vec{k},t) = (H_0+\hat{V}(t))x(\vec{k},t)$$

Till now no approximations have been made. We now decompose these variables in terms of harmonics of ω, neglecting second and higher harmonics. We write

$$x(\vec{k},t) = x_s(\vec{k},t) + x_+(\vec{k},t)e^{i\omega t} + x_-(\vec{k},t)e^{-i\omega t},$$

$$\hat{V}(t) = e^{i\omega t}\ V_+ + e^{-i\omega t}\ V_-$$

where,

$$V_+ = \begin{pmatrix} 0 & v_F\vec{\sigma}_{AB}\cdot\frac{e}{c}\vec{A}^*(0) & 0 \\ 0 & 0 & -2v_F\vec{\sigma}_{AB}\cdot\frac{e}{c}\vec{A}^*(0) \\ 0 & 0 & 0 \end{pmatrix}$$

$$V_- = \begin{pmatrix} 0 & 0 & 0 \\ 2v_F\vec{\sigma}_{BA}\cdot\frac{e}{c}\vec{A}(0) & 0 & 0 \\ 0 & -v_F\ \vec{\sigma}_{BA}\cdot\frac{e}{c}\vec{A}(0) & 0 \end{pmatrix}$$

We have to stress at this stage that we are trying to determine $x(\vec{k},t)$ so that we may then compute $X(\vec{0},t) = \frac{1}{A}\sum_{\vec{k}} x(\vec{k},t)$ which is a gauge invariant rather that $x(\vec{k},t)$ itself. The very definition of a slowly varying function means that we are entitled to consider $|\dot{x}_\pm(\vec{k},t)| \ll |x_\pm(\vec{k},t)|\omega$.

$$i\partial_t x_s(\vec{k},t) = H_0 x_s(\vec{k},t) + \hat{V}_+ x_-(\vec{k},t) + \hat{V}_- x_+(\vec{k},t), \tag{2.26}$$

$$(-\omega - H_0)\ x_+(\vec{k},t) = \hat{V}_+ x_s(\vec{k},t)\ ;\ (\omega - H_0)\ x_-(\vec{k},t) = \hat{V}_-\ x_s(\vec{k},t). \tag{2.27}$$

From this we may derive an equation for the slowly varying part of the fundamental quantities of this work,

$$i\partial_t x_s(\vec{k},t) = H_{full}\ x_s(\vec{k},t) \tag{2.28}$$

where,

$$H_{full} = \begin{pmatrix} -\frac{2\omega_R^2\omega}{((2v_Fk)^2-\omega^2)} & -(k_x-ik_y)v_F\left(1-\frac{2\omega_R^2}{((2v_Fk)^2-\omega^2)}\right) & 0 \\ 2(k_x+ik_y)v_F\left(-1+\frac{2\omega_R^2}{((2v_Fk)^2-\omega^2)}\right) & 0 & 2(k_x-ik_y)v_F\left(1-\frac{2\omega_R^2}{((2v_Fk)^2-\omega^2)}\right) \\ 0 & (k_x+ik_y)v_F\left(1-\frac{2\omega_R^2}{((2v_Fk)^2-\omega^2)}\right) & \frac{2\omega_R^2\omega}{((2v_Fk)^2-\omega^2)} \end{pmatrix} \tag{2.29}$$

In this case three regimes occur naturally :

$$(i)\ \ \omega \gg 2v_Fk \quad (ii)\ \ \omega \approx 2v_Fk \quad (iii)\ \ \omega \ll 2v_Fk.$$

The first case is what we have been calling ARWA. The second case is the conventional RWA. The third case is equivalent to the free particle situation. We will always assume $\omega \gg \omega_R$.

(i)

$$H_{full} \approx \begin{pmatrix} \frac{2\omega_R^2}{\omega} & -(k_x - ik_y)v_F & 0 \\ -2(k_x + ik_y)v_F & 0 & 2(k_x - ik_y)v_F \\ 0 & (k_x + ik_y)v_F & -\frac{2\omega_R^2}{\omega} \end{pmatrix}$$

(ii)

$$H_{full} \approx \begin{pmatrix} -\frac{2\omega_R^2\omega}{((2v_Fk)^2-\omega^2)} & (k_x - ik_y)v_F\frac{2\omega_R^2}{((2v_Fk)^2-\omega^2)} & 0 \\ 2(k_x + ik_y)v_F\frac{2\omega_R^2}{((2v_Fk)^2-\omega^2)} & 0 & -2(k_x - ik_y)v_F\frac{2\omega_R^2}{((2v_Fk)^2-\omega^2)} \\ 0 & -(k_x + ik_y)v_F\frac{2\omega_R^2}{((2v_Fk)^2-\omega^2)} & \frac{2\omega_R^2\omega}{((2v_Fk)^2-\omega^2)} \end{pmatrix}$$

(iii)

$$H_{full} \approx \begin{pmatrix} 0 & -(k_x - ik_y)v_F & 0 \\ -2(k_x + ik_y)v_F & 0 & 2(k_x - ik_y)v_F \\ 0 & (k_x + ik_y)v_F & 0 \end{pmatrix}$$

We may formally write the solution as $U(t) = e^{-itH_{full}}$,

$$x_s(\vec{k}, t) = U(t)\ x_s(\vec{k}, 0)$$

$$x_s(\vec{k}, t \to -\infty) = U(-\infty)\ x_s(\vec{k}, 0).$$

In case of ARWA (i) using Mathematica we may show that,

$$U_{(i)}(-\infty) = \begin{pmatrix} \frac{(kv_F\omega)^2}{2((kv_F\omega)^2+\omega_R^4)} & \frac{(k_x-ik_y)v_F\omega\omega_R^2}{2((kv_F\omega)^2+\omega_R^4)} & \frac{(k_x-ik_y)^2v_F^2\omega^2}{2((kv_F\omega)^2+\omega_R^4)} \\ \frac{(k_x+ik_y)v_F\omega\omega_R^2}{((kv_F\omega)^2+\omega_R^4)} & \frac{\omega_R^4}{((kv_F\omega)^2+\omega_R^4)} & \frac{(k_x-ik_y)v_F\omega\omega_R^2}{((kv_F\omega)^2+\omega_R^4)} \\ \frac{(k_x+ik_y)^2v_F^2\omega^2}{2((kv_F\omega)^2+\omega_R^4)} & \frac{(k_x+ik_y)v_F\omega\omega_R^2}{2((kv_F\omega)^2+\omega_R^4)} & \frac{(kv_F\omega)^2}{2((kv_F\omega)^2+\omega_R^4)} \end{pmatrix}$$

In general we may write,

$$U_{(i)}(t) = U_{(i)}(-\infty) + e^{2it\frac{\sqrt{\omega_R^4+(kv_F\omega)^2}}{\omega}}\ U_{(i)+} + e^{-2it\frac{\sqrt{\omega_R^4+(kv_F\omega)^2}}{\omega}}\ U_{(i)-}$$

where

$$U_{(i)+} = \begin{pmatrix} \frac{(k_F v_F\omega)^2+2\omega_R^4-2\omega_R^2\sqrt{(kv_F\omega)^2+\omega_R^4}}{4(\omega_R^4+(kv_F\omega)^2)} & -\frac{(k_x-ik_y)v_F\omega(\omega_R^2-\sqrt{(kv_F\omega)^2+\omega_R^4})}{4(\omega_R^4+(kv_F\omega)^2)} & -\frac{(k_x-ik_y)^2v_F^2\omega^2}{4(\omega_R^4+(kv_F\omega)^2)} \\ -\frac{(k_x+ik_y)v_F\omega(\omega_R^2-\sqrt{(kv_F\omega)^2+\omega_R^4})}{2(\omega_R^4+(kv_F\omega)^2)} & \frac{(kv_F\omega)^2}{2(\omega_R^4+(kv_F\omega)^2)} & -\frac{(k_x-ik_y)v_F\omega(\omega_R^2+\sqrt{\omega_R^4+(kv_F\omega)^2}}{2(\omega_R^4+(kv_F\omega)^2)} \\ -\frac{(k_x+ik_y)^2v_F^2\omega^2}{4(\omega_R^4+(kv_F\omega)^2)} & -\frac{(k_x+ik_y)v_F\omega(\omega_R^2+\sqrt{(kv_F\omega)^2+\omega_R^4})}{4(\omega_R^4+(kv_F\omega)^2)} & \frac{(kv_F\omega)^2+2\omega_R^4+2\omega_R^2\sqrt{(kv_F\omega)^2+\omega_R^4}}{4(\omega_R^4+(kv_F\omega)^2)} \end{pmatrix}$$

$$U_{(i)-} = \begin{pmatrix} \frac{(k_F v_F\omega)^2+2\omega_R^4+2\omega_R^2\sqrt{(kv_F\omega)^2+\omega_R^4}}{4(\omega_R^4+(kv_F\omega)^2)} & -\frac{(k_x-ik_y)v_F\omega(\omega_R^2+\sqrt{(kv_F\omega)^2+\omega_R^4})}{4(\omega_R^4+(kv_F\omega)^2)} & -\frac{(k_x-ik_y)^2v_F^2\omega^2}{4(\omega_R^4+(kv_F\omega)^2)} \\ -\frac{(k_x+ik_y)v_F\omega(\omega_R^2+\sqrt{(kv_F\omega)^2+\omega_R^4})}{2(\omega_R^4+(kv_F\omega)^2)} & \frac{(kv_F\omega)^2}{2(\omega_R^4+(kv_F\omega)^2)} & -\frac{(k_x-ik_y)v_F\omega(\omega_R^2-\sqrt{\omega_R^4+(kv_F\omega)^2}}{2(\omega_R^4+(kv_F\omega)^2)} \\ -\frac{(k_x+ik_y)^2v_F^2\omega^2}{4(\omega_R^4+(kv_F\omega)^2)} & -\frac{(k_x+ik_y)v_F\omega(\omega_R^2-\sqrt{(kv_F\omega)^2+\omega_R^4})}{4(\omega_R^4+(kv_F\omega)^2)} & \frac{(kv_F\omega)^2+2\omega_R^4-2\omega_R^2\sqrt{(kv_F\omega)^2+\omega_R^4}}{4(\omega_R^4+(kv_F\omega)^2)} \end{pmatrix}$$

In case of RWA we may see that,

$$U_{(ii)}(-\infty) = \begin{pmatrix} \frac{2(v_Fk)^2}{((2v_Fk)^2+\omega^2)} & \frac{(k_x-ik_y)v_F\omega}{((2v_Fk)^2+\omega^2)} & \frac{2(k_x-ik_y)^2v_F^2}{((2v_Fk)^2+\omega^2)} \\ \frac{2(k_x+ik_y)v_F\omega}{((2v_Fk)^2+\omega^2)} & \frac{\omega^2}{((2v_Fk)^2+\omega^2)} & \frac{2(k_x-ik_y)v_F\omega}{((2v_Fk)^2+\omega^2)} \\ \frac{2v_F^2(k_x+ik_y)^2}{((2v_Fk)^2+\omega^2)} & \frac{(k_x+ik_y)v_F\omega}{((2v_Fk)^2+\omega^2)} & \frac{2(v_Fk)^2}{((2v_Fk)^2+\omega^2)} \end{pmatrix}$$

and similar matrices $U_{(ii)+}$ and $U_{(ii)-}$ so that,

$$U_{(ii)}(t) = U_{(ii)}(-\infty) + U_{(ii)+}e^{2it\frac{\sqrt{\omega^2+(2v_Fk)^2}\omega_R^2}{\omega^2-(2v_Fk)^2}} + U_{(ii)-}e^{-2it\frac{\sqrt{\omega^2+(2v_Fk)^2}\omega_R^2}{\omega^2-(2v_Fk)^2}}$$

Finally in the free case $2v_Fk \gg \omega \gg \omega_R$ ($\theta_k = Tan^{-1}(\frac{k_y}{k_x})$),

$$U_{(iii)}(t) = \begin{pmatrix} cos^2(v_Fkt) & \frac{i}{2}sin(2v_Fkt)e^{-i\theta_k} & sin^2(v_Fkt)e^{-2i\theta_k} \\ ie^{i\theta_k}sin(2v_Fkt) & cos(2v_Fkt) & -isin(2v_Fkt)e^{-i\theta_k} \\ sin^2(v_Fkt)e^{2i\theta_k} & -\frac{i}{2}sin(2v_Fkt)e^{i\theta_k} & cos^2(v_Fkt) \end{pmatrix}$$

We have to compute the gauge invariant quantity,

$$\sum_{\vec{k}} x_s(\vec{k},t) = \sum_{\vec{k}} U(t)U^{-1}(-\infty)x_{eq}(\vec{k})$$

where $x_{eq}(\vec{k})$ is the equilibrium value of the vector x. While doing so we note that the dominant contribution comes from the ARWA regime. The conventional RWA in fact

is quite singular since the frequency associated with it is $2\frac{\sqrt{\omega^2+(2v_Fk)^2}\omega_R^2}{\omega^2-(2v_Fk)^2}$. This diverges in the RWA regime when $\omega \sim 2v_Fk$. This means we may ignore this contribution while evaluating the slowly varying contributions since a divergent frequency means the dependent variables average out to zero due to rapid oscillations. Similarly the free case has frequency $2v_F|k| \gg \omega \gg \omega_R$ which may also be ignored while evaluating the slowest contributions. Thus the slowest contributions to the gauge invariant quantities comes from the ARWA regime and corresponds to the anomalous Rabi frequency $2\frac{\sqrt{\omega_R^4+(kv_F\omega)^2}}{\omega}$. The gauge invariant current density associated with ARWA has already been computed in an earlier section.

This discussion clearly shows that non-resonant excitations produce slow time varying currents in graphene. This feature is unique to graphene and is attributable to the pseudospin character of the graphene Hamiltonian as we have pointed out on several occasions. This feature is absent in the toy model which we shall discuss in the next section that shares all qualities of graphene except pseudospin. The discussion in this section also shows that the concept of anomalous Rabi frequency is a gauge invariant notion since the gauge invariant current has been shown oscillate with this frequency.

2.6 Toy model: Analogous to graphene except "pseudospin"

In conventional semiconductors, the dispersion of carriers is parabolic and three dimensional, and no pseudospin-like term is present unlike graphene, where the off-diagonal terms present in the Hamiltonian show pseudospin. The notion of pseudospin requires elaboration. Since a Hamiltonian of the form $H = v_F\vec{\sigma}\cdot\vec{p}$ is unitarily equivalent to $H = v_F|p|\sigma_z$ which is purely diagonal it is not proper to attribute pseudospin to the presence of off-diagonal terms alone. While these two forms are unitarily equivalent, cast in real space, one of them is local and the other is not. By this we mean in the former case an identification $p \to -i\frac{d}{dx}$ poses no difficulty in interpretation whereas in the second case it is problematic. The problem becomes even more severe with minimal coupling to a vector potential. Hence we may unambigiously claim that there is a qualitative difference between the local graphene Hamiltonian and its diagonalised non-local version. It is the original form of the Hamiltonian $H = v_F\vec{\sigma}\cdot\vec{p}$ that becomes $H = v_F\vec{\sigma}\cdot(\vec{p}-\frac{e}{c}\vec{A}(t))$ upon minimal coupling to a vector potential. It is the

non-diagonal but local nature of this Hamiltonian that leads to anomalous Rabi oscillations. A nondiagonal local Hamiltonian is said to possess pseudospin whereas a local diagonal Hamiltonian such as $H = \frac{p^2}{2m_e}\sigma_z$ does not posesses pseudospin and shows no anomalous Rabi oscillation. Nonlinear optical processes have been extensively studied in semiconductors[46]. We now wish to present an exactly solvable analog of the graphene Hamiltonian identical to the latter in all respects except one - namely that no pseudospin character is present. We then go on to show that the cross-over phenomenon we saw earlier for graphene is absent in the exactly solvable model. Thus the crossover to a new smaller 'anamolous' Rabi frequency may be directly attributed to the pseudo-spin character of the Hamiltonian of graphene. Consider the following Hamiltonian,

$$H = H_0 + H_I$$

where,

$$H_0 = \sum_{\vec{p}} v_F|p|(c^\dagger_{\vec{p}}\, c_{\vec{p}} + d^\dagger_{\vec{p}}\, d_{\vec{p}}),\ H_I = \sum_{\vec{p}} \left(-\frac{e}{mc}\vec{A}(t)\cdot\vec{p}_{vc}\ c^\dagger_{\vec{p}}\, d^\dagger_{-\vec{p}} + c.c.\right),$$

where, $c^\dagger$, (c) is the creation (annihilation) operator corresponding to electron associated with conduction band whereas $d^\dagger$, (d) is for holes associated with valence band. This model is identical to graphene in all respects - the (kinetic energy) dispersion is linear, the system is two dimensional, the band gap is zero and there is particle hole symmetry. The only thing absent is pseudospin. The quantities of interest are $p(\vec{k},t) = \langle d_{-\vec{k}}\, c_{\vec{k}}\rangle$, $n_e(\vec{k},t) = \langle c^\dagger_{\vec{k}} c_{\vec{k}}\rangle$, $n_h(\vec{k},t) = \langle d^\dagger_{-\vec{k}} d_{-\vec{k}}\rangle$, $n(\vec{k},t) = n_e(\vec{k},t) + n_h(\vec{k},t)$. Using same procedure as in earlier section, the equation of motion is given as,

$$i\partial_t n(\vec{k},t) = \frac{2e}{mc}\left(-\vec{A}(t)\cdot\vec{p}_{vc}\ p^*(\vec{k},t) + \vec{A}^*(t)\cdot\vec{p}^*_{vc}\ p(\vec{k},t)\right), \tag{2.30}$$

$$i\partial_t p(\vec{k},t) = 2v_F|k|\ p(\vec{k},t) - \frac{e}{mc}\vec{A}(t)\cdot\vec{p}_{vc}\ (1 - n(\vec{k},t)). \tag{2.31}$$

One could apply the same two ideas on these equations to see what differences emerge from the graphene case. As it happens, due to a high degree of symmetry these equations may be solved exactly unlike the graphene case which is quite messy. The final results

may be easily verified by simple substitution (here $\Delta = \omega - 2v_F|k|$ is the detuning),

$$n(\vec{k},t) = \frac{4Z^*Z(1-\cos(\Omega_R t))}{\Omega_R^2}, \tag{2.32}$$

$$p(\vec{k},t) = e^{-i\omega t}\ \ \frac{Z(-\Delta + \Delta\cos(\Omega_R t) + i\Omega_R \sin(\Omega_R t))}{\Omega_R^2} \tag{2.33}$$

where $\Omega_R = (\Delta^2 + 4Z^*Z)^{\frac{1}{2}}$ is the effective Rabi frequency and $Z = \frac{e}{mc}\vec{A}(0)\cdot\vec{p}_{vc}$ (we have chosen $n(\vec{k},0) = p(\vec{k},0) = 0$). For zero detuning the Rabi frequency is $2|Z|$. In the other extreme, we obtain a result similar to the graphene case but with some differences. In the large frequency limit, we may expand the effective Rabi frequency in powers of ω^{-1} as,

$$\Omega_R = (\Delta^2 + 4Z^*Z)^{\frac{1}{2}} \approx (\omega - 2v_F|k| + \frac{2Z^*Z}{\omega})$$

then Eq.(2.33) becomes,

$$p(\vec{k},t) = \frac{Z}{\omega}(-e^{-i\omega t} + e^{it(-2v_F|k| + \frac{2Z^*Z}{\omega})}) \tag{2.34}$$

Thus the part that oscillates with the external frequency (ω) has a constant amplitude making the current in frequency domain a delta function - a very different result from what we saw in the graphene case. Alternatively, one may obtain the same result using the ARWA procedure we employed for graphene Bloch equations (2.2) and (2.3),

$$p_+(\vec{k},t) \approx -\frac{Z}{\omega}\ ;\ n_f(\vec{k},t) = -\frac{2Z}{\omega}\ p_s^*(\vec{k},t)\ ;\ n_s(\vec{k},t) = O(\frac{1}{\omega^2})$$

and

$$(i\partial_t - 2v_F|k|)p_s(\vec{k},t) \approx -\ \frac{2Z^*Z}{\omega}\ p_s(\vec{k},t).$$

Thus the solution given earlier, Eq.(2.34), is consistent with these equations. Hence we may expect our predictions in the case of graphene to be valid since the methods have been validated by testing against an exact solution. Analogous to the graphene case we may use the exact solution to extract the a.c. current in the frequency and time

domains. For $\omega^{'} > 0$ (define $\Delta^{'} = \sqrt{\omega^{'2} - 4Z^{*}Z}$),

$$\begin{aligned} \vec{j}_{slow,EXACT}(\omega^{'}) &= \vec{K}\ \delta(\omega^{'}) + \sum_{s=\pm 1} s\vec{p}_{vc}\frac{A}{4v_F^2}\theta(\omega - s\Delta^{'})(\omega - s\Delta^{'}) \\ & \frac{Z(s\frac{\Delta^{'}}{2} + \frac{1}{2}\omega^{'})}{\omega^{'2}}\frac{\theta(\omega^{'} - \sqrt{4Z^{*}Z})}{\Delta^{'}}\omega^{'}, \end{aligned} \tag{2.35}$$

where $\vec{K}$ is some constant that depends also on the lattice spacing, $\Omega_R = (\Delta^2 + 4Z^{*}Z)^{\frac{1}{2}}$, $\Delta = \omega - 2v_F|k|$.

The current density in time domain is given by,

$$\vec{J}_{slow}(t) = \vec{p}_{vc}\frac{A}{(2\pi)}\frac{\omega}{2v_F}\ \frac{iZ}{v_F}\frac{\pi}{2}\quad {}_0F^1[1, -t^2Z^{*}Z]Sign[t], \tag{2.36}$$

where ${}_0F^1$ is the regularized Hypergeometric function.

One can see from this exact result (Eq.(2.35)) that there is a spike at zero frequency followed by a gap and then power-law behavior near a threshold at the canonical Rabi frequency $\omega_R = \sqrt{4Z^{*}Z}$. This may be contrasted with the approximate result described in Eq.(2.34) from where we may derive,

$$\vec{j}_{slow,ARWA}(\omega^{'}) = \vec{K}\ \delta(\omega^{'}). \tag{2.37}$$

Thus the behavior at very low frequencies is well described by ARWA but not at higher frequencies. As a final comparison we study the exact result in the resonant limit (conventional RWA) when detuning is small. In this case Eq.(2.33) reduces to,

$$p(\vec{k}, t) \approx e^{-i\omega t}\ (Zi)\ \frac{\sin(\Omega_R t)}{\Omega_R}$$

using this result, the current density in frequency domain can be written as,

$$\vec{j}_{slow,RWA}(\omega^{'}) = \sum_{s=\pm 1}\frac{sAe\vec{\sigma}_{AB}\ Z}{4\pi}\theta(\omega - s\Delta^{'})\pi(\omega - s\Delta^{'})\ \frac{\theta(\omega^{'} - \sqrt{4Z^{*}Z})}{\Delta^{'}} \tag{2.38}$$

The equations Eq.(2.35), Eq.(2.37) and Eq.(2.38) are particularly illuminating. We see that the exact current is nothing but the sum of the RWA and ARWA currents so long

as we focus only on the threshold or singular behavior. Thus we may write,

$$\vec{j}_{EXACT}(\omega^{'}) = \vec{j}_{RWA}(\omega^{'}) + \vec{j}_{ARWA}(\omega^{'}).$$

When $\omega^{'}$ is close to the conventional Rabi frequency, the exact current is well approximated by the simple RWA current. However when the frequency $\omega^{'}$ is close to the anomalous Rabi frequency (in this case it is zero) then the exact current is well approximated by the ARWA current. We expect a similar observation to hold in the case of graphene where the equations cannot be solved exactly due to pseudospin.

Having an exact solution to test approximations against is always a boon and we have convincingly demonstrated that the scheme that we applied to graphene is valid. From this description, it is clear that conventional RWA shows threshold behavior near the canonical Rabi frequency, whereas ARWA shows possible threshold behavior or other type of singular behavior at a 'crossed over' Rabi frequency, typically much smaller than the conventional Rabi frequency. We can see that the phenomenon of crossover is quite generic, except that in the case of graphene it is more interesting since the singular behavior in the crossed over low frequency regime is also a power law threshold behavior. More importantly, in case of models with pseudospin the 'anomalous' Rabi frequency is non-zero. Before we move to a description of the plots, it is desirable to have a deeper understanding of why the graphene equations are not exactly soluble whereas the pseudospin-less model has an exact solution. A comparison of Eq.(2.2), Eq.(2.3) with Eq.(2.33), Eq.(2.33) shows why. The latter equations are invariant under a phase transformation $p(\vec{k},t) \rightarrow p(\vec{k},t)\ e^{i\theta}$, $\vec{A}(t) \rightarrow \vec{A}(t)\ e^{i\theta}$ and $n(\vec{k},t) \rightarrow n(\vec{k},t)$ whereas the Eq.(2.2) and Eq.(2.3) are not. This symmetry may be exploited to generate a solution. The Noether constant associated with this symmetry may be written down as,

$$Q = n(\vec{k},t)\Delta + 4Re\left(\frac{e}{mc}\vec{p}^{\,*}_{vc} \cdot \vec{A}^{*}(t)\ p(\vec{k},t)\right). \tag{2.39}$$

The absence of such a symmetry means that the polarization and occupation involve all higher harmonics in the external frequency whereas this is not the case in the exactly solvable model, the polarization is expressible in terms of a prefactor $e^{-i\omega t}$ times a slowly varying term. In other words, the presence of pseudospin means that the equations are not exactly solvable. This also seems to lead to two non-trivial Rabi frequencies rather than one for the integrable model. We do not have a deeper understanding of this phenomenon other than to attribute this to (or to the lack of) pseudospin.

Till now we have discussed the phenomenon of anomalous Rabi oscillations in graphene in presence of continuous intense optical field, in the next section we will show that pulses of a finite duration also produce anomalous Rabi oscillations.

2.7 Anomalous Rabi oscillations with pulsed non-resonant excitation

It is well known that finite duration pulses also produce Rabi oscillations. Here the new ingredient that enters into the formalism is known as the "area of the pulse" defined as the area under the pulse envelope well described in various textbooks[45]. We now wish to show that similar considerations apply when one studies graphene far from resonance. At this stage, a few words regarding the choice of gauge seems appropriate. Typically one starts with the density matrix $\rho_{i,j}(\mathbf{P},\mathbf{P}^{'})$ (a bilinear in the fields) where $\mathbf{P}$ is the canonical momentum. Here $\rho_{i,j}(\mathbf{P},\mathbf{P}^{'})$ describes the distribution and transitions in the canonical momentum space. For example, $\rho_{1,1}(\mathbf{P},\mathbf{P})$ is the probability to find the particle in the lower band with canonical momentum $\mathbf{P}$. In the case of length gauge, interaction is described by the potential energy $\hat{V} = e\mathbf{r}\cdot\mathbf{E}(t)$ and "p-space" corresponds to kinetic momentum. Thus, in this case $\rho_{i,j}(\mathbf{p},\mathbf{p}^{'})$ is the probability to find the particle in the upper band with kinetic momentum $\mathbf{p}$. The relation between kinetic and canonical momentum is $\mathbf{p} = \mathbf{P} - \frac{e}{c}\mathbf{A}(t)$. In the velocity gauge, only when $\mathbf{A}(t < t_i) = 0$ (before the pulse) and when $\mathbf{A}(t > t_f) = 0$ (after the pulse) one may regard $\mathbf{P}$ as the kinetic (physical) momentum.

We now present a physical explanation of slow oscillations similar to Rabi, far from resonance. The Rabi frequency describes the rate of the oscillations of the state's populations and it is meaningful for a resonant interaction. In case of graphene it should describe the rates of interband transitions and with an appropriate choice of the "interaction area" one should be able to obtain desired electron-hole superposition states. Hence we wish to show that due to the interaction with wave pulse ($\mathbf{A} = 0$ before and after the interaction) one can obtain nonzero inter-band transitions due to slow oscillations far from resonance. The situation close to resonance in atomic (two-level) systems is well described in various text books[45]. The far from resonance condition is something we have been calling ARWA. Strictly speaking, the only criterion that applies in case of ARWA is that ω - the external driving frequency - is the largest.

For the case of pulsed excitation, the vector potential is $\vec{A}(t) = \vec{A}_s(t)e^{-i\omega t}$ where $\vec{A}_s(t)$ is the slowly varying part of the vector potential. In ARWA, no assumption is needed regarding the relative sizes of the quantity we call $z_R(t) = v_F(\vec{\sigma}_{BA} \cdot \frac{e}{c}\vec{A}_s(t))$ and $2v_F|k|$. For pulsed excitation $\vec{A}_s(t) = 0$ before and after the pulse has passed. Hence in these regimes $2v_F|k| \gg |z_R| = 0$, however at all times one has to ensure that $\omega \gg |z_R|, 2v_F|k|$. Notice that by definition, $z_R(t)$ is complex. Thus while, $z_R(t) = v_F(\vec{\sigma}_{BA} \cdot \frac{e}{c}\vec{A}_s(t))$ whereas $z_R^*(t) = v_F(\vec{\sigma}_{AB} \cdot \frac{e}{c}\vec{A}_s^*(t))$. For a pulse, $\vec{A}_s(t) \equiv 0$ when $t > t_f$ and $t < t_i$ where $T = t_f - t_i$ is the pulse duration. From an earlier section we may write down the ARWA equations for a pulse instead of a continuous wave train,

$$p_+(\vec{k}, t) \approx -\frac{z_R(t)}{\omega} n_s(\vec{k}, t) \; ; \quad n_f(\vec{k}, t) \approx \frac{2z_R(t)}{\omega} \; p_s^*(\vec{k}, t)$$

and,

$$p_-(\vec{k}, t) \approx -\frac{2z_R^*(t)z_k^*}{\omega^2} \; p_s(\vec{k}, t)$$

Therefore, the equation for slowly varying coefficients become

$$i\partial_t p_s(\vec{k}, t) = z_k^* \; n_s(\vec{k}, t) - \frac{2z_R^*(t)z_R(t)}{\omega} \; p_s(\vec{k}, t)$$

and

$$\partial_t n_s(\vec{k}, t) = 4 \; Im \left(z_k \; p_s(\vec{k}, t) \right)$$

where $z_k = v_F(k_x - ik_y)$. The only assumptions involved in deriving these have been that ω is the largest of the frequencies so that $|\dot{X}| \ll \omega|X|$. We now define $\omega_R^2(t) \equiv z_R^*(t)z_R(t)$, as the (square of the) effective Rabi frequency for the pulse. By substituting one equation into another we get,

$$\partial_t n_s(\vec{k}, t) = 4 \; Im \left(z_k \; p_s(\vec{k}, t) \right)$$

$$i\partial_t p_s(\vec{k}, t) = z_k^* \; n_s(\vec{k}, t) - \frac{2\omega_R^2(t)}{\omega} \; p_s(\vec{k}, t)$$

In case $\omega_R(t)$ varies slowly ($|\dot{\omega}_R(t)| \ll \omega_R^2$), we my write the approximate solution by replacing ω_R by $\omega_R(t)$ the earlier solution for a continuous wave train. The only difference now is that instead of $\Omega_R t$ we have to write $\Phi(t)$, defined by the following

expression,

$$\Phi(t) \equiv \int_{t_i}^{t} dt^{'} \Omega_R(t^{'}) dt^{'}$$

which is nothing but the area of the pulse. For example if $\Phi = \pi$ an atom in the grand state initially, ends up in the excited state at the end of the pulse. A pulse with this area is known as a π pulse. If the pulse area is 2π the atom ends up back in its initial state. Thus we can see that the cyclic nature is completely determined by the area of the pulse. Hence, in case of a pulse, the earlier solution in presence of a continuous wave train modified as follows,

$$n_s(\vec{k}, t) = n_s(\vec{k}, t_i) \ \cos\Phi(t)$$

$$p_s(\vec{k}, t) = \frac{\Omega_{R,*} z_k^* n_s(\vec{k}, t_i)}{4i(v_F k)^2} \left(\sin\Phi(t) - i \frac{2\omega_{R,*}^2}{\Omega_{R,*}\omega} \ \cos\Phi(t) \right) \tag{2.40}$$

$$\Omega_R(t) = 2\frac{\sqrt{\omega_R^4(t) + (v_F|k|)^2\omega^2}}{\omega} \tag{2.41}$$

and $n_s(\vec{k}, t_i) = \frac{\omega(v_F|k|)}{\omega_{R,*}^2}$, $p_0(\vec{k}) = -\frac{k_x + ik_y}{2|k|}$ is the value of polarization at $t = t_i$ (we only discuss undoped graphene). Where we have defined $\omega_R(t) = v_F|\vec{\sigma}_{BA} \cdot \frac{e}{c}\vec{A}_s(t)|$ as Rabi frequency. (we may use the average value of this namely $\omega_{R,*}$ outside the argument of trignometric functions). Since $n_s(t) = n_A(t) - n_B(t)$ measures the population excess of the A sublattice relative to the B sublattice, we see a quasi-sinusoidal oscillation where one sublattice is filled initially and the other is empty and over time the situation is reversed and so on until the pulse lasts. Once the pulse is switched off, close to the bottom of the bands $v_F|k| \approx 0$ we see that the population excess freezes to a value determined entirely by the total area of the pulse $\Phi_{max} = \int_{t_i}^{t_f} dt^{'} \Omega_R(t^{'}) dt^{'}$. Thus,

$$n_s(\vec{k}, t_f) = n_s(\vec{k}, t_i) \ \cos\Phi_{max}$$

for a pulse such that $\Phi_{max} = \pi$ we see a complete inversion of population. Thus the situation is entirely analogous to the resonant two-level case except that the conventional Rabi frequency is replaced by the anomalous Rabi frequency. This is only true on time scales small compared to $(2v_F|k|)^{-1}$. For longer time scales, the inversion is not

permanent and it also oscillates with the frequency $2v_F|k|$. As pointed out earlier, the anomalous Rabi frequency far from resonance arises due to pseudospin and is peculiar to graphene.

The next section is devoted to addressing what superficially appears to be a non-issue, viz. why we chose a complex vector potential instead of a real one. In linear response theory, the choice is a matter of convenience. An exponential time dependence is far more convenient to deal with than a trignometric one, since upon differentiation an exponential remains the same apart from multiplicative constants. Hence choosing a complex exponential time dependence has become customary. But when we go beyond linear response, higher powers of the fields mean that these two choices are no longer equivalent.

2.8 Issue of the vector potential: Real vs complex

Here we show that treating the vector potential as a real quantity leads to a formula for the Rabi frequency found by Mishchenko[54] whereas treating it as complex with one branch only viz. $e^{-i\omega t}$ leads to our formula[53]. We favor treating the vector potential complex since it simplifies the introduction of higher harmonics while paying the small price of getting a trigonometric factor wrong in the final formula for the Rabi frequency. This is a small price to pay since the discrepancy between the two results is significant only when the electric field and the momentum are in the same direction. While summing over momenta to find the current density, all directions are included and thus the discrepancy is mitigated. To see this more clearly we proceed as follows. The graphene Hamiltonian is,

$$H = \psi_A^\dagger v_F \vec{\sigma}_{AB} \cdot (\vec{p} - \frac{e}{c}\vec{A}(t))\psi_B + \psi_B^\dagger v_F \vec{\sigma}_{BA} \cdot (\vec{p} - \frac{e}{c}\vec{A}^*(t))\psi_A$$

The polarization and populations are defined as,

$$p(t) = \psi_A^\dagger(t)\psi_B(t);\ p^*(t) = \psi_B^\dagger(t)\psi_A(t);$$
$$n(t) = \psi_A^\dagger(t)\psi_A(t) - \psi_B^\dagger(t)\psi_B(t)$$

Thus equation of motion,

$$i\,\partial_t\, n(t) = 2v_F\,\vec{\sigma}_{AB}\cdot(\vec{p}-\frac{e}{c}\vec{A}(t))\,p(t) - c.c.$$
$$i\,\partial_t\, p(t) = v_F\,\vec{\sigma}_{BA}\cdot(\vec{p}-\frac{e}{c}\vec{A}^*(t))\,n(t)$$
$$i\,\partial_t\, p^*(t) = -v_F\,\vec{\sigma}_{AB}\cdot(\vec{p}-\frac{e}{c}\vec{A}(t))\,n(t)$$

Choices:

(i) Mishchenko : $\vec{A}(t) = \vec{A}^*(t) = -\hat{x}\frac{cE}{\omega}sin(\omega t)$.

(ii) Enamullah et.al.[53] : $\vec{A}(t) = (A_x(0)\hat{x} + A_y(0)\hat{y})e^{-i\omega t}$, $\vec{A}^*(t) = (A_x^*(0)\hat{x} + A_y^*(0)\hat{y})e^{i\omega t}$

First Mishchenko's theorem: If $\vec{A}(t)$ is real and linearly polarized along $\vec{p}$, there are no Rabi oscillations.

Proof: In this case we may write $\frac{e}{c}\vec{A}(t) = \vec{p}a(t)$ so that $\vec{\sigma}_{AB}\cdot\vec{p} = p_x - ip_y = p_-$. This means,

$$i\partial_t n(t) = 2v_F p_-(1-a(t))p(t) - 2v_F p_+(1-a(t))p^*(t),$$
$$i\partial_t p(t) = v_F p_+(1-a(t))n(t), i\partial_t p^*(t) = -v_F p_-(1-a(t))n(t).$$

Set $p_-p(t) - p_+p^*(t) \equiv z(t)$. This gives the following simplified coupled equations:

$$i\partial_t z(t) = 2v_F|p|^2(1-a(t))n(t),$$
$$i\partial_t n(t) = 2v_F(1-a(t))z(t).$$

There is a bilinear conserved quantity associated with these equations that may be exploited to generate a solution. $z^2(t) - |p|^2\, n^2(t) = -C^2$ where C is a constant. This means we may write,

$$z(t) = i\,C\,\cos\theta(t);\ |p|\,n(t) = C\,\sin\theta(t).$$

Therefore,

$$\theta(t) = \theta(0) + 2v_F|p|(t - \int_0^t dt^{'}a(t^{'})).$$

Setting $a(t) = \frac{a^{'}(0)}{\omega}\ \sin(\omega t)$ we conclude that at resonance, $\omega = 2v_F|p|$, the quantities $z(t)$ and $n(t)$ have no terms that have a frequency other than the harmonics of ω, i.e. no Rabi frequency.

Corollary: If $\frac{e}{c}\vec{A}(t) = \vec{p}a(0)e^{-i\omega t}$ is complex but linearly polarized along $\vec{p}$, there are Rabi oscillations with the frequency the same as what is found in text books on two-level systems.

Here we have three coupled equations:

$$i\partial_t n(t) = 2v_F\ p_-(1 - a(0)e^{-i\omega t})p(t) - 2v_F\ p_+(1 - a^*(0)e^{i\omega t})p^*(t),$$
$$i\partial_t p(t) = v_F\ p_+\ (1 - a^*(0)e^{i\omega t})\ n(t), i\partial_t p^*(t) = -v_F\ p_-\ (1 - a(0)e^{-i\omega t})\ n(t).$$

In this situation the three coupled equations do not reduce to two.

To solve the above equations we employ the conventional RWA where we set $\omega = 2\epsilon + \Delta$ and ignore terms that are varying with frequency $2\omega, 4\omega$ e.t.c. This yields the following conventional Rabi frequency, $\Omega^2 = (\Delta^2 + |a(0)|^2(pv_F)^2)$. Since $\frac{e}{c}\vec{A}(t) = \vec{p}a(0)e^{-i\omega t}$, it follows that, $\frac{v_F e}{c}(\vec{\sigma}_{BA} \cdot \vec{A}(0)) = v_F p_+ a(0)$ i.e. the Rabi frequency become,

$$\omega_R = |\frac{v_F e}{c}\vec{\sigma}_{BA} \cdot \vec{A}(0)| = v_F|p||a(0)|.$$

This means the Rabi frequency is what is found in the context of two-level atoms, i.e. $\Omega = \sqrt{\Delta^2 + \omega_R^2}$. Thus we see there are qualitative differences in treating the field as having a real sinusoidal time dependence versus a complex exponential time dependence. We prefer the complex exponential since allows us to maintain contact with the two-level system and is also easier to handle than the trigonometric functions when higher harmonics are involved. We are more interested in establishing the general results that graphene exhibits peudospin-linked anomalous Rabi oscillations rather than obtaining an accurate and realistic formula for the Rabi frequency in terms of the components of the fields. With this limited goal in mind, a mathematically elegant method that can bring out these ideas is more desirable than one that is tedious but more realistic.

Second Mishchenko's theorem: If $\vec{A}(t)$ is real and linearly polarized making an angle χ_p with the vector $\vec{p}$, conventional Rabi oscillations exist with Rabi frequency $\omega_R = \frac{ev_F E}{\omega}\sin(\chi_p)$. Set $\frac{e}{c}\vec{A}(t) = -\frac{e\ E}{\omega}\ \hat{x}\ \sin(\omega t)$. Without loss of generality we have

chosen the x axis to coincide with the direction of the linearly polarized field.

Proof: This theorem has been proved in Mishchenko's paper[54]

Existence theorem of ARO : Even when the vector potential is chosen real and sinusoidal, anomalous Rabi oscillations are seen even though the dependence of the anomalous Rabi frequency on the components of the electric field depend on whether the fields are treated as (i) complex and exponential or (ii) real and sinusoidal.

In the work[53] we proved (i).

To prove (ii) we set,

$$\vec{A}(t) = Re(\vec{A}_0 e^{-i\omega t})$$

where $\vec{A}_0 = \vec{A}_0(\cos(\theta)\hat{x} + \sin(\theta)e^{i\delta}\hat{y})$ where θ, δ, ω and A_0 are real. The real vector potential is given by, $\vec{A}(t) = \vec{A}_0\ \cos(\theta)\ \hat{x}\ \cos(\omega t) + A_0\ \sin(\theta)\ \hat{y}\ \cos(\omega t - \delta)$ where θ is the angle made by the electric field and the x-axis and δ is the phase difference between the x and y components and A_0 is the amplitude, all real quantities. We follow the ARWA procedure,

$$\begin{aligned} n(t) &= n_s(t) + n_f(t)e^{-i\omega t} + n_f^*(t)e^{i\omega t} \\ p(t) &= p_s(t) + p_+(t)e^{-i\omega t} + p_-(t)e^{i\omega t} \end{aligned} \tag{2.42}$$

After comparing the coefficient we have,

$$\begin{aligned} \omega n_f(t) &= -2v_F\frac{e}{c}A_0\ \cos\theta\ \frac{1}{2}\left(p_s(t) - p_s^*(t)\right) + i2v_F\frac{e}{c}A_0\ \sin\theta\ \frac{1}{2}\left(p_s(t) + p_s^*(t)\right)e^{i\delta}, \\ \omega p_+(t) &= -v_F\frac{e}{c}A_0\ \cos\theta\ \frac{1}{2}n_s(t) - v_F\frac{e}{c}iA_0\ \sin\theta\ \frac{1}{2}e^{i\delta}n_s(t), \\ -\omega p_-(t) &= -v_F\frac{e}{c}A_0\ \cos\theta\ \frac{1}{2}n_s(t) - v_F\frac{e}{c}iA_0\ \sin\theta\ \frac{1}{2}e^{-i\delta}n_s(t), \end{aligned}$$

together with,

$$\begin{aligned} p_s(t) &= \frac{(v_F\frac{e}{c}A_0)^2}{\omega}\ \sin(2\theta)\sin\delta\frac{1}{4p_-v_F}n_s(t) + \frac{1}{4p_-v_F}i\partial_t n_s(t), \\ n_s(t) &= n_s(0)\ \cos(\omega_{ARWA}t). \end{aligned}$$

The anomalous Rabi frequency is given by,

$$\omega_{ARWA} = (4v_F^2 p^2 + \frac{(v_F \frac{e}{c} A_0)^4}{\omega^2} \sin^2(2\theta) \sin^2\delta)^{\frac{1}{2}} \tag{2.43}$$

We see that when the fields are real, the anomalous Rabi frequency is zero when the electric field is linearly polarized. We saw in the earlier work that the anomalous Rabi frequency is simply related to the conventional one through the relation $\omega_{ARWA}(p = 0) = \frac{2\omega_{RWA}^2(\Delta=0)}{\omega}$ when we treat the fields as complex exponential time varying fields. We now evaluate the conventional Rabi frequency and see if the same relationship between conventional and anomalous Rabi frequency holds when the fields are real and sinusoidal. One finds the result, $\Omega_{RWA} = \sqrt{\omega_{RWA}^2 + \Delta^2}$ where the zero detuning conventional Rabi frequency is,

$$\omega_{RWA} = \frac{A_0 e v_F}{c} \sqrt{(1 - \cos(2\theta)\cos(2\chi_p) - \cos(\delta)\sin(2\theta)\sin(2\chi_p))}$$

where $\chi_p = tan^{-1}(p_y/p_x)$. We see that this relationship is not strictly obeyed now. However magnitude wise, it is still true that $\omega_{ARWA} \sim \frac{\omega_{RWA}^2}{\omega}$. The main point we are making is that no matter what, there is such a thing as anomalous Rabi oscillations in graphene which is absent in conventional (pseudospinless) systems whose frequency is smaller compared to the zero detuned conventional Rabi frequency (ω_{RWA}) by a factor of $\frac{\omega_{RWA}}{\omega}$. These two approaches (real versus complex fields) are equivalent when considering linear equations but for nonlinear systems such as the one we consider here, they are different. Mathematically, this may understood as follows: while $Im(e^{i\omega t}) = \sin(\omega t)$ so that the two approaches are the same for linear fields, from the observation that $Im(e^{2i\omega t}) \neq (\sin(\omega t))^2$ we may conclude that it does not work in nonlinear (Rabi-like) situations. While Mishchenko's[54] approach has the appeal that it uses a physical real electric field, our approach has the appeal that the model with complex vector potentials (the Hamiltonians are real, of course) is able to map the graphene system at resonance to the two-level system with the Rabi frequency given by the textbook value which depends on the electric field alone (it does not vanish in some situations unlike Mishchenko's). Furthermore, our approach of using time varying complex exponentials renders calculations involving higher harmonics (which is the norm in few-layer graphene e.g. or while considering higher order effects such as Bloch Siegert shift) quite easy and elegant unlike what would be the case had we insisted on using real fields.

2.9 Interpolation between RWA and ARWA regimes

In this section, we present an analytical method for interpolating between the RWA and ARWA regimes and obtain a Rabi frequency that crosses over from the conventional Rabi frequency ω_R close to resonance to the anomalous Rabi frequency $\frac{2\omega_R^2}{\omega}$ far from resonance. This exercise enables us to uncover precisely how the crossover takes place and what new features if any may be expected in the intermediate region. Further, it is possible to write down an analytical expression for the nonlinear current in graphene in the coherent regime in the absence of excitonic effects - an important and new development in its own right. The interpolation scheme presented here is two-tiered. In the first instance, we ignore frequency doubling effects and demonstrate the nature of the crossover including in the intermediate region. In the second instance we generalize the approach to include frequency doubling effects and compare with the results obtained by ignoring these effects. It must be stressed that a novel combination of fully analytical and fully numerical approach (next section) presented in this chapter is designed to highlight coherent optical processes unique to graphene attributable to pseudospin.

The interpolation is effected by the use of Fourier transforms. The k-dependence may be suppressed in polarization and density so that the Bloch equations (2.2) and (2.3)may be written compactly as,

$$i\ \dot{n}(t) = 2(z_k^* - z_R^*\ e^{i\omega t})p(t) - 2(z_k - z_R\ e^{-i\omega t})p^*(t) \tag{2.44}$$

and,

$$i\ \dot{p}(t) = (z_k - z_R\ e^{-i\omega t})\ n(t). \tag{2.45}$$

Use the following definition of the Fourier transforms,

$$P(\omega) = \int_{-\infty}^{\infty} \frac{d\omega}{2\pi} e^{-i\omega t}\ p(t);\ \ N(\omega) = \int_{-\infty}^{\infty} \frac{d\omega}{2\pi} e^{-i\omega t}\ n(t),$$

after substituting, the Eq. (2.44) and Eq. (2.45) become,

$$-\omega^{'}\ N(\omega^{'}) = 2z_k^* P(\omega^{'}) - 2z_k P^*(-\omega^{'}) + 2z_R P^*(-\omega^{'} - \omega) - 2z_R^*\ P(\omega^{'} - \omega), \tag{2.46}$$

and,

$$-\omega^{'}\ P(\omega^{'}) = (z_k\ N(\omega^{'}) - z_R\ N(\omega + \omega^{'})). \tag{2.47}$$

With the help of equation (2.46) and (2.47) we obtain the following eigenvalue equation,

$$-\omega^{'}\ N(\omega^{'}) = -\frac{2z_k^*}{\omega^{'}}(z_k\ N(\omega^{'}) - z_R\ N(\omega+\omega^{'}))$$

$$-\frac{2z_k}{\omega^{'}}(z_k^*\ N(\omega^{'}) - z_R^*\ N(-\omega+\omega^{'})) + 2z_R\frac{1}{\omega^{'}+\omega}(z_k^*\ N(\omega^{'}+\omega) - z_R^*\ N(\omega^{'}))$$

$$-2z_R^*\ \frac{1}{(-\omega^{'}+\omega)}(z_k\ N(\omega^{'}-\omega) - z_R\ N(\omega^{'})). \tag{2.48}$$

To solve we make further assumptions about the importance of harmonics. In the first instance we make the assumption that frequency doubling effects are absent. This is the same as saying that we neglect a term such as $N(\omega^{'} \pm 2\omega)$. One is then led to the following formula for the eigenvalue $\omega^{'}$,

$$D_0(\omega^{'}) = (\omega+\omega^{'}) - \frac{4(v_F|k|)^2}{\omega+\omega^{'}} - \frac{2\omega_R^2}{\omega^{'}+2\omega} - \frac{2\omega_R^2}{\omega^{'}}$$

and,

$$0 = D_0(\omega^{'}-\omega) - 4(v_F|k|)^2\omega_R^2\ \frac{\left(\frac{1}{\omega+\omega^{'}}+\frac{1}{\omega^{'}}\right)^2}{D_0(\omega^{'})} + 4(v_F|k|)^2\omega_R^2\ \frac{\left(\frac{1}{\omega^{'}-\omega}+\frac{1}{\omega^{'}}\right)^2}{D_0(-\omega^{'})} \tag{2.49}$$

The above (Eq.(2.49)) has ten solutions apart from the trivial one $\omega^{'}=0$. Of these, only one of them is positive and a meromorphic function of the other variables such as $v_F|k|$ (according to Mathematica). This is the Rabi frequency. In the regime $\omega \gg \omega_R$ and $\omega \gg 2v_F|k|$ i.e. in ARWA regime we may write the solution of (Eq.(2.49)) as,

$$\omega^{'} = \frac{2\sqrt{(v_F|k|)^2\omega^2+\omega_R^4}}{\omega}\ (1 - \frac{\omega_R^2}{\omega^2} + ...)$$

This is the same result we derived earlier.

Conversely, in the resonant case i.e. in RWA regime ($\omega = 2v_F|k| + \Delta$ where $\Delta \ll 2v_F|k|$) we get,

$$\omega^{'} = \sqrt{\Delta^2+\omega_R^2} + \frac{(\omega_R^2\ \Delta)}{(4\sqrt{\Delta^2+\omega_R^2}\ v_F|k|)} + O\left(\frac{1}{(v_F|k|)^2}\right) \tag{2.50}$$

which is precisely the result obtained from RWA. Also of interest is the correction term that shows deviation from the prediction of RWA. This is needed since eventually RWA

gives way to ARWA. Now it is natural to become curious as to what happens in the region between RWA and ARWA. In other words, what additional features if any are seen on this crossover route. To answer this we have plotted in Fig.(2.1), the effective (or generalized) Rabi frequency $\Omega_{eff} = \omega^{'}$ versus $e_k = v_F|k|$ in units of $\omega_R = 1$ and by choosing $\omega = 100$ in the same units. Also shown is the answer to the same question when frequency doubling effects are included but triple frequencies are excluded. This involves solving a slightly more complicated set of equations shown below.

$$D_1(\omega^{'}) = D_0(\omega^{'}) - 4(v_F|k|)^2\omega_R^2 \frac{\left(\frac{1}{2\omega+\omega^{'}} + \frac{1}{(\omega^{'}+\omega)}\right)^2}{D_0(\omega^{'}+\omega)}$$

The equation to be solved is,

$$0 = D_0(\omega^{'}-\omega) - 4(v_F|k|)^2\omega_R^2 \frac{\left(\frac{1}{\omega+\omega^{'}} + \frac{1}{\omega^{'}}\right)^2}{D_1(\omega^{'})} + 4(v_F|k|)^2\omega_R^2 \frac{\left(\frac{1}{\omega^{'}-\omega} + \frac{1}{\omega^{'}}\right)^2}{D_1(-\omega^{'})} \quad (2.51)$$

From the way it is written it is easy to suspect that in general, including all harmonics amounts to solving the equations,

$$0 = D_0(\omega^{'}-\omega) - 4(v_F|k|)^2\omega_R^2 \frac{\left(\frac{1}{\omega+\omega^{'}} + \frac{1}{\omega^{'}}\right)^2}{D_{n+1}(\omega^{'})} + 4(v_F|k|)^2\omega_R^2 \frac{\left(\frac{1}{\omega^{'}-\omega} + \frac{1}{\omega^{'}}\right)^2}{D_{n+1}(-\omega^{'})} \quad (2.52)$$

where,

$$D_{n+1}(\omega^{'}) = D_n(\omega^{'}) - 4(v_F|k|)^2\omega_R^2 \frac{\left(\frac{1}{(n+2)\omega+\omega^{'}} + \frac{1}{(\omega^{'}+(n+1)\omega)}\right)^2}{D_n(\omega^{'}+\omega)}$$

An examination of the plots (Fig.(2.1)) show that the effective Rabi frequency upon inclusion of second harmonics may be well approximated by the following formula,

$$\Omega(v_F|k| < \frac{\omega}{4}) = \frac{2\sqrt{(v_F|k|)^2\omega^2 + \omega_R^4}}{\omega} \quad \rightarrow ARWA$$

$$\Omega(\frac{\omega}{4} < v_F|k| < \frac{3\omega}{4}) = \sqrt{\omega_R^2 + (\omega - 2v_F|k|)^2} \quad \rightarrow RWA$$

$$\Omega(\frac{3\omega}{4} < v_F|k| < \frac{3\omega}{2}) = \sqrt{\frac{\omega_R^4}{\omega^2} + 4(\omega - v_F|k|)^2} \rightarrow RWA \quad 2^{nd}\ Harmonic\ Generation$$

$$\Omega(v_F|k| > \frac{3\omega}{2}) = \omega$$

This function is continuous if we assert that $\omega \gg \omega_R$. We may see different regimes and the different kinds of Rabi frequency associated with those regimes. In addition to ARWA we also see that there is an anomalous RWA at frequency $\omega = v_F|k|$ *provided* we include the effect of second harmonics. This effect is absent if we ignore frequency doubling phenomena. Of these Rabi frequencies, the one that is associated with a region close to the tip of the Dirac cone corresponds to ARWA. Thus for obtaining low energy physics we expect ARWA to be more important than RWA. The earlier sections have thoroughly studied the effects of ARWA on the induced current in the system. Now we move on to a description of a purely numerical solution to the Bloch equations.

2.10 Numerical solution of the Bloch equation

So far the efforts have been purely analytical. It is worthwhile to attempt a numerical solution of Bloch equations which would once and for all validate the assertions made in the other sections. This is especially desirable since we are dealing with a simple system that neglects Coulomb terms and is easily solved with present day computing resources. This has already been done by Mischenko[54] and Mikhailov[106–108] among others. Thus the present section while not particularly novel is still important since it is needed to make contact with the analytical approaches of earlier sections. Besides, the focus of our efforts (highlighting the pseudo-spin origin of the cross-over phenomenon) is somewhat different from these authors. We also stress that numerical approaches though powerful, fail to provide explicit formulas (as distinct from numerical values) for quantities such as the anomalous Rabi frequency that is the central new concept.

We have used the NDSolve routine (non-stiff Adams method or a stiff Gear backward differentiation formula) of Mathematica to generate the plots shown here. They fully confirm the expectations of earlier sections and provide a solid foundation on which to base future analytical explorations involving excitons and so on.

2.11 Results and discussion

In this section, we plot the results obtained thus far in order to visualize the cross-over phenomenon. The Fig.(2.1) is the central result. It shows the dependence of

the effective Rabi frequency on the band energy $v_F|k|$ for a fixed value of external frequency ($\omega = 100$) and Rabi frequency for zero detuning ($\omega_R = 10$). The black solid line which includes only the slowly varying contribution captures only the ARWA regime correctly while completely missing the conventional RWA result. The blue dot-dashed line includes the first harmonic in the external frequency in addition to slowly varying terms, correctly captures both the ARWA and RWA regimes. Upon inclusion of second harmonic terms we see the emergence of a new regime which we may call higher rotating wave approximation regime (HRWA). This new regime is solely to due the frequency doubling phenomenon and the effective Rabi frequency goes through a minimum in this region. In Fig.(2.2), between the anomalous Rabi frequency and ω_R (usual Rabi frequency) the current is obtained using ARWA. The threshold behavior of the current at the anomalous Rabi frequency is seen where the current goes to zero as a power law. Above and close to the second threshold (namely, ω_R) there is a power law divergence. This region is well described by the conventional RWA. This situation for graphene is in contrast with the exactly solvable model that possess all the qualities of graphene except pseudospin. The blue dotted curve shows that there is only one non-zero threshold frequency namely ω_R where there is a power law behavior. The smaller frequency where something singular occurs is exactly at zero frequency. In Fig.(2.3) we see the slowly varying part of the current density with time. The red curve is ARWA and the blue curve is RWA. The frequency associated with the red curve is small compared to the frequency associated with the blue curve for reasons we have already alluded to.

Fig.(2.4) depicts the overall slow current (both thresholds included) in the time domain. We may see the beats are quite different in the two cases. In the exactly solvable case (blue dotted) there is only one non-zero characteristic frequency (ω_R) thus the beats are regular. In the graphene case (red solid) the beat train may be seen to undulate. This undulation occurs with a smaller frequency which is nothing but the anomalous Rabi frequency. This is made more explicit in the next plot Fig.(2.5) where we plot the function $f(t) = \sin(t) + \sin(10t)$ as a function of time and this also exhibits the undulation. Thus the undulation is due to a linear superposition of waves with the anomalous and usual Rabi frequencies.

One definitive indication for the presence of an anomalous Rabi frequency would be to test for the variation of the undulation frequency with the external driving frequency but keeping the conventional Rabi frequency ω_R fixed. If the undulation frequency

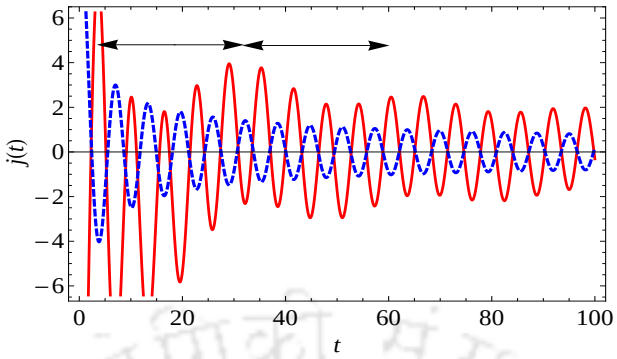

Figure 2.4: This figure depicts the overall slow current in the time domain. The beat frequency associated with the dotted blue plot (exactly solvable model) is the conventional Rabi frequency, whereas in the case of graphene (solid red plot) these beats are also undulating (arrows) with a smaller frequency.

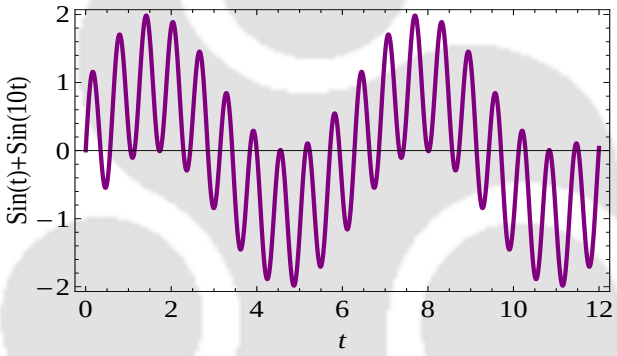

Figure 2.5: A plot of $f(t) = \sin(t) + \sin(10t)$ versus t shows that undulation of beat trains is a simple consequence of linear superposition of two frequencies.

appears to be inversely related to the external driving frequency then that would be a confirmation of the cross-over phenomenon. Fig.(2.6) shows a density plot of the effective Rabi frequency versus the band energy $v_F|k|$ and the Rabi frequency for zero detuning ω_R (related to the intensity of radiation). The most prominent feature of this plot is the alternating dark and light blue regions depicting minima and maxima of the Rabi frequency before they give way to a yellow region of constant Rabi frequency. One also sees a faint periodic dependence of the effective Rabi frequency on the conventional Rabi frequency for band energies corresponding to the light blue regions.

The Fig.(2.7), Fig.(2.8), Fig.(2.9) and Fig.(2.10) are the numerical solution (exact) of the Bloch equation in different regimes. We consider ARWA for Fig.(2.7) and

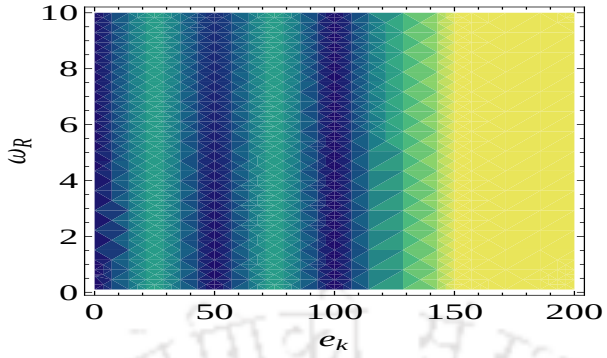

Figure 2.6: This density plot shows the effective Rabi frequency versus the band energy $e_k = v_F|k|$ and the Rabi frequency for zero detuning ω_R for a fixed external frequency $\omega = 100$ in generalized units.

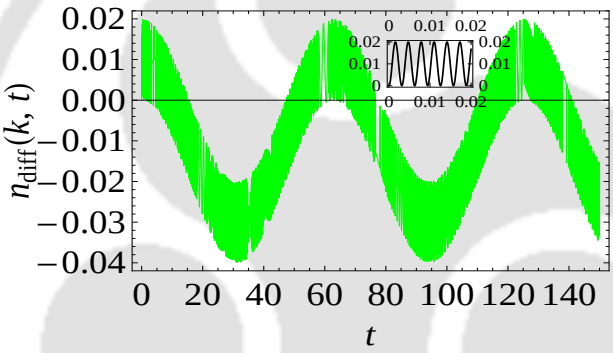

Figure 2.7: This figure depicts the variation of the slowly as well as rapidly varying part (inset) of $n_{diff}(\vec{k}, t)$ versus t. To plot, we have chosen these parameters : $z_k = 0.001, z_R = 10, \omega = 2000$. In the terminology, this corresponds to ARWA. The anomalous Rabi frequency obtained numerically (frequency of the slow part) matches with the analytical result quoted.

Fig.(2.8) and RWA for Fig.(2.9) and Fig.(2.10). The frequencies obtained analytically for $n_{diff}(\vec{k}, t)$ and $p(\vec{k}, t)$ within these approximations are verified by these numerical results. In Fig.10 the inset shows a feeble oscillatory behavior of an otherwise monotonic curve. The frequency we deduce by examining the inset is - twice the external frequency. Since we have chosen to ignore harmonic generation (in the first instance) in our approximations (including in RWA) we do not expect to reproduce this feature analytically. In figures (2.7), (2.8) and (2.9), the frequency of the slowly varying oscillations corresponds to either the standard or the anomalous Rabi frequency, the rapid oscillations are due to the frequency of the externally applied field. In Fig. (2.10)

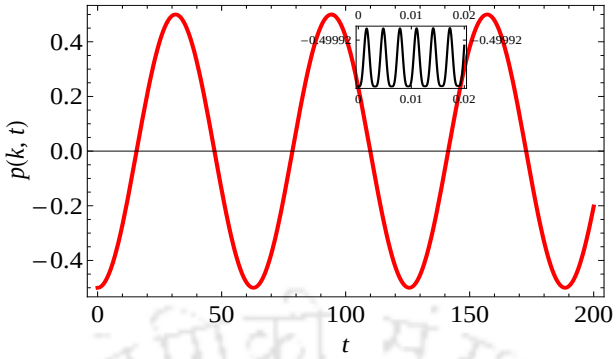

Figure 2.8: The above plot shows the variation of slowly as well as rapidly varying part (inset) of the polarization $Re[p(\vec{k},t)]$ versus time within ARWA limit and to plot we have taken the parameters as $z_k = 0.001, z_R = 10, \omega = 2000$. The frequencies obtained from this plot match with expectation both in the low and high frequency regions.

however, the frequency of the rapidly varying part is twice the external frequency (2ω).

Before we conclude it is worthwhile pointing out that ignoring relaxation terms misses some saturation phenomena discussed by Mischenko[54]. Our present focus is rather different and this omission is therefore justifiable. Next, even though we have ignored frequency doubling effects for the most part, we argue that for some purposes this is not an unreasonable approximation. Indeed graphene's optical response is highly nonlinear and one has to take into account higher harmonics[106–108]. However, we take the point of view that only the leading harmonics may be extracted from the series and studied independently.

If $\vec{J}(t)$ is the total current including all higher harmonics then we may extract the slowly varying part of the current by multiplying this by $e^{i\omega t}$ and averaging over one cycle of the external frequency. Thus, $\vec{J}_{slow}(t) = \frac{1}{\tau}\int_t^{t+\tau} dt'\ e^{i\omega t'}\ \vec{J}(t')$.

This is justified in the context of the results shown in Fig.(2.1) where higher harmonics are important only for band energies of the order of the external driving frequency - in other words where the Dirac cone approximation is likely to be questionable. Thus while there are certainly going to be modifications upon inclusion of higher harmonics (such as the emergence of additional minima in the plot of effective Rabi frequency versus the band energy), we expect the presence of two Rabi scales - ω_R and $\frac{2\omega_R^2}{\omega}$ to be robust as it is related to the Bloch equations of graphene lacking symmetry under phase transformations and the presence of pseudospin in graphene. Lastly, ignoring excitonic effects is justified if the excitonic binding energies are very different from the two Rabi

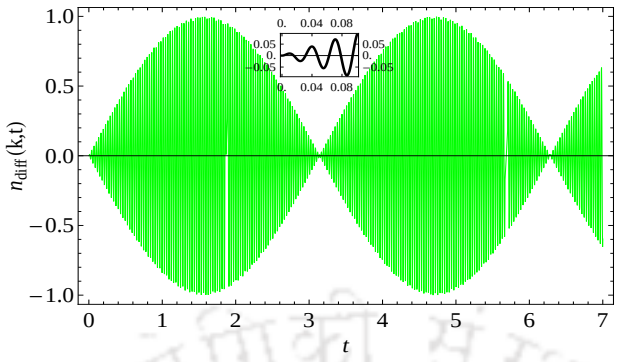

Figure 2.9: This figure depicts the slowly as well as rapidly varying part (inset) of $n_{diff}(\vec{k},t)$ versus t. To plot we have taken the parameters as $z_k = 100, z_R = 1, \omega = 200$. This corresponds to standard RWA. The frequencies obtained are consistent with expectations in both the high and low frequency regions.

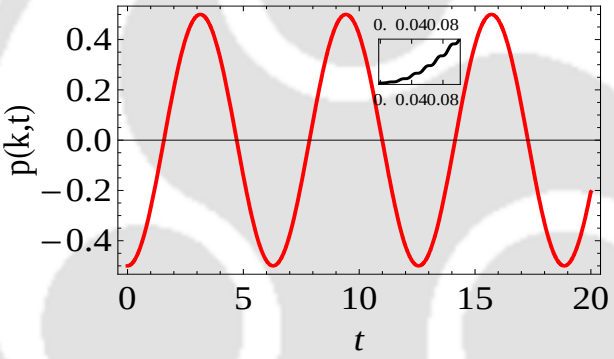

Figure 2.10: The above plot shows the slowly as well as rapidly varying part (inset) of $Re[p(\vec{k},t)]$ versus time. To plot we have taken the parameters as $z_k = 100, z_R = 1, \omega = 200$. This corresponds to RWA with zero detuning. The smaller Rabi frequency matches with expectations however the higher frequency (inset) is due to second harmonic generation which we have ignored in some of the analytical calculations.

frequencies so that they may be resolved. Besides, the anomalous Rabi frequency has a well defined dependence on the external frequency whereas the excitonic energies are independent of the external frequency. Incoherent effects (mainly due to phonon relaxation) have been evaluated in great detail by Romanets et.al.[110] who show that they operate on a time scale of $0.1 - 0.2ps$ and argue that Rabi oscillations may be easily observed at femtosecond time scales with pump intensities of $3 - 30GW/cm^2$.

In this chapter, we have derived the Bloch equations for carriers in graphene. We have employed successive approximations in order to solve these equations. First we

ignore the relaxation terms and focus on the coherent processes. Next we ignore the higher harmonics in the external driving frequency thereby ignoring frequency doubling effects. Lastly we derive expressions for the effective Rabi frequency when Coulomb interactions are absent, postponing the more interesting discussion of excitonic optical Stark effect and so on for later publications. The effective Rabi frequency in general is shown to obey a secular equation of a high degree. Further simplifications are made by examining limiting cases such as when detuning is small or when the wave number of the polarization/density is small compared to the external driving frequency (divided by Fermi velocity), an exercise that illustrates the phenomenon of crossover of Rabi frequency. We also compute the current density (nonlinear response) and demonstrate that the slowly varying part of the current density exhibits threshold behavior in frequency domain with threshold frequency $\frac{2\omega_R^2}{\omega}$ and with exponent equal to 1/2.

2.12 Conclusions

In conclusion, we have studied the nonlinear electromagnetic response of graphene theoretically. The main technical advancement reported here is the use of an alternative to the well-known rotating wave approximation (which we have called 'asymptotic rotating wave approximation'). This alternative approach applicable far from resonance is able to show that for systems with pseudospin such as graphene, a second anomalous Rabi frequency is present and the current density in the frequency domain exhibits a crossover from one type of singular behavior close to the normal Rabi frequency to another type of singular behavior close to the (typically smaller) anomalous Rabi frequency. A comparison with an exactly solvable model identical to graphene in all respects except lacking in pseudospin shows that the second anomalous Rabi frequency is peculiar to models with pseudospin. This exactly solvable model also validates the asymptotic rotating wave approximation (this approximation on the solvable model agrees with the appropriate limit of the exact solution) which is the new technique advocated here. An analytical interpolation method that interpolates between these two regimes shows new minima in the effective Rabi frequency brought about by frequency doubling.

The alternative to the rotating wave approximation namely, asymptotic RWA should pave the way for a detailed study of excitonic and other effects in graphene based systems and is hence likely to be of broad significance.

Chapter 3

Detection of anomalous Rabi oscillations in graphene

3.1 Introduction

Theoretical prediction of any physical phenomena is fully convincing only if it is verified experimentally. This chapter is devoted to the study of above predicted anomalous Rabi oscillations[53] in graphene using pump-probe spectroscopy[57,58,62,114,115]. Typically, incoherent optical properties such as optical dephasing and relaxation of band electrons in semiconductors are studied using the pump-probe experiment[45,46] in which two successive laser pulses are used, one to prepare the system in a certain way, called pump pulse and one to test it after a variable time delay, called probe pulse. To study a phenomenon such as optical dephasing and relaxation of nonequilibrium photoexcited band electrons one has to use femtosecond laser pulses because the characteristic time scales for these phenomena, be they carrier-carrier scattering or carrier-phonon scattering are very short. Carrier relaxation in semiconductors is explained by incoherent interactions such as Coulomb carrier-carrier scattering and carrier-phonon (optical or acoustical) scattering, both phenomena occur in interaband as well as interband transitions of semiconductors. Coherent optical responses e.g. the Excitonic Optical Stark Effect (EOSE) of a semiconductor[116–118] may also be studied using the pump-probe technique in which the pump pulse excites the material energetically below the exciton resonance and probe pulse monitors the transmission change at exciton resonance. Recent observations on relaxation dynamics of photoexcited electrons in graphene on

different substrate depends upon the number of layers with the shortest time constant of 150 fs for single layer graphene. So it is appropriate to investigate such nonlinear properties in case of two dimensional single layer graphene (SLG), bilayer graphene (BLG), trilayer graphene (TLG) and multi layer graphene (MLG) where the bands are linear in the case of SLG, parabolic in BLG and cubic in trilayer but all of them possess a property unique to these systems viz. - pseudospin. Therefore, while typically, pump probe spectroscopy is used to investigate incoherent phenomena such as dephasing, it has also been used to study coherent phenomena such as EOSE. The next section explains how to study an equally interesting coherent optical phenomenon viz. anomalous Rabi oscillations using pump probe spectroscopy.

3.2 Problem formulation

In this chapter, we present a theoretical description of how to detect the anomalous Rabi oscillations (ARO) in graphene and verify the theoretical value of anomalous Rabi frequency with existing experimental data[115]. The suggested experimental method we favor to detect the anomalous Rabi frequency is the ultrafast pump probe technique.
We start the chapter with a study of coherent Bloch equations for graphene in presence of a pump field considered as a pulse. This is followed by a study of linearized Bloch equations for a weak probe pulse. The main outcome of this study is the prediction that the differential transmission coefficient (the probe transmission with and without the pump) is an oscillatory function of the pump-probe delay, all else remaining fixed. The frequency of these oscillations are shown to be identical to the anomalous Rabi frequency thereby providing an explicit experimental method to study these anomalous oscillations. Furthermore these oscillations are robust in the sense that they persist even with dephasing and so on but with a diminished amplitude.

3.3 Experimental results on the relaxation dynamics in graphene

The method of choice for measuring transient relaxation phenomena is the pump probe experiment. Dephasing and other relaxation rates are often obtained by measuring the dependence of the differential transmission coefficient on the time delay between pump

and probe pulses. One sees an exponential decay as function of the delay and the decay constant is nothing but the dephasing rate. It is interesting to note that by studying the details of this plot in graphene more carefully, we are able to also infer the presence of anomalous Rabi oscillations which is a coherent phenomenon. This is explained in detail in a later section.

Recently, a large number of experiments on the relaxation of the carrier dynamics in graphene on different substrates has been performed[57,58,62–66,114,119]. Some of the experimental efforts are summarized below. Ultrafast relaxation of photogenerated carriers in epitaxially grown graphene layers on SiC substrate[62] depends upon the intraband carrier-carrier and intraband carrier-phonon scattering. The plot between the differential transmission coefficient $\left(\frac{T-T_0}{T_0}\right)$ where, $T(T_0)$ is the probe transmission coefficient with (without) pump field, vs time delay between pump and probe pulse shows two type of relaxation (τ_1) and (τ_2) with different pump pulse energy and different temperature. The fast relaxation time (τ_1) with range nearly (70-120) fs and the slow relaxation time (τ_2) with the range (0.4-1.2) ps. Fast relaxation (τ_1) is due to the consequence of the intraband carrier-carrier scattering leads to the quaisequilibrium states with a Fermi-Dirac distribution which is consistent with the theoretically predicted intraband carrier-carrier relaxation in graphene[120]. The slower time delay (τ_2) is attributed to the further thermalization such as intraband carrier-phonon scattering.

The experimental plot between the differential transmission coefficient $\left(\frac{T-T_0}{T_0}\right)$ vs delay time between pump and probe pulses of carrier relaxation in graphene on mica substrate using femtosecond laser[58] is almost the same as earlier experiments[62] barring some intermittent discrepancies in sign. The plot shows the initial increase (almost linear) in differential transmission coefficient is due to Pauli blocking or due to the repulsion by the initially generated electron-hole density on further generated photoelectrons. The subsequent decrease in transmission coefficient is due to intra-band carrier-carrier and intra-band carrier-phonon scattering. One conclusion of this experiment is that carrier relaxation in graphene is almost same as that of graphite. This means coupling between different graphite layers play a minor role in ultrafast carrier relaxation. Wang[66] et. al. studied the relaxation dynamics of hot optical phonons in few-layer and multi-layer graphene grown on a silicon carbide substrate and found that the optical phonon cooling on short time scale are independent of factors such as growth technique, number of graphene layers and type of substrate. Time resolved terahertz spectroscopy has been a powerful tool in the investigation of carrier dynam-

ics in semiconductors[121]. The work on multi-layer graphene nanostructures[122,123] are particularly relevant for applications to optoelectronics.

Another experiment performed by Kumar et.al.[57] on the relaxation dynamics of carriers in graphene with different solvents using a femtosecond laser also shows the two types of relaxation, fast relaxation (τ_1) in the range of (130-330) fs and slow relaxation (τ_2) in (3.5-4.9) ps. Fast relaxation is related to the carrier-carrier scattering while slower one related to the carrier-phonon scattering.

The experiments performed by the above authors specially Dawalty et.al.[62], Kumar et.al.[57] and Breusing et.al.[58] are the one we shall be studying closely in order to infer the presence of anomalous Rabi oscillations in graphene.

In the following section, we perform a theoretical analysis of the pump-probe experiment where we calculate probe susceptibility of the system of interest as a function of the area of the pump pulse assuming the probe is a delta function (broad band) in time. Anomalous Rabi oscillations manifest themselves as periodic oscillations of the probe susceptibility as a function of pump duration at each probe frequency where the pump probe delay is assumed to be zero. The period associated with these oscillations corresponds to the anomalous Rabi frequency. It has been estimated by the authors cited that a quasi-equilibrium state due to Coulomb scattering is reached in graphene in a time scale of $\sim 100 - 250$ fs and phonon assisted energy relaxation takes place in a time scale of $1 - 2$ ps. This means that the phenomena of the present work are seen clearly when a sufficient number of oscillations fit into a time scale of the order of 250 fs. This in turn translates into a constraint on the peak electric field of the pulses used. More detailed numerical estimates will be provided in the results and discussion section.

Subsequent to this, we theoretically analyse the more commonly performed version of the pump-probe experiment where the pump and probe pulses are identical except that the probe pulse is much weaker than the pump pulse and arrives after a certain time delay. The differential transmission coefficient is studied as a function of the pump-probe delay yielding information about relaxation phenomena. We shall see that a closer examination of this dependence also reveals anomalous Rabi oscillations which appears to have been seen also in the actual pump-probe experiment performed by Breusing et.al.[58].

3.4 Coherent Bloch equations in presence of an intense optical pump pulse

In what follows, we describe the effect of a finite duration pump pulse on the time evolution of the polarization and densities of charge carriers in graphene. This has been done in detail in our earlier work[53] hence we shall be content at reproducing only the salient features. Upon extinguishing the pump pulse, the dynamical quantities in the system temporarily freeze to their respective values determined by the so-called area of the pulse[45]. These then serve as background for the probe pulse that follows immediately afterward (this assumption makes the analysis simpler, later we also include time delay). The idea is that, a study of the probe susceptibility as a function of the pump pulse duration is able to extract the anomalous Rabi frequency - a characteristic unique to the graphene systems as we have already pointed out.

3.4.1 Bloch equations for single layer graphene

The Hamiltonian for the low energy spectrum of graphene in presence of an intense optical pump pulse may be written in the second quantization language as[4,35],

$$\hat{H} = \sum_{p,\alpha,\beta} v_F \ \vec{\sigma}_{\alpha,\beta} \cdot (\vec{p} - \frac{e}{c}\vec{A}(t)) \ \hat{c}^{\dagger}_{p,\alpha}\hat{c}_{p,\beta},$$

where all the parameters have defined in chapter 2 except the complex vector potential $\vec{A}(t) = \vec{A}_s(t)\ e^{-i\omega t}$, corresponds to the pump pulse and $\vec{A}_s(t)$ is the slowly varying envelope function (in chapter 2, this was independent of time for all time) for the duration of the pulse. With the help of Heisenberg's equation of motion we have derived the equation of motion for the elements of reduced density matrix $n_{diff}(\vec{k},t) = n_A(\vec{k},t) - n_B(\vec{k},t) = \langle c^{\dagger}_{k,A}(t)c_{k,A}(t)\rangle - \langle c^{\dagger}_{k,B}(t)c_{k,B}(t)\rangle$ and $\langle c^{\dagger}_{k,A}(t)c_{k,B}(t)\rangle = p(\vec{k},t)$. The optical Bloch equation without Coulomb interaction in presence of pump field taken as pulse (similar derivation as in chapter 2) is given by,

$$i\ \partial_t\ n_{diff}(\vec{k},t) = 2(z_k - z^*_A(t))\ p(\vec{k},t) - 2(z^*_k - z_A(t))\ p^*(\vec{k},t) \tag{3.1}$$

$$i\ \partial_t\ p(\vec{k},t) = (z^*_k - z_A(t))\ n_{diff}(\vec{k},t) \tag{3.2}$$

where we define, $z_k = v_F(\vec{\sigma}_{AB} \cdot \vec{k})$ and $z_A(t) = v_F(\vec{\sigma}_{BA} \cdot \frac{e}{c}\vec{A}(t))$. These Bloch equations may be solved using an alternative to the well-known rotating wave approximation (RWA), which have called asymptotic RWA (ARWA)[53]. A detailed justification for the use of this approximation is given in the previous chapter. Hence we can directly write the pump solution as follows,

$$n_f(\vec{k},t) \approx \frac{2z_R(t)}{\omega}\ p_s^*(\vec{k},t),\ p_+(\vec{k},t) \approx -\frac{z_R(t)}{\omega}n_s(\vec{k},t),\ p_-(\vec{k},t) \approx -\frac{2z_R^*(t)z_k^*}{\omega^2}\ p_s(\vec{k},t)$$

and the equilibrium value of polarization and number density are given by (before the pump field)

$$p_s(\vec{k}, t \leq T_i) = -\frac{k_x + ik_y}{2|k|} = -\frac{z_k^*}{2v_F|k|};\ \ n_s(\vec{k}, t \leq T_i) = 0$$

where we take the pump pulse field to be in the interval $T_i < t < T_f$. The solution for slowly varying part is,

$$n_s(\vec{k}, t \geq T_i) = n_s(\vec{k}, T_i)\ \cos\Phi(t), n_s(\vec{k}, T_i) = \frac{\omega(v_F|k|)}{\omega_R^2(\bar{t})}$$

$$p_s(\vec{k}, t \geq T_i) = \frac{\Omega_R(\bar{t})z_k^*\omega}{4i(v_F|k|)\omega_R^2(\bar{t})}\left(\sin\Phi(t) - i\ \frac{2\omega_R^2(\bar{t})}{\omega\ \Omega_R(\bar{t})}\cos\Phi(t)\right)$$

where $\Omega_{AR}(\vec{k},t)$ is the generalized anomalous Rabi frequency given by the following expression,

$$\Omega_{AR}(\vec{k},t) = \sqrt{4(v_F|k|)^2 + \left(\frac{2\omega_R^2(t)}{\omega}\right)^2}$$

the quantity $\Phi(\vec{k},t) = \int_{T_i}^{t} \Omega_R(\vec{k},t')\ dt'$ is called 'the area of pulse'. The quantity $\omega_R^2(t) = z_R^*(t)z_R(t) = |v_F\frac{e}{c}(\vec{\sigma}_{BA}\cdot\vec{A}_s(t))|^2$ is the square of the conventional Rabi frequency at zero detuning, changing adiabatically in time as a function of the pump envelope field. Also, $\omega_R^2(\bar{t}) = \frac{\int_{T_i}^{t} dt'\ \omega_R^2(t')}{(t-T_i)}$ is the time average of the square of the conventional Rabi frequency. For the purposes of the present work, we choose the shape of the slowly varying part

of vector potential $\vec{A}_s(t)$ as,

$$\begin{aligned}\vec{A}_s(t) &= \frac{\sqrt{2}\vec{A}(0)}{\sqrt{T_f-T_i}}(t-T_i)^{\frac{1}{2}}\Theta(\frac{T_i+T_f}{2}-t)\Theta(T_f-t)\\ &+ \frac{\sqrt{2}\vec{A}(0)}{\sqrt{T_f-T_i}}(T_f-t)^{\frac{1}{2}}\Theta(t-\frac{T_i+T_f}{2})\Theta(T_f-t)\end{aligned}$$

The precise shape, of course, does not matter since the basic physics we are after is, establishing the phenomenon of anomalous Rabi oscillations. The expression for the area of pulse becomes ($\phi(k)=\sqrt{16(v_F|k|)^2+(T_f-T_i)^2Z^2}$),

$$\Phi(\vec{k},t\geq T_f)=\frac{1}{4}(T_f-T_i)\phi(k)+\frac{2(v_F|k|)^2}{Z}\log\left|\frac{\phi(k)+(T_f-T_i)Z}{\phi(k)-(T_f-T_i)Z}\right|+2v_F|k|(t-T_f),$$

where, $Z=\frac{4|z_{max}|^2}{\omega(T_f-T_i)}$. In the discussion that follows, we assume that the probe pulse is immediately applied upon extinguishing the pump pulse and the former is of such a short duration that it is legitimate to use a delta function probe. The main reason for this assumption is we want only the anomalous Rabi frequency to contribute to the area of the pulse and not the free particle dispersion (even if k is small $2v_F|k|(t_{pr}-T_f)$ may not be small if $t_{pr}\gg T_f$). In this case, the time average of Rabi frequency and generalized Rabi frequencies become,

$$\omega_R^2(\bar{t})=\frac{\int_{T_i}^{T_f}dt'\ \omega_R^2(t')}{(T_f-T_i)}=\frac{|z_{max}|^2}{2},\quad \Omega_{AR}(\vec{k},\bar{t})=\sqrt{4(v_F|k|)^2+\frac{|z_{max}|^4}{\omega^2}}$$

and for the small value of band momentum 'k' the area of the pulse may be simply written as,

$$\Phi(t_{pr}) = (T_f-T_i)\frac{|z_{max}|^2}{\omega}=(T_f-T_i)\frac{2\omega_R^2(\bar{t})}{\omega}$$

In passing, we note that the Bloch equations are a special case of what is known as the Floquet equation[124] in mathematics. This formalism has also been used extensively in the physics literature especially in the field of atomic physics where atom-light interactions are studied[125]. The Rabi frequency that we deduce (both anomalous and conventional) are known as Floquet exponents. In this sense, there is nothing myste-

rious about the anomalous Rabi frequency or indeed the conventional one. However, the point we have been stressing is that these exponents vanish in some regime for peudospinless systems whereas they do not when there is pseudo spin (hence the adjective 'anomalous'). In the present situation, according to that theory, there are three Floquet exponents that add up to zero. Since they are symmetrically placed, one of them is zero the other two are equal and opposite in sign. This is the Rabi frequency. However, this theory does not provide a simple analytical expression for these coefficients and in most situations, they have to be obtained numerically if the exact answer is needed. Hence our analytical approach, though approximate unlike the numerical approach, is needed to establish the general relationships between the Rabi frequency and models under study and regimes considered.

3.5 Linear response due to the probe pulse

The effect generated by the pump pulse in graphene may be studied by the probe field which being weak, obeys linearized Bloch equations. In order to linearize the Bloch equations, we make the following substitution,

$$n_{diff}(\vec{k},t) \rightarrow n_{diff}(\vec{k},t) + \delta n_{diff}(\vec{k},t), p(\vec{k},t) \rightarrow p(\vec{k},t) + \delta p(\vec{k},t),$$
$$z_A(t) \rightarrow z_A(t) + \delta z_A(t)$$

where, $\delta n_{diff}(\vec{k},t)$, $\delta p(\vec{k},t)$ are the linear response functions due to the probe pulse $\delta z_A(t)$. Obtaining the probe response involves ignoring the nonlinear terms, i.e. terms involving products of the changes in polarizations and number densities. For the purposes of the present section, we also assume that the probe pulse is applied just after the pump pulse i.e. there is a very short time duration between the pump pulse and the probe pulse. The next subsections are devoted to the effect of the probe pulse on single layer graphene driven out of equilibrium by the pump pulse.

3.5.1 Linear response of graphene

The Bloch equations (3.1) and (3.2) may be linearized to yield,

$$
\begin{aligned}
&i\ \partial_t \delta n_{diff}(\vec{k},t) = 2z_k\ \delta p(\vec{k},t) - 2z_k^*\ \delta p^*(\vec{k},t) + Q(\vec{k},t),\\
&i\ \partial_t \delta p(\vec{k},t) = z_k^*\ \delta n_{diff}(\vec{k},t) - \delta z_A(t)\ n_s(\vec{k},t),\\
&i\ \partial_t \delta p^*(\vec{k},t) = -z_k\ \delta n_{diff}(\vec{k},t) + \delta z_A^*(t)\ n_s(\vec{k},t)
\end{aligned}
$$

where, $Q(\vec{k},t) = -2\delta z_A^*(t)\ p_s(\vec{k},t) + 2\delta z_A(t)\ p_s^*(\vec{k},t)$. To derive the above linearized Bloch equations we ignore terms such as $z_A(t)\times\delta p(\vec{k},t),\ z_A(t)\times\delta p(\vec{k},t),\ z_A(t)\times\delta z_A(t)$ since we assume as in the previous section, that there is a finite time duration (very short) between the pump pulse and probe pulse i.e. we are discussing the case of non-overlapping pump and probe pulses.

We solve these coupled equations with initial condition $\delta n_{diff}(\vec{k},t_{pr}) = 0$ and $\delta p(\vec{k},t_{pr}) = 0$ at time $t = t_{pr}$ and assume that the probe field is weak and a very short duration pulse so that one can assume it as a delta function probe (for theoretical simplification). In other words we set, $\delta z_A(t) = (\delta z_{A,max} t_{pr})\ \delta(t - t_{pr})$. After solving above equations in presence of a probe field we get the following expression for $\delta n_{diff}(\vec{k},t)$ and $\delta p(\vec{k},t)$ as,

$$
\begin{aligned}
&\delta n_{diff}(\vec{k},t) = -iQ(t_{pr})\Theta(t-t_{pr})\cos(2|z_k|(t-t_{pr}))\\
&+\frac{n_s(t_{pr})}{|z_k|}2Re\left(z_k\delta A(t_{pr})\right)\Theta(t-t_{pr})\cos(2|z_k|(t-t_{pr}))
\end{aligned}
$$

and

$$
\begin{aligned}
&\delta p(\vec{k},t) = -\frac{n_s(\vec{k},t_{pr})}{z_k}\ Im\left(z_k(\delta z_{A,max}t_{pr})\right)\Theta(t-t_{pr})\\
&+\frac{i\ n_s(\vec{k},t_{pr})}{z_k}\ Re\left(z_k\ \delta z_{A,max}t_{pr}\right)\cos(2v_F|k|(t-t_{pr}))\\
&\Theta(t-t_{pr}) + \frac{2i|z_k|}{z_k}\ Im\Big((\delta z_{A,max}t_{pr})\ p_s^*(\vec{k},t_{pr})\Big)\\
&\sin(2v_F|k|(t_{pr}-t))\ \Theta(t-t_{pr})
\end{aligned}
$$

where $Q(\vec{k},t_{pr}) = -2\delta z_A^*(t_{pr})\ p_s(\vec{k},t_{pr}) + 2\delta z_A(t_{pr})\ p_s^*(\vec{k},t_{pr})$ and $\Theta(x)$ is Heaviside's step function. Take the Fourier transform of $\delta p(\vec{k},t)$ followed by summation over 'k' we

have,

$$\delta p(\omega^{'}) = \sum_k \frac{|k|v_F}{4i} \frac{\Omega_R(\bar{t})\omega}{v_F|k|\omega_R^2(\bar{t})} \left(\sin\Phi + i\frac{2\omega_R^2(\bar{t})}{\omega\Omega_R(\bar{t})}\right) \frac{2v_F|k|}{(2v_F|k|)^2-\omega^{'2}} \frac{2\pi i e v_F}{\omega^{'}} \delta E(\omega^{'}) + \sum_k i n_s(t_{pr})\delta z_A(t_{pr}) \left(-\frac{i}{\omega^{'}} + \frac{i\omega^{'}}{(2v_F|k|)^2-\omega^{'2}}\right) \frac{2\pi i e v_F}{\omega^{'}} \delta E(\omega^{'})$$

where we have used the following relations,

$$\int_{t_{pr}}^{+\infty} e^{-i\omega^{'}t} \sin(2v_F|k|(t-t_{pr}))\, dt = \frac{2v_F|k|}{(2v_F|k|)^2-\omega^{'2}} e^{-i\omega^{'}t_{pr}},$$

$$\int_{t_{pr}}^{+\infty} e^{-i\omega^{'}t}\, dt = -\frac{i}{\omega^{'}} e^{-i\omega^{'}t_{pr}},$$

$$\int_{t_{pr}}^{+\infty} e^{-i\omega^{'}t} \cos(2v_F|k|(t-t_{pr}))\, dt = \frac{i\omega^{'}}{(2v_F|k|)^2-\omega^{'2}} e^{-i\omega^{'}t_{pr}},$$

$$\delta z_A(t_{pr})\, e^{-i\omega^{'}t} = \frac{2\pi i e v_F}{\omega^{'}} \delta E(\omega^{'}).$$

The probe susceptibility may be defined by the following relation,

$$\delta p(\omega^{'}) = \chi(\omega^{'})\, \delta E(\omega^{'}),$$

where $\delta E(\omega^{'})$ is the electric field due to the probe. Extracting the probe susceptibility and then apply the ARWA limit we have,

$$\chi(\omega^{'}) = \sum_k i\frac{\omega|k|^2}{2m\omega_R^2(\bar{t})}\delta z_A(t_{pr}) \left(-\frac{i}{\omega^{'}} + \frac{i\omega^{'}}{(2v_F|k|)^2-\omega^{'2}}\right) \frac{2\pi i e v_F}{\omega^{'}} \cos\Phi$$

$$\chi(\omega^{'}) \sim \cos\Phi.$$

We may see that the probe susceptibility depends upon the area of the pump pulse and it has oscillatory behavior as a function of the duration of the pump field. Further simplification implies the following expression,

$$\frac{\chi(\omega^{'})}{\chi_{\max}(\omega^{'})} = \cos\Phi, \quad \Phi = \frac{v_F^2}{\hbar^2\omega^3}|\vec{\sigma}_{BA}\cdot e\vec{E}_{max}|^2(T_f - T_i). \tag{3.3}$$

Here we have restored Planck's constant to facilitate experimental verification of our

central claim viz. Eq.(3.3). Also, $\chi_{\max}(\omega^{'})$ is the susceptibility when $\cos\Phi = 1$. The central result of Eq.(3.3) may be depicted graphically as shown by the diagram in results section.

3.5.2 Experimental verification of ARO's: Differential transmission coefficient

The above description was an ideal pump probe experiment where the probe duration is taken to be much smaller than the pump duration, so much so that we have used an ideal delta function in time to describe the probe. This enables an elegant analytical solution of the probe susceptibility at each probe frequency. This solution also clearly and easily brings out the important physics we are after viz. that the probe susceptibility is a sinusoidal function of the pump duration with the probe frequency and the pump Rabi frequency (electric field strength) remaining fixed. The period of these oscillations is the anomalous Rabi frequency. Realistic experiments[57,58,62,114] typically use the same pulse for pump and probe except that the probe beam is much less intense than the pump and comes after a time delay following the pump. Therefore, in order to compare with existing experimental data we wish to study this problem. When delays are present it is important to take into account dephasing rates.

In presence of a decaying term, the optical Bloch equations (3.1) and (3.2) can be written as,

$$\partial_t n_{diff}(\vec{k},t) = 4Im\left(v_F\vec{\sigma}_{AB}\cdot(\vec{k}-\frac{e}{c}\vec{A}^{*}(t))p(\vec{k},t)\right) \tag{3.4}$$

$$i\,\partial_t p(\vec{k},t) = v_F\vec{\sigma}_{BA}\cdot(\vec{k}-\frac{e}{c}\vec{A}(t))n_{diff}(\vec{k},t) - i\frac{p(\vec{k},t)-p_0(\vec{k})}{T_2} \tag{3.5}$$

Here $\frac{1}{T_2}$ is the polarization dephasing rate (we ignore the decaying term due to electron-hole recombination viz. population decay since it is small in comparison to $\frac{1}{T_2}$) and $p_0(\vec{k}) = -\frac{z_k^*}{2v_F|k|}$ is the equilibrium polarization. The above equation ensures that the polarization decays to the equilibrium value after a time large compared to T_2 once the pump is turned off.

The probe response of Eq.(3.4) and Eq.(3.5) are given by,

$$\partial_t\delta n_{diff}(\vec{k},t) = 4v_F Im(\vec{\sigma}_{AB}\cdot(-\frac{e}{c}\delta\vec{A^{*}}(t))\,p(\vec{k},t)) + 4v_F Im((\vec{\sigma}_{AB}\cdot\vec{k})\,\delta p(\vec{k},t)), \tag{3.6}$$

$$i\,\partial_t \delta p(\vec{k},t) = v_F \vec{\sigma}_{BA}\cdot(-\frac{e}{c}\delta\vec{A}(t))n_{diff}(\vec{k},t) + v_F(\vec{\sigma}_{BA}\cdot\vec{k})\;\delta n_{diff}(\vec{k},t) - i\frac{\delta p(\vec{k},t)}{T_2}. \quad (3.7)$$

We have solved these equations using the the methods already outlined to obtain the following formulas for the transmission coefficient. In graphene we think of the induced field as proportional to the induced current which is in turn proportional to the polarization. Therefore we choose the contribution to the signal induced by the probe pulse as,

$$\delta\vec{\pi}(t) = v_F\vec{\sigma}_{AB}\;\delta p(t) + v_F\vec{\sigma}_{BA}\;\delta p^*(t)$$

where $\delta p(t) = \frac{1}{A}\sum_{\mathbf{k}}\delta p(\mathbf{k},t)$. The signal due to the probe only is chosen for dimensional consistency as $\delta\vec{\pi}_{ext}(t) = \frac{ev_F^2}{c^2}\delta\mathbf{E}_{ext}(t)$. The net transmitted signal is $\delta\vec{\pi}_{trans}(t) = \delta\vec{\pi}_{ind}(t) + \delta\vec{\pi}_{ext}(t)$ where $\delta\vec{\pi}_{ind}(t)$ is the induced signal that propagates in the same direction as $\delta\vec{\pi}_{ext}(t)$. The transmitted intensity is $\langle\delta\vec{\pi}^*_{trans}(t)\cdot\delta\vec{\pi}_{trans}(t)\rangle$ where the average denotes time average and the incident intensity is $\langle\delta\vec{\pi}^*_{ext}(t)\cdot\delta\vec{\pi}_{ext}(t)\rangle$. The transmission coefficient is,

$$\frac{\Delta T}{T_0} = \frac{\langle\delta\vec{\pi}^*_{trans}(t)\cdot\delta\vec{\pi}_{trans}(t)\rangle}{\langle\delta\vec{\pi}^*_{ext}(t)\cdot\delta\vec{\pi}_{ext}(t)\rangle}.$$

What we are really interested in is the change in this coefficient with and without the pump. This means we have to calculate $\frac{\Delta T_+ - \Delta T}{T_0}$ where ΔT_+ refers to the probe transmission with the pump and ΔT is the same without the pump. In present case the induced signal is much weaker that the incident probe signal (it is well known that graphene is quite transparent $\sim 97\%$), hence we may write for the differential transmission coefficient,

$$\eta \equiv \frac{\Delta T_+ - \Delta T}{T_0} =$$
$$\frac{\langle\delta\vec{\pi}^*_{ext}(t)\cdot(\delta\vec{\pi}_{ind,+}(t) - \delta\vec{\pi}_{ind}(t))\rangle + \langle(\delta\vec{\pi}^*_{ind,+}(t) - \delta\vec{\pi}^*_{ind}(t))\cdot\delta\vec{\pi}_{ext}(t)\rangle}{\langle\delta\vec{\pi}^*_{ext}(t)\cdot\delta\vec{\pi}_{ext}(t)\rangle}$$

We have computed η explicitly and it may be written as,

$$\eta = -\frac{ic^2}{\omega^2 A}\sum_{\mathbf{k}}\; e^{\lambda_2\tau}\frac{1}{\tau_d}\;\frac{(e^{\lambda_2\tau_d}-1)^2}{\Omega_{ARWA}(0)} + c.c. \quad (3.8)$$

where,

$$\lambda_2 = -\frac{1}{2T_2} - \frac{\Omega^2_{ARWA}(0)}{2T_2\Omega^2_{ARWA}(k)} - i\Omega_{ARWA}(k) \quad (3.9)$$

and $\Omega_{ARWA}(k)$ is the effective anomalous Rabi frequency and τ is the time delay between

the end of the pump pulse and start of the probe pulse. Also τ_d is the common duration of the pump and probe pulses. This may be explicitly evaluated for graphene to yield,

$$\eta = -\frac{c^2}{(4\pi v_F^2(\tau+\tau_d)(\tau+2\tau_d)\omega^2)}$$

$$\times((4+\frac{2\tau}{\tau_d})\ \cos\left(\frac{2\omega_R^2}{\omega}(\tau+\tau_d)\right)\ e^{-\frac{(\tau+\tau_d)}{T_2}} - \frac{(\tau+\tau_d)}{\tau_d}\ \cos\left(\frac{2\omega_R^2}{\omega}(\tau+2\tau_d)\right)\ e^{-\frac{(\tau+2\tau_d)}{T_2}}$$

$$+(-3-\frac{\tau}{\tau_d}-\frac{2\tau_d}{\tau})\ \cos\left(\frac{2\omega_R^2}{\omega}\tau\right)\ e^{-\frac{\tau}{T_2}}) \tag{3.10}$$

It is clear that the above formula is consistent with the claims of the earlier discussion which involved using a delta function probe, viz. that the susceptibility is a sinusoidal function of the pulse duration. Here however some differences are expected since both the pump pulse and the probe pulse have the same duration which means harmonics of the anomalous Rabi frequency are also seen since a term such as $\cos\left(\frac{2\omega_R^2}{\omega}(\tau_{d,probe}+\tau_{d,pump})\right)$ also appears, which in the earlier discussion simply reduced to $\cos\left(\frac{2\omega_R^2}{\omega}\tau_d\right)$ since $\tau_{d,probe}=0$ but here since $\tau_{d,probe}=\tau_{d,pump}=\tau_d$ there are harmonics as well. In this case, $T_2 \gg \tau \gg \tau_d$. If we also ensure that $\frac{2\omega_R^2}{\omega}\tau \sim 10$ so that there are around 10 anomalous Rabi oscillations in the duration between pump and probe, this phenomenon is seen clearly in the periodic variation of the differential transmission coefficient as a function of delay. This formula also shows good agreement with experimental data[57,58,62,114]. Specifically, in the work of Breusing et al.[58], a $7fs$ pump and probe pulse was used with pump fluence of $0.2mJ/cm^2$ corresponding to an intensity of $I_0 = 2.857 \times 10^{14} Watt/m^2$ and the r.m.s. electric field corresponding to this intensity is $E = 3270.0\ kV/cm$. The central frequency of the pump corresponds to $\hbar\omega = 1.5eV$ and the polarization dephasing time is taken to be $T_2 = 140fs$. This leads to the following realistic values for the various frequency scales. The driving frequency is $\omega = 2.27 \times 10^{15} rad/sec$, the conventional Rabi frequency is $\omega_R = 2.19 \times 10^{14} rad/sec$ and the anomalous Rabi frequency is $\Omega_{ARWA} = \frac{2\omega_R^2}{\omega} = 4.2 \times 10^{13} rad/sec$. This means that in the duration of each pulse there are ~ 16 oscillations with frequency ω, making this notion well-defined. Also within the decay time there are ~ 6 anomalous Rabi oscillations making this also easily detectable. We may see that these numbers are completely consistent with the assumptions made in the asymptotic rotating wave approximation - each differ from the other by an order of magnitude or more. Now we

wish to plot the theoretical analog (see figure 3.1) of the data shown in Fig.1(c) of Breusing et al.[58].

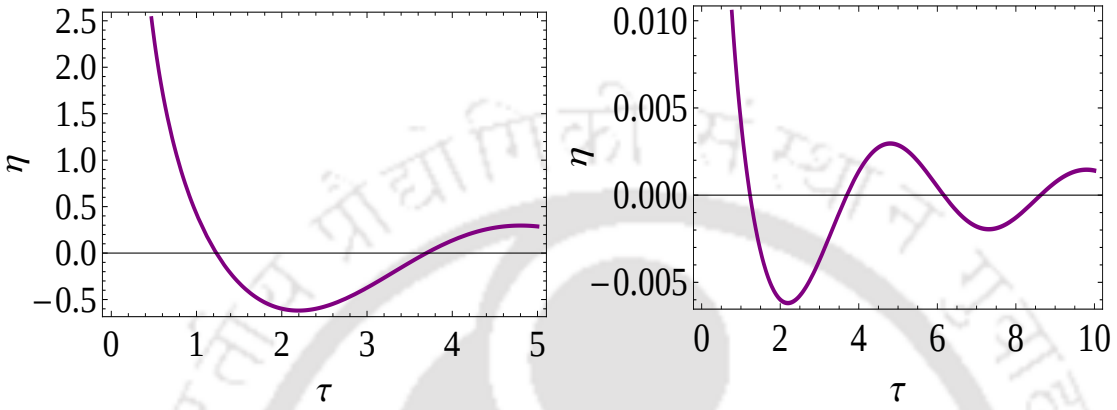

Figure 3.1: These figures depicts the variation of differential transmission coefficient (η) versus the time duration between the pump and probe field (τ).

In that work we see the following important features. The change in transmission is positive for time delays $\tau < 300fs$ and negative thereafter. The data points show oscillatory behavior superimposed on an overall decay. The claim we are making is that this oscillatory behavior is nothing but the anomalous Rabi oscillation. Indeed, an estimation of the period of these oscillations from Fig 1(c) of Breusing et al. gives a period of $107fs$. This corresponds to a circular frequency of $5.8 \times 10^{13} rad/sec$ which is rather close to the anomalous Rabi frequency $\Omega_{ARWA} = 4.2 \times 10^{13} rad/sec$. Other features of this plot Fig.1(c) of Breusing et al. that are in broad agreement with Eq.(3.10) are, (a) In both these plots, there is an sharp drop in the magnitude with increasing delays especially for small delays (b) In both these plots there is the all important oscillation superimposed on this decay whose frequencies are in good agreement - a signature of anomalous Rabi oscillation (c) Both change sign after a certain time delay (however the numerical values of those times do not match, also the numerical values of the coefficient do not match at all, ours is a bit too high).

The important point is that the oscillatory behavior is characteristic and robust and common to both theory and experiment.

3.6 Results and discussion

In this section, we plot a graph obtained from Eq.(3.3) which reveals that the susceptibility due to the probe field depends upon the area of pump pulse. This area is proportional to the pump pulse duration $(T_f - T_i)$, provided the conventional Rabi frequency is held fixed. The frequency of oscillations of the probe susceptibility as a function of pump pulse duration is just the anomalous Rabi frequency.

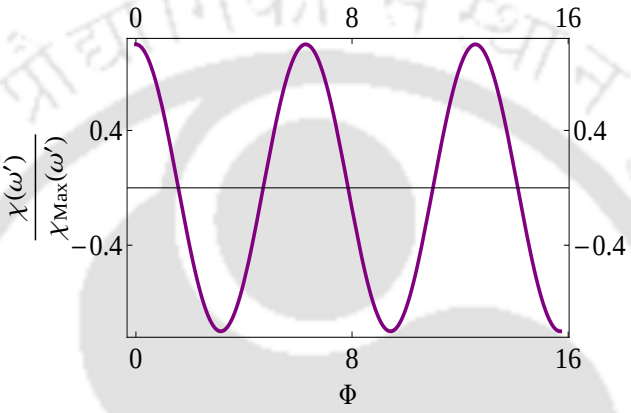

Figure 3.2: The figure depicts the variation of probe susceptibility with the area of the pump pulse.

At this stage, it is desirable to perform some numerical estimates to decide when these phenomena are going to be seen most clearly. The basic idea is that within a relaxation time, sufficient number of oscillations should occur so that one may then extract a proper frequency. Assuming the relaxation time to be T_2 we expect,

$$\Omega_{a-Rabi} \equiv \frac{v_F^2}{\hbar^2\omega^3}|\vec{\sigma}_{BA} \cdot e\vec{E}_{max}|^2 \sim 10\frac{2\pi}{T_2},$$

corresponding to 10 anomalous Rabi oscillations within a time interval of T_2. Also we choose the external pump frequency to be 10 times the anomalous Rabi frequency. This means that the frequency of the pump pulse is $\nu = \frac{100}{T_2}$. According to Ulbricht et.al.[121], the maximum electric field generated by terahertz radiation pulses is, $E_{max} \sim 120 - 400$ kV/cm corresponding to pump frequency of 0.6×10^{12} Hz to 4×10^{12} Hz. From our assumptions, this means that the relaxation time is constrained to be between $T_2 = 25$ ps to $T_2 = 167$ ps. But other works[62,63] have shown that phonon assisted energy relaxation in graphene is in the subpicosecond time scale ($\sim 0.4 - 1.7$ ps), therefore it

appears that a hundred times higher frequency than THz may be required. However just for purposes of getting some insight into the various time scales and electric fields involved, let us for the moment assume that a $T_2 \sim 25$ ps can be achieved.

In this case, $E_{max} \sim 131$ kV/m is the peak field needed. This is two orders of magnitude smaller than the maximum that can be achieved using THz pulses. Therefore this experiment is indeed quite feasible.

Alternatively, graphene mimicked using cold atoms[126] could also be a possibility where such constraints may be circumvented as the experiments can be tailor-made to a theory's specifications. The surface states of a three dimensional topological insulator are also Dirac fermions[127,128] but they possess conventional spin rather than pseudo spin. The analysis of the present work shows that in such systems too (gapped or without gap), anomalous Rabi oscillations may be expected.

3.7 Conclusions

The work contained in this chapter has shown how pump-probe experiments can detect anomalous Rabi oscillations in graphene. Anomalous Rabi oscillations are like conventional Rabi oscillations - periodic exchange of energy between the light field and the system in question. However, instead of these oscillations taking place close to the resonance criterion where the applied frequency is nearly equal to the frequency for creating a particle-hole pair, anomalous Rabi oscillations are seen when the external frequency is larger than all others in the system. We have shown that these anomalous oscillations have a frequency equal to $\frac{2\omega_R^2}{\omega}$ where ω_R is the conventional Rabi frequency and ω is the applied frequency. These anomalous oscillations have been shown in an earlier work to be solely due to pseudo-spin/conventional spin, Dirac-fermion nature of the quasiparticles. These qualities are shared by both the graphene system and surface states of topological insulators. These anomalous oscillations manifest themselves in the pump-probe experiment as a periodic variation of the probe susceptibility as a function of pump duration when the conventional Rabi frequency is held fixed or as a periodic variation of the differential transmission coefficient as a function of pump-probe delay with other parameters held fixed.

Chapter 4

Quantum Rabi oscillations in graphene

4.1 Introduction

The previous two chapters discussed the phenomenon of matter-field interaction, where the EM field was treated as purely classical. However, there are several cases where a classical description of the radiation field is not valid. Experimentally observed quantum phenomena such as photoelectric effect, Raman effect, stimulated emission and absorption, spontaneous emission etc. can not be explained by the classical theory of radiation, these phenomena are explained only by quantum aspect of the radiation field. Semiclassical analogue of the Rabi oscillations, resulting from the interaction of the light field with a two level system shows sinusoidal oscillations (infinite wave train) in the absence of any relaxation terms. Treating the radiation field quantum mechanically[47–49], some new phenomena are observed in Rabi oscillations known as quantum 'collapse' and 'revival'. From a semiclassical perspective, an atom in an excited state cannot make a transition to a lower level in the absence of an external field whereas in the quantum case, this transition is possible even in a vacuum because of spontaneous emission (zero point quantum fluctuations of radiation). A solvable model of quantum radiation interacting with a two-level system has been given by Jaynes and Cummings[129,130]. The most interesting phenomena in this model are the collapse and revival oscillations that occur when the electromagnetic (EM) field is in a coherent state[131–134]. These phenomena may be intuitively understood as follows. The population density consists of a sum of oscillating terms, each corresponding to a well-defined photon number n and each term oscillates with a particular Rabi frequency proportional to $\sqrt{n+1}$[130]. In this

case, one may see that even without any relaxation, the distribution of Rabi frequencies produces an initial dephasing ('collapse') in the sinusoidal Rabi oscillations[129]. The basic reason is, if two neighboring terms oscillate 180° out of phase, they destructively interfere whereas if they are in phase, there is constructive interference[47]. In case of collapse, the various contributions destructively interfere thereby producing the effect of decay or dephasing. Revival is purely a quantum phenomenon, however. Revival refers to the resurrection of previously extinguished oscillations due to destructive interference gradually diminishing, progressively revealing the original oscillations. It depends not only upon the coherent state of photons but also on the statistical distribution of photon numbers. A continuous photon distribution would lead to a collapse just like as in a classical field, but no revivals. The experimental realization of the interaction between a two level atom and a quantized electromagnetic field have been experimentally observed in experiments[103] such as cavity quantum electrodynamics (CQED), performed with circular Rydberg atoms (atoms excited to highly quantum number state) and center-of-mass motion of a trapped ion. Rabi oscillations have long been studied in semiconductors[46] as well, where energy levels are replaced by bands. Rabi oscillations in graphene has been studied by Mischenko[54] and Ishikawa[55] using the well known rotating wave approximation[45] (RWA) close to resonance. Recently, we predicted anomalous Rabi oscillations in graphene that occur far from resonance using an alternative to RWA which we have been calling asymptotic rotating wave approximation[53] (ARWA). This is the regime where the incident optical frequency is much higher than the frequency corresponding to particle hole energy.

In this chapter, we wish to show that the phenomenon of anomalous Rabi oscillations occur even when the EM field is quantum, thereby establishing unequivocally that the ARO are due to pseudospin and not due to approximations or assumptions we have made.

4.2 Problem formulation

The preceding chapters were devoted to the study of the Rabi oscillations using optical Bloch equations in the presence of not only a continuous optical field but also with a pump pulse. In this chapter, we describe the phenomenon of Rabi oscillations in the presence of a purely quantum field which shows collapse and revival along with Rabi oscillations.

We start this chapter with the probability amplitude equation to study anomalous Rabi oscillations in the presence of a quantum field. The result obtained is compared with the model of pseudospinless graphene. Thereafter we study the interpolation between the RWA and ARWA regime. This is followed by a description of collapse and revival phenomena in presence of a coherent radiation field. Which is then followed by result and discussion section with various plots.

4.3 Quantum Rabi oscillations in graphene: Probability amplitude equation

The Hamiltonian for the low energy spectrum of graphene near the Dirac points in presence of a quantum field is given by the following expression,

$$\hat{H} = c_A^\dagger \ (\vec{\sigma}_{AB} \cdot \vec{\epsilon}) \ c_B + c_B^\dagger \ (\vec{\sigma}_{BA} \cdot \vec{\epsilon}) \ c_A + \lambda \ b \ c_B^\dagger c_A + \lambda^* \ c_A^\dagger c_B \ b^\dagger + \omega \ b^\dagger b, \tag{4.1}$$

where the first two terms represents the low energy Hamiltonian of graphene, third and fourth terms represents the interaction between graphene with quantum field and the last term represents the field Hamiltonian, $[b, b^\dagger] = 1$ are the photon operators, '$\vec{\epsilon}$' represents the momentum dependent vector and 'λ' is the coupling constant.

In order to study differences that emerge when radiation is treated classically or quantum mechanically, it is best to keep the matter sector as simple as possible. To this end, we assert that all processes in case of graphene involve just one electron either on site A or B. This means that in case of graphene, the only initial non-zero amplitudes are, $\langle 0, 1, n|\Phi(t)\rangle_{in}$ and $\langle 1, 0, n|\Phi(t)\rangle_{in}$, where the suffix "$in$" stand for initial state. Using Schrodinger/Dirac equation, $i\hbar\frac{\partial}{\partial t}|\Phi(t)\rangle = \hat{H}|\Phi(t)\rangle$ and with the unitary transformation $\langle 0, 1, n|\Phi(t)\rangle_{in} = \langle 0, 1, n|\Phi(t)\rangle \ e^{-i\omega nt}$, $\langle 1, 0, n|\Phi(t)\rangle_{in} = \langle 1, 0, n|\Phi(t)\rangle \ e^{i\omega nt}$, one can get the general probability amplitude equation as follows (setting $\hbar = 1$) (for the derivation see the Appendix-C),

$$i\partial_t\langle 0, 1, n|\Phi(t)\rangle = \vec{\sigma}_{BA} \cdot \vec{\epsilon} \ \langle 1, 0, n|\Phi(t)\rangle + \sqrt{n+1}\lambda \ e^{-i\omega t} \ \langle 1, 0, n+1|\Phi(t)\rangle \tag{4.2}$$

and,

$$i\partial_t\langle 1, 0, n+1|\Phi(t)\rangle = \vec{\sigma}_{AB} \cdot \vec{\epsilon} \ \langle 0, 1, n+1|\Phi(t)\rangle + \sqrt{n+1}\lambda^* \ e^{i\omega t} \ \langle 0, 1, n|\Phi(t)\rangle. \tag{4.3}$$

These equations may be solved in two different regimes near conventional resonance it may be solved using the well known RWA where as far from resonance it is solved using the ARWA technique.

In this section, we explore the two main regions where Rabi oscillations occur according to our earlier work[53] and see if they still survive in the extreme quantum limit of the radiation field. In that work, we showed that Rabi oscillations in graphene occur at resonance when the external frequency matches the particle-hole frequency – an unsurprising result shared by many systems such as two-level atoms, semiconductors and so on. But we found that grapheme, due to the pseudospin degree of freedom, exhibits anomalous Rabi oscillations for frequencies much higher than the frequency associated with particle-hole creation. We find below that both types of oscillations survive in the ultra quantum limit as well. Indeed there are even zero-point anomalous Rabi oscillations in a vacuum. This means that the notion of ARO is robust and not an artifact of any approximations.

4.3.1 Anomalous Rabi oscillations

In order to solve the graphene amplitude equations Eq.(4.2) and Eq.(4.3) in the regime where the incident applied frequency (ω) is much higher than the frequency corresponding to particle hole energy (2ϵ), we use the ARWA method, within this approximation we set,

$$\langle\rangle = \langle\rangle_s + \langle\rangle_+ \; e^{-i\omega t} + \langle\rangle_- \; e^{i\omega t}$$

Inserting this into the full amplitude equations Eq.(4.2) and Eq.(4.3) and comparing the coefficients we obtain (keeping in mind that $|i\partial_t g_{s,\pm}| \ll |\omega g_{s,\pm}|$),

$$\begin{aligned}
\langle 0,1,n|\Phi(t)\rangle_+ &= \frac{\sqrt{n+1}\lambda}{\omega}\ \langle 1,0,n+1|\Phi(t)\rangle_s, \\
\langle 1,0,n+1|\Phi(t)\rangle_+ &= \frac{(\vec{\sigma}_{AB}\cdot\vec{\epsilon})}{\omega}\ \langle 0,1,n+1|\Phi(t)\rangle_+, \\
\langle 0,1,n|\Phi(t)\rangle_- &= -\frac{(\vec{\sigma}_{BA}\cdot\vec{\epsilon})}{\omega}\ \langle 1,0,n|\Phi(t)\rangle_-, \\
\langle 1,0,n+1|\Phi(t)\rangle_- &= -\frac{\sqrt{n+1}\lambda^*}{\omega}\ \langle 0,1,n|\Phi(t)\rangle_s,
\end{aligned}$$

and the equations for the slow part of the amplitude,

$$\left(i\partial_t + \frac{(n+1)|\lambda|^2}{\omega}\right)\ \langle 0,1,n|\Phi(t)\rangle_s = (\vec{\sigma}_{BA}\cdot\vec{\epsilon})\ \langle 1,0,n|\Phi(t)\rangle_s, \tag{4.4}$$

$$\left(i\partial_t - \frac{n|\lambda|^2}{\omega}\right)\ \langle 1,0,n|\Phi(t)\rangle_s = (\vec{\sigma}_{AB}\cdot\vec{\epsilon})\ \langle 0,1,n|\Phi(t)\rangle_s \tag{4.5}$$

To obtain the amplitude Rabi frequency we set $i\partial_t \equiv \Omega$ which correspond to a secular equation for Ω.

$$|\lambda|^4 n(1+n) - |\lambda|^2\omega\Omega + \omega^2(\epsilon-\Omega)(\epsilon+\Omega) = 0 \tag{4.6}$$

Therefore the amplitude Rabi frequency is,

$$\Omega_{\pm}(n) = \frac{-|\lambda|^2 \pm \sqrt{|\lambda|^4(1+2n)^2 + 4\epsilon^2\omega^2}}{2\omega} \tag{4.7}$$

This is the Rabi frequency associated with the probability amplitude: $\psi_{\pm} \sim e^{i\Omega_{\pm}t}$. But the current density is defined as, $j \sim \psi_+^{\dagger}\psi_-$, hence the actual Rabi frequency in the ARWA regime associated with the current density is,

$$\Omega_{AR}(n) = 2\frac{\sqrt{|\lambda|^4(n+\frac{1}{2})^2 + \epsilon^2\omega^2}}{\omega} \tag{4.8}$$

In the semi-classical limit, when $n = n^0 \gg 1$ we obtain the formula of our earlier work viz. $\Omega_{AR}(n^0) = 2\sqrt{\omega_R^4 + \epsilon^2\omega^2}/\omega$, where $\omega_R = \sqrt{n^0}|\lambda|$.

4.3.1.1 Single photon anomalous Rabi oscillations

The equation for generalized anomalous Rabi frequency Eq.(4.8) suggest that the same effect survives also in the single (or even zero) photon limit. The smallest anomalous Rabi frequency is one for which $n = 0$. We see that zero-point fluctuations of the photon field leads to anomalous Rabi oscillations even in a vacuum, which is detectable only when $\frac{|\lambda|^2}{2} \gg \epsilon\omega$. In this case of single photon limit the expression for the generalized Rabi frequency is given by the following expression,

$$\Omega_{AR}^{(n=1)} = 2\frac{\sqrt{\frac{|\lambda|^4}{4} + \epsilon^2\omega^2}}{\omega}$$

Thus *anomalous* Rabi oscillations present in the single photon limit. Now we wish to ascertain if *conventional* Rabi oscillations are also present in the single photon limit.

4.3.2 Conventional Rabi oscillations

In this section, we study the other extreme limit where the incident frequency is nearly equal to the frequency corresponding to particle hole energy. This is the RWA regime: $\omega \approx 2\epsilon$. In the semiclassical case we replace $(n+1)$ from the probability amplitude equations Eq.(4.2) and Eq.(4.3) to n we have (in matrix form),

$$i\frac{\partial}{\partial t}\begin{pmatrix} \langle 0,1,n|\Phi(t)\rangle \\ \langle 1,0,n|\Phi(t)\rangle \end{pmatrix} = \begin{pmatrix} 0 & \epsilon_{BA} \\ \epsilon_{AB} & 0 \end{pmatrix}\begin{pmatrix} \langle 0,1,n|\Phi(t)\rangle \\ \langle 1,0,n|\Phi(t)\rangle \end{pmatrix} + \begin{pmatrix} 0 & \lambda\sqrt{n}\, e^{-i\omega t} \\ \lambda^*\sqrt{n}\, e^{i\omega t} & 0 \end{pmatrix}\begin{pmatrix} \langle 0,1,n|\Phi(t)\rangle \\ \langle 1,0,n|\Phi(t)\rangle \end{pmatrix}$$

where, $\vec{\sigma}_{BA}\cdot\vec{\epsilon} = \epsilon_{BA}$ and $\vec{\sigma}_{AB}\cdot\vec{\epsilon} = \epsilon_{AB}$. To obtain the expression for generalized Rabi frequency, diagonalize the first matrix then after make the following substitution,

$$\begin{pmatrix} \langle 0,1,n|\Phi(t)\rangle \\ \langle 1,0,n|\Phi(t)\rangle \end{pmatrix} = \begin{pmatrix} \frac{\epsilon_{BA}}{|\epsilon|} & -\frac{\epsilon_{BA}}{|\epsilon|} \\ 1 & 1 \end{pmatrix}\begin{pmatrix} \langle 0,1,\tilde{n}|\Phi(t)\rangle \\ \langle 1,0,\tilde{n}|\Phi(t)\rangle \end{pmatrix}$$

The matrix equation which we have got after the above substitution, make the further substitution,

$$\langle 0,1,\tilde{n}|\Phi(t)\rangle = e^{-i\epsilon t}\,\langle 0,1,\tilde{\tilde{n}}|\Phi(t)\rangle;\;\; \langle 1,0,\tilde{n}|\Phi(t)\rangle = e^{i\epsilon t}\,\langle 1,0,\tilde{\tilde{n}}|\Phi(t)\rangle,$$

using the RWA approximation we have,

$$i\partial_t\,\langle 0,1,\tilde{\tilde{n}}|\Phi(t)\rangle = \frac{\lambda\sqrt{n}}{2|\epsilon|}\,\epsilon_{AB}\,e^{-i\Delta t}\,\langle 1,0,\tilde{\tilde{n}}|\Phi(t)\rangle,$$

and,

$$i\partial_t\,\langle 1,0,\tilde{\tilde{n}}|\Phi(t)\rangle = \frac{\lambda^*\sqrt{n}}{2|\epsilon|}\,\epsilon_{BA}\,e^{i\Delta t}\,\langle 0,1,\tilde{\tilde{n}}|\Phi(t)\rangle$$

where, $\Delta = \omega - 2|\epsilon|$. A solution of these coupled equations yield the amplitude Rabi frequency as $\Omega_{R,\pm} = \frac{1}{2}(\Delta \pm \sqrt{\Delta^2 + n|\lambda|^2})$ since the amplitude is $\psi_\pm \sim e^{i\Omega_{R,\pm}t}$. This means that the slow part of the current oscillates as $j_s(t) \sim e^{i\Omega_R t}$, where, Ω_R is the

generalized Rabi frequency given by the following expression,

$$\Omega_R = \sqrt{\Delta^2 + \omega_R^2},$$

where, $\omega_R = \sqrt{n}|\lambda|$ is defined as Rabi frequency with zero detuning.

4.3.2.1 Conventional Rabi oscillations: Single photon limit

Consider the special limit where there is only one photon present. In this case, in an amplitude such as $\langle 0, 1, n|\Phi(t)\rangle$ the value of n is either one or zero. Hence the amplitude equations Eq.(4.2) and Eq.(4.3) for graphene reduces as follows,

$$\begin{aligned}
i\partial_t \langle 0,1,0|\Phi(t)\rangle &= (\vec{\sigma}_{BA}\cdot\vec{\epsilon})\,\langle 1,0,0|\Phi(t)\rangle + \lambda e^{-i\omega t}\,\langle 1,0,1|\Phi(t)\rangle,\\
i\partial_t \langle 0,1,1|\Phi(t)\rangle &= (\vec{\sigma}_{BA}\cdot\vec{\epsilon})\,\langle 1,0,1|\Phi(t)\rangle,\\
i\partial_t \langle 1,0,1|\Phi(t)\rangle &= (\vec{\sigma}_{AB}\cdot\vec{\epsilon})\,\langle 0,1,1|\Phi(t)\rangle + \lambda^* e^{i\omega t}\,\langle 0,1,0|\Phi(t)\rangle,\\
i\partial_t \langle 1,0,0|\Phi(t)\rangle &= (\vec{\sigma}_{AB}\cdot\vec{\epsilon})\,\langle 0,1,0|\Phi(t)\rangle
\end{aligned}$$

A solution to these coupled equations yield the amplitude Rabi frequency as,

$$\Omega_R = \frac{1}{2}\,(\Delta \pm \sqrt{\Delta^2 + \lambda^2}),$$

since the current density is defined as, $j \sim \psi_+^\dagger \psi_-$, the Rabi frequency associated with the current is given by the following expression,

$$\Omega_R = \sqrt{\Delta^2 + \lambda^2}.$$

Thus we can see that conventional Rabi oscillations are also present in the single photon limit in graphene (details missing from this section are contained in appendix)

4.3.3 Collapse and revival

In this section, we study the phenomenon of collapse and revival oscillations. These are well explained in various textbooks on quantum optics[45,47]. The phenomenon of collapse is the extinguishing of Rabi oscillations after a large number of cycles. This could be a purely classical effect brought about by dephasing, or more interestingly it could be due to the quantum nature of light which causes destructive interference that

progressively builds up and finally destroys the oscillations. This is in fact the case in the exactly solvable Jaynes Cummings (JC) model which describes a two level system coupled to a single mode photon. While collapse could be due to any one of these causes, the reverse phenomenon viz. revival is a purely quantum effect. Dephasing is irreversible and therefore cannot be the reason for revival. Revivals are caused when the destructive interference due to the quantum nature of light progressively diminishes revealing the original Rabi oscillations. We wish to study these phenomena both in the exactly solvable pseudospinless model (JC model) and also in graphene. Close to resonance $\omega \sim 2\epsilon$, both graphene and the JC model show identical behavior. Hence the collapse and revival oscillations in this case are identical to what may be found in textbooks. We therefore focus on the other extreme case namely far from resonance where only graphene is expected to show Rabi-like oscillations. Collapse and revival phenomena occur when the radiation is in a coherent state.

In the textbooks, the photon number states are used as basis where the calculations involve a saddle point approximation around a classical average number of photons $n = \langle n \rangle + \delta n$ which then leads to a closed formula for the dynamical variables which then is seen to exhibit collapse and revival oscillations. To see this, we first explicitly solve the equations Eq.(4.4) and Eq.(4.5). Since the terms $\langle ... \rangle_{\pm}$ are smaller than $\langle ... \rangle_s$ by factors of $\frac{\lambda}{\omega}$ or $\frac{\epsilon}{\omega}$, we may apply the initial conditions on the slow parts without introducing much error. We assert, $|\Phi(t)\rangle_s = |1,0\rangle|w\rangle$ where $|w\rangle$ is the boson coherent state[47,48,134] can be expressed in terms of vacuum state as,

$$|w\rangle = e^{-\frac{1}{2}\bar{w}w} e^{wb^\dagger} |0\rangle.$$

Solving Eq.(4.4) and Eq.(4.5) with the following initial condition at $t = 0$,

$$\langle 0,1,n|\Phi(0)\rangle_s = 0, \quad \langle 1,0,n|\Phi(0)\rangle_s = e^{-\frac{1}{2}\bar{w}w} \frac{w^n}{\sqrt{n!}}$$

we have the solution for slowly varying part,

$$\langle 0,1,n|\Phi(t)\rangle_s = -e^{-\frac{1}{2}\bar{w}w} \frac{w^n}{\sqrt{(n)!}} \frac{\epsilon^2}{\epsilon_{AB}\Omega_{AR}(n)} (e^{-i\Omega_-(n)t} - e^{-i\Omega_+(n)t}), \tag{4.9}$$

$$\langle 1,0,n|\Phi(t)\rangle_s = e^{-\frac{1}{2}\bar{w}w}\frac{\bar{w}^n}{\sqrt{n!}}\frac{1}{2\Omega_{AR}(n)}\left[\left(\omega\ \Omega_{AR}(n)+(2n+1)|\lambda|^2\right)e^{-i\Omega_+(n)t}\right.$$
$$\left.+\left(\omega\ \Omega_{AR}(n)-(2n+1)|\lambda|^2\right)e^{-i\Omega_-(n)t}\right] \tag{4.10}$$

and the solution for rapidly varying part,

$$\langle 0,1,n|\Phi(t)\rangle_+ = \frac{\lambda\sqrt{n+1}}{\omega}\ e^{-\frac{1}{2}\bar{w}w}\frac{w^{(n+1)}}{\sqrt{(n+1)!}}\frac{1}{2\omega\Omega_{AR}(n+1)}$$
$$\left[\left(\omega\ \Omega_{AR}(n+1)+(2n+3)|\lambda|^2\right)e^{-i\Omega_+(n+1)t}\right.$$
$$\left.+\left(\omega\ \Omega_{AR}(n+1)-(2n+3)|\lambda|^2\right)e^{-i\Omega_-(n+1)t}\right], \tag{4.11}$$

$$\langle 1,0,n|\Phi(t)\rangle_- = \frac{n\lambda^*}{\omega}\ e^{-\frac{1}{2}\bar{w}w}\frac{w^{n-1}}{\sqrt{n!}}\frac{\epsilon_{BA}}{\Omega_{AR}(n-1)}(e^{-i\Omega_-(n-1)t}-e^{-i\Omega_+(n-1)t}) \tag{4.12}$$

where the amplitude Rabi frequencies come out to be,

$$\Omega_\pm(n) = \frac{-|\lambda|^2 \pm 2\sqrt{|\lambda|^4(n+\frac{1}{2})^2+\epsilon^2\omega^2}}{2\omega}. \tag{4.13}$$

The polarization function in case of graphene can be defined as,

$$p(t) = \langle\Phi(t)|c_A^\dagger c_B|\Phi(t)\rangle,$$

inserting the completeness condition the above equation becomes,

$$p(t) = \sum_{n_A,n_B,n_\nu,n'_A,n'_B,n'_\nu}\langle\Phi(t)|n_A,n_B,n_\nu\rangle\langle n_A,n_B,n_\nu|c_A^\dagger c_B|n'_A,n'_B,n'_\nu\rangle\langle n'_A,n'_B,n'_\nu|\Phi(t)\rangle,$$

using the definition of creation (annihilation) operator we have,

$$p(t) = \sum_{n_A,n_B,n_\nu}\langle\Phi(t)|n_A,n_B,n_\nu\rangle\sqrt{n_A}\sqrt{n_B+1}\ \langle n_A-1,n_B+1,n_\nu|\Phi(t)\rangle,$$

only two possibility exist either ($n_A = 1$, $n_B = 0$) or ($n_A = 0$, $n_B = 1$) we have,

$$p(t) = \sum_{n=0}^{\infty} \langle \Phi(t)|1,0,n\rangle\langle 0,1,n|\Phi(t)\rangle. \tag{4.14}$$

In case of ARWA, the amplitude $\langle 0,1,n|\Phi(t)\rangle$ and $\langle \Phi(t)|1,0,n\rangle$ can be written as,

$$\langle 0,1,n|\Phi(t)\rangle = \langle 0,1,n|\Phi(t)\rangle_s + \langle 0,1,n|\Phi(t)\rangle_+ \, e^{-i\omega t} + \langle 0,1,n|\Phi(t)\rangle_- \, e^{i\omega t}$$

and,

$$\langle \Phi(t)|1,0,n\rangle = \langle 1,0,n|\Phi(t)\rangle_s^* + \langle 1,0,n|\Phi(t)\rangle_+^* \, e^{i\omega t} + \langle 1,0,n|\Phi(t)\rangle_-^* \, e^{-i\omega t}.$$

Since the amplitude $\langle \Phi(t)|1,0,n\rangle$ is the complex conjugate of $\langle 1,0,n|\Phi(t)\rangle$. Substituting these values in to the Eq.(4.14) and equating only the amplitude of the part of that oscillates as $e^{-i\omega t}$ is (we are interested only to take the coefficient of $e^{-i\omega t}$ because only this will survive after summing over 'k' and we can neglect the coefficient of $e^{i\omega t}$ since it contain $\frac{1}{\omega}$ term),

$$\begin{aligned} p_+(t) \;=\; & \sum_{n=0}^{\infty} \big((\langle 1,0,n|\Phi(t)\rangle_s)^* \; \langle 0,1,n|\Phi(t)\rangle_+ \\ & + (\langle 1,0,n+1|\Phi(t)\rangle_-)^* \; \langle 0,1,n+1|\Phi(t)\rangle_s \big) , \end{aligned}$$

after substituting all the values in to above polarization equation we have,

$$\begin{aligned} & p_+(t) = \sum_{n=0}^{\infty} \lambda \, e^{-\frac{1}{2}\bar{w}w} \frac{w(w\bar{w})^n}{n!\; 4\omega^3} \frac{1}{\Omega_{AR}(n)\Omega_{AR}(n+1)} \\ & \Big[\big(\omega \; \Omega_{AR}(n) + (2n+1)|\lambda|^2\big) \, e^{i\Omega_+(n)t} + \big(\omega \; \Omega_{AR}(n) - (2n+1)|\lambda|^2\big) \, e^{i\Omega_-(n)t} \Big] \\ & \Big[\big(\omega \; \Omega_{AR}(n+1) + (2n+3)|\lambda|^2\big) \, e^{-i\Omega_+(n+1)t} + \big(\omega \; \Omega_{AR}(n+1) - (2n+3)|\lambda|^2\big) \, e^{-i\Omega_-(n+1)t} \Big] \\ & - \sum_{n=0}^{\infty} \; e^{-\frac{1}{2}\bar{w}w} \frac{(w\bar{w})^n}{\bar{w}\; n!} \; \frac{n\lambda|\epsilon|^2}{\omega} \frac{1}{\Omega_{AR}(n-1)\Omega_{AR}(n)} \left((e^{i\Omega_-(n-1)t} - e^{i\Omega_+(n-1)t}) \right. \\ & \left. (e^{-i\Omega_-(n)t} - e^{-i\Omega_+(n)t}) \right) . \end{aligned}$$

Using the saddle point approximation we have (suppose we have the maximum distri-

bution at $n = \bar{n}$),

$$
\begin{aligned}
p_+(t) = & \sum_{n=0}^{\infty} e^{-\frac{1}{2}\bar{w}w} \frac{w\lambda(\bar{n})^n}{n!\ 4\omega^3} \frac{1}{\Omega_{AR}(\bar{n})\Omega_{AR}(\bar{n}+1)} \\
& \Big[\big(\omega\ \Omega_{AR}(\bar{n}) + (2\bar{n}+1)|\lambda|^2\big)\, e^{i(\Omega_+(\bar{n})+(n-\bar{n})\Omega'_+(\bar{n}))t} \\
& + \big(\omega\ \Omega_{AR}(\bar{n}) - (2\bar{n}+1)|\lambda|^2\big)\, e^{i(\Omega_-(\bar{n})+(n-\bar{n})\Omega'_-(\bar{n}))t} \Big] \\
& \Big[\big(\omega\ \Omega_{AR}(\bar{n}+1) + (2\bar{n}+3)|\lambda|^2\big)\, e^{-i(\Omega_+(\bar{n}+1)+(n-\bar{n})\Omega'_+(\bar{n}+1))t} \\
& + \big(\omega\ \Omega_{AR}(\bar{n}+1) - (2\bar{n}+3)|\lambda|^2\big)\, e^{-i(\Omega_-(\bar{n}+1)+(n-\bar{n})\Omega'_-(\bar{n}+1))t} \Big] \\
& - \sum_{n=0}^{\infty} e^{-\bar{w}w} \frac{(\bar{n})^n}{\bar{w}\ n!} \frac{\bar{n}\lambda|\epsilon|^2}{\omega} \frac{1}{\Omega_{AR}(\bar{n}-1)\Omega_{AR}(\bar{n})} \Big(e^{i(\Omega_-(\bar{n}-1)-(n-\bar{n})\Omega'_-(\bar{n}-1))t} \\
& - e^{i(\Omega_+(n-1)-(n-\bar{n})\Omega'_+(\bar{n}-1))t} \Big) \Big(e^{-i(\Omega_-(\bar{n})-(n-\bar{n})\Omega'_-(\bar{n}))t} - e^{-i(\Omega_+(\bar{n})-(n-\bar{n})\Omega'_+(\bar{n}))t} \Big),
\end{aligned}
$$

further simplification gives (for $\bar{n} \gg 1$),

$$
\begin{aligned}
p_+(t) \ \approx \ & \sum_{n=0}^{\infty} \frac{\lambda}{\omega}\ w\ e^{-\bar{n}} \frac{\bar{n}^n}{n!} \frac{(2\epsilon^2 + (\frac{1}{2}\Omega'_{AR}(\bar{n}) - \frac{2|\lambda|^2}{\omega})(\frac{1}{2}\Omega_{AR}(\bar{n}) + \frac{\bar{n}|\lambda|^2}{\omega}))}{\Omega^2_{AR}(\bar{n})} \\
& e^{i\Omega_{AR}(\bar{n})t} e^{i(n-\bar{n})\Omega'_{AR}(\bar{n})t}.
\end{aligned} \tag{4.15}
$$

This expression shows that there is a threshold behavior in the current density[53] in frequency domain with the threshold frequency (with $\epsilon = 0$) given by $\Omega_{AR,0} = 2\frac{(\bar{n}+1/2)|\lambda|^2}{\omega}$. Thus we shall be content at examining the expressions in this situation. The induced current density is given by $j(t) = j_+(t)e^{-i\omega t}$ where $j_+(t) = \sum_{\mathbf{k}} p_+(t)$ where $\epsilon = v_F|k|$. Therefore the envelope of the current density is,

$$
j_+(t) = \frac{1}{2\pi} \frac{|\lambda|^2}{4iv_F^2\omega t} \sum_{n=0}^{\infty} \frac{\lambda}{\omega}\ w\ e^{-\bar{n}}\ \frac{\bar{n}^n}{n!} e^{i\frac{2|\lambda|^2(\bar{n}+\frac{1}{2})}{\omega}t} e^{i(n-\bar{n})\frac{2|\lambda|^2}{\omega}t}. \tag{4.16}
$$

We see that the current density in the time domain has an oscillatory behavior governed by the threshold anomalous Rabi frequency $\Omega_{AR,0}$ and an envelope that has a power law decay ($\sim t^{-1}$) with exponent -1. This exponent is characteristic of the the linear dispersion of the single layer graphene quasiparticles, e.g. this exponent is different in bilayer graphene. After summing over all momenta we obtain Eq.(4.16) and if we plot the real part of its current density ($j_+(t)$) versus dimensionless time variable ($\frac{|\lambda^2|}{\omega}t$),

shows the anomalous collapse and revival but with the decreasing envelope amplitude governed by the factor $\frac{1}{t}$. The method for evaluating this sum over the integer n is described by Eberly et. al.[131] and also in various textbooks[45,47]. It involves noting that the Poisson distribution is sharply peaked at $n = \bar{n} \equiv \bar{w}w$ for $\bar{w}w \gg 1$ so that we may write $n = \bar{n} + (n - \bar{n})$ and ignore terms of order $(n - \bar{n})^2$ and higher. However it is important to retain the discrete summation over n (rather than replace by integration e.g.) since this leads to the phenomenon of revivals.

4.3.3.1 Collapse and revival time

From the expression (4.15), it is possible to extract the collapse and revival times. Revival occurs when successive terms interfere constructively. Thus if t_{rev} represents the revival time then $e^{i\Omega'_{AR}(\bar{n})t_{rev}} = 1$. This means the oscillations revive roughly (because we used the saddle point approximation) after every t_{rev} such that,

$$t_{rev} = \frac{2\pi m}{\Omega'_{AR}(\bar{n})}$$

where $m = 1, 2, ...$

To study the phenomenon of collapse, take the following terms from the expression (4.15) and let us say it as I,

$$I = \sum_{n=0}^{\infty} e^{-\bar{n}} \frac{\bar{n}^n}{n!} e^{i\Omega_{AR}(\bar{n})t} e^{i(n-\bar{n})\Omega'_{AR}(\bar{n})t}$$

after performing the summation we have,

$$I = e^{i\Omega_{AR}(\bar{n})t} e^{-i\bar{n}\Omega'_{AR}(\bar{n})t} e^{-\bar{n}} \; e^{\bar{n} \; Exp[it\Omega'_{AR}(\bar{n})]}$$

collapse occurs on a time scale small compared to t_{rev} so that we may expand as,

$$Exp[it\Omega'_{AR}(\bar{n})] \approx 1 + it\Omega'_{AR}(\bar{n}) + \frac{1}{2}(it\Omega'_{AR}(\bar{n}))^2 + ...$$

then we have,

$$I \approx e^{i\Omega_{AR}(\bar{n})t} \; e^{-\bar{n}\frac{1}{2}t^2\Omega'^2_{AR}(\bar{n})}$$

We define collapse time t_{col} as the time at which the amplitude is 1/10 of the original.

This means,

$$e^{-\bar{n}\frac{1}{2}t_{col}^2\Omega_{AR}'^2(\bar{n})} = \frac{1}{10}$$

so that,

$$t_{col} = \sqrt{\frac{2\log(10)}{\bar{n}\Omega_{AR}'^2(\bar{n})}}$$

We note that $\frac{t_{rev}}{t_{col}} = 2\pi\sqrt{\frac{\bar{n}}{2\log(10)}}$ which means it is sufficient to study any one of these times as a function of other parameters. Consider the two revival times: the revival time of conventional Rabi oscillation $t_{rev,R} = \frac{2\pi}{\Omega_R'(\bar{n})}$ and the revival time of anomalous Rabi oscillation $t_{rev,AR} = \frac{2\pi}{\Omega_{AR}'(\bar{n})}$. But we know from the earlier discussion that, $\Omega_R(\bar{n}) = \sqrt{\bar{n}}|\lambda|$ and $\Omega_{AR}(\bar{n}) = \frac{2\Omega_R^2(\bar{n})}{\omega} \approx \frac{2\bar{n}|\lambda|^2}{\omega}$ so that, $\Omega_R'(\bar{n}) = \frac{1}{2\sqrt{\bar{n}}}|\lambda|$ and $\Omega_{AR}'(\bar{n}) \approx \frac{2|\lambda|^2}{\omega}$. Therefore,

$$t_{rev,AR} = \frac{\omega\pi}{|\lambda|^2}; \quad t_{col,AR} = \frac{1}{2\pi}\sqrt{\frac{2\log(10)}{\bar{n}}}\frac{\omega\pi}{|\lambda|^2};$$

$$t_{rev,R} = \frac{4\pi\sqrt{\bar{n}}}{|\lambda|}; \quad t_{col,R} = \frac{1}{2\pi}\sqrt{2\log(10)}\frac{4\pi}{|\lambda|};$$

Till now we have discussed the coherent interaction of graphene with quantized EM field and demonstrated the phenomenon of anomalous Rabi oscillations. In the next section we compare the result obtained so far with the exactly solvable analogue of graphene which does not have pseudospin and show that the anomalous Rabi oscillations in graphene is because of its pseudospin nature.

4.4 Exactly solvable analogue of graphene: "Pseudospinless" graphene

In this section, we introduce a model that describes two species of fermionic oscillators coupled to a single mode photon. This is meant to isolate and highlight the role played by pseudospin in determining the nature of anomalous Rabi oscillations far from resonance in the presence of a quantized single mode photon field. We demonstrate through an exact solution and otherwise the central result viz. that anomalous oscillations far from resonance occur only in graphene or graphene-like systems that possess pseudospin. In addition, conventional Rabi oscillations seen in pseudospinless systems (e.g. the Jaynes Cummings model) are of course, also present.

Here we wish to show that in the ARWA limit, the amplitude of the part of current density which oscillates with the frequency of the external radiation in case of pseudospinless graphene is constant, whereas in the case of graphene this amplitude oscillates slowly with the anomalous Rabi frequency which we have already shown in the previous section.The Hamiltonian for the pseudospinless graphene that possesses all the attributes of graphene barring pseudospin is obtained by making the correspondence $c_A \rightarrow d^\dagger$, $c_B^\dagger \rightarrow c^\dagger$, where $d^\dagger$ creates one hole in the valence band and $c^\dagger$ creates one electron in the conduction band, but now the kinetic energy is chosen to be purely diagonal.

$$\hat{H}_{PSL} = \epsilon\ (c^\dagger c + d^\dagger\ d) + \lambda\ c^\dagger\ d^\dagger\ b + \lambda^*\ b^\dagger\ d\ c + \omega\ b^\dagger b. \tag{4.17}$$

Here the subscript 'PSL' stand for a pseudospinless system. These Hamiltonians are designed so that when the fields are treated classically, $b = \sqrt{n}$ - a constant, the results, both for graphene and the peudospinless system, are identical to the ones found in our earlier work[53]. Hence the reason for this particular choice of Hamiltonians. Furthermore, the Hamiltonian in Eq.(4.17) which we have been calling[53] PSL graphene deserves such an epithet only because we choose to think of ϵ as being linearly related to the momentum. Since the kinetic term is purely diagonal, it is also 'pseudospinless'. We make use of the observation that this model is exactly solvable even when b is an operator. This is not surprising since this model may be mapped to the well-known Jaynes-Cummings model through the following identifications,

$$\sigma_+ = c^\dagger d^\dagger;\ \sigma_- = dc$$

together with a unitary transformation on the photons which means we replace b with $be^{-i\omega t}$.

4.4.1 Equation of motion for the probability amplitude

A pseudospinless graphene system can be treated as a conventional semiconductor with zero band gap and linear energy-momentum relation near the vicinity of vanishing energy. In case of the PSL system each state has either (i) no electron or hole or (ii) one electron and one hole. This means the only non-zero amplitudes are $\langle 0, 0, n|\Phi(t)\rangle_{PSL,in}$ and $\langle 1, 1, n|\Phi(t)\rangle_{PSL,in}$. Using the Schrodinger/Dirac equation followed by the unitary transformation, the equation of motion for the probability amplitudes is given as (detail

calculations contained in the Appendix-C),

$$i\partial_t \langle 0,0,n|\Phi(t)\rangle_{PSL} = \sqrt{n}\lambda^* \; e^{i\omega t}\langle 1,1,n-1|\Phi(t)\rangle_{PSL}, \tag{4.18}$$

$$(i\partial_t - 2\epsilon) \;\; \langle 1,1,n-1|\Phi(t)\rangle_{PSL} = \sqrt{n}\lambda \; e^{-i\omega t}\langle 0,0,n|\Phi(t)\rangle_{PSL}, \tag{4.19}$$

where, the state $\langle 0,0,n|\Phi(t)\rangle_{PSL,in}$ and $\langle 0,0,n|\Phi(t)\rangle_{PSL}$ are related with the unitary transformation. Unlike the graphene equations Eq.(4.2) and Eq.(4.3) that require domain-specific approximate methods for their solution (to be discussed subsequently), the equations for the pseudospinless model viz. Eq.(4.18) and Eq.(4.19) are exactly solvable by virtue of being the same as the equations for the Jaynes Cummings model. The current density in case of graphene is defined by, $\vec{j} = \vec{\sigma}_{AB}c_A^\dagger c_B + \vec{\sigma}_{BA}c_B^\dagger c_A$, whereas in case of a pseudospinless system it is, $\vec{j}_{PSL} = -\vec{p}_{vc}(c^\dagger d^\dagger + dc)$. We wish to evaluate, the expectation value of current density in both the cases. In the case of graphene's toy model, we assume that there is one electron so that we have two possible states $(n_A, n_B) = (0,1),(1,0)$

$$\langle\vec{j}(t)\rangle = \vec{\sigma}_{BA}\sum_n \langle\Phi(t)|0,1,n\rangle\langle 1,0,n|\Phi(t)\rangle + \vec{\sigma}_{AB}\sum_n \langle\Phi(t)|1,0,n\rangle\langle 0,1,n|\Phi(t)\rangle,$$

whereas in case of pseudospinless system, we assert that (n_c, n_d) is either (0,0) or (1,1),

$$\langle\vec{j}_{PSL}(t)\rangle = -\vec{p}_{vc}\sum_n \left(\langle\Phi(t)|1,1,n\rangle\langle 0,0,n|\Phi(t)\rangle + \langle\Phi(t)|0,0,n\rangle\langle 1,1,n|\Phi(t)\rangle\right) \tag{4.20}$$

In case of graphene, the polarization function in our earlier work was defined by the following expression,

$$p(t) = \langle\Phi(t)|c_A^\dagger c_B|\Phi(t)\rangle = \sum_n \langle\Phi(t)|1,0,n\rangle\langle 0,1,n|\Phi(t)\rangle$$

whereas in case of PSL it is,

$$p_{PSL}(t) = \langle\Phi(t)|dc|\Phi(t)\rangle = \sum_n \langle\Phi(t)|0,0,n\rangle\langle 1,1,n|\Phi(t)\rangle \tag{4.21}$$

We now make the observation that the equations Eq.(4.18) and Eq.(4.19) for the PSL system (essentially the Jaynes Cummings model) may be solved through the following

substitution.

$$\langle 0,0,n|\Phi(t)\rangle_{PSL} = \langle 0,0,n|\Phi(t)\rangle_{PSL,r}\ e^{i\omega t} \tag{4.22}$$

We have observed earlier[53] that this is tied to the global symmetry, $\langle 1,1,n|\Phi(t)\rangle_{PSL} \rightarrow \langle 1,1,n|\Phi(t)\rangle_{PSL}\ e^{i\theta}$, $\langle 0,0,n|\Phi(t)\rangle_{PSL} \rightarrow \langle 0,0,n|\Phi(t)\rangle_{PSL}$, $\lambda \rightarrow e^{i\theta}\lambda$ enjoyed by the PSL equations. With this substitution, the solution for the PSL equations may be written down as follows,

$$\langle 0,0,n|\Phi(t)\rangle_{PSL,r} = \frac{e^{-\frac{1}{2}t(2i\epsilon+i\omega+iz)}}{2z}(2\epsilon(e^{itz}) + \omega + z + e^{itz}(-\omega+z)) \tag{4.23}$$

and,

$$\langle 1,1,n-1|\Phi(t)\rangle_{PSL} = -\frac{e^{-\frac{1}{2}t(2i\epsilon+i\omega+iz)}(-1+e^{itz})\lambda}{z}\sqrt{n} \tag{4.24}$$

where, $z = \sqrt{4n|\lambda|^2 + (-2\epsilon+\omega)^2}$. Substituting the above values of probability amplitudes into Eq.(4.20) and extracting the coefficient of $e^{-i\omega t}$ within ARWA limit allow us to conclude that there are no anomalous Rabi oscillations in this situation. The only Rabi oscillations occur close to resonance viz. $\omega \sim 2\epsilon$. However, the graphene system may not be solved by a simple substitution. But there are some limits in which the graphene system may also be studied. One is the semi-classical radiation limit. In this case $n = n^0 \gg 1$, a fixed quantity. Since now we may set $n-1 \approx n$, the equations Eq.(4.2) and Eq.(4.3) instead of being an infinite tower (in the variable n) of coupled equations, just becomes two coupled equations. One may then proceed to study them either using the conventional rotating wave approximation (RWA) or the newly introduced asymptotic RWA[53] valid far from resonance where we encountered the phenomenon of anomalous Rabi oscillation.

4.4.2 Analysis of 'pseudospinless' probability amplitude equations within ARWA

In order to examine the phenomenon of anomalous Rabi oscillations in 'pseudospinless' model of graphene in the extreme non-resonance condition we make the following substitutions in to the Eq.(4.18) and Eq.(4.19),

$$\langle 0,0,n|\Phi(t)\rangle_{PSL} = \langle 0,0,n|\Phi(t)\rangle + \langle 0,0,n|\Phi(t)\rangle_{+}\ e^{-i\omega t} + \langle 0,0,n|\Phi(t)\rangle_{-}\ e^{i\omega t}$$

and

$$\langle 1,1,n-1|\Phi(t)\rangle_{PSL} = \langle 1,1,n-1|\Phi(t)\rangle_s + \langle 1,1,n-1|\Phi(t)\rangle_+ \, e^{-i\omega t} + \langle 1,1,n-1|\Phi(t)\rangle_- \, e^{i\omega t}.$$

Upon substitution, the solution for the rapidly varying part becomes,

$$\langle 0,0,n|\Phi(t)\rangle_+ = 0, \quad \langle 0,0,n|\Phi(t)\rangle_- = -\frac{\sqrt{n}\lambda^*}{\omega} \, \langle 1,1,n-1|\Phi(t)\rangle_s,$$
$$\langle 1,1,n-1|\Phi(t)\rangle_+ = \frac{\sqrt{n}\lambda}{\omega} \, \langle 0,0,n|\Phi(t)\rangle_s, \quad \langle 1,1,n-1|\Phi(t)\rangle_- = 0$$

and the equation for the slowly varying part is,

$$i\partial_t \langle 0,0,n|\Phi(t)\rangle_s = \frac{n|\lambda|^2}{\omega} \, \langle 0,0,n|\Phi(t)\rangle_s,$$
$$i\partial_t \langle 1,1,n-1|\Phi(t)\rangle_s = \left(2\epsilon - \frac{n|\lambda|^2}{\omega}\right) \, \langle 1,1,n-1|\Phi(t)\rangle_s$$

leads to the following solution,

$$\langle 0,0,n|\Phi(t)\rangle_s = c_1 \, e^{-i\frac{n|\lambda|^2}{\omega}t}, \quad \langle 1,1,n-1|\Phi(t)\rangle_s = c_2 \, e^{2i\epsilon t} e^{-i\frac{n|\lambda|^2}{\omega}t},$$

where c_1 and c_2 are constants.

within ARWA limit, the Eq.(4.20) can be written as (we are interested to take only the coefficient of $e^{-i\omega t}$),

$$\begin{aligned}\langle \vec{j}_{PSL,+}(t)\rangle \;=\; & -\vec{p}_{vc} \sum_n \left(\langle \Phi(t)|1,1,n\rangle_s \langle 0,0,n|\Phi(t)\rangle_+ + \langle \Phi(t)|1,1,n\rangle_- \langle 0,0,n|\Phi(t)\rangle_s\right) \\ & -\vec{p}_{vc} \sum_n \left(\langle \Phi(t)|0,0,n\rangle_s \langle 1,1,n|\Phi(t)\rangle_+ + \langle \Phi(t)|0,0,n\rangle_- \langle 1,1,n|\Phi(t)\rangle_s\right)\end{aligned}$$

After substituting the value of probability amplitudes in the above expression leads to a constant term, we may conclude that there are no anomalous Rabi oscillations present in 'pseudospinless' model of graphene far extreme non-resonance.

4.5 Interpolation

As in the earlier work[53], we wish to find a single formula for the Rabi frequency that interpolates between the two regimes discussed above. The best way to solve

the graphene equations is by use of Fourier transforms. This method yielded[53] one formula for the Rabi frequency valid both close to resonance and far from resonance which matches with the results obtained by solving these equations separately in those limits. To this end, we make the following identifications.

$$\langle 0,1,n|\Phi(t)\rangle = \int_{-\infty}^{\infty} \frac{d\omega^{'}}{2\pi}\, e^{-i\omega^{'}t}\, f_{01}(n,\omega^{'});$$

$$\langle 1,0,n|\Phi(t)\rangle = \int_{-\infty}^{\infty} \frac{d\omega^{'}}{2\pi}\, e^{-i\omega^{'}t}\, f_{10}(n,\omega^{'}), \tag{4.25}$$

where, $f_{01}(n,\omega^{'})$ is the Fourier transform of $\langle 0,1,n|\Phi(t)\rangle$. Substituting these into the graphene equations above yields the following set of coupled double recursion relations,

$$\omega^{'}\ f_{01}(n,\omega^{'}) = \vec{\sigma}_{BA}\cdot\vec{\epsilon}\, f_{10}(n,\omega^{'}) + \sqrt{n+1}\lambda\ f_{10}(n+1,\omega^{'}-\omega), \tag{4.26}$$

$$\omega^{'}\ f_{10}(n+1,\omega^{'}) = \vec{\sigma}_{AB}\cdot\vec{\epsilon}\, f_{01}(n+1,\omega^{'}) + \sqrt{n+1}\lambda^{*}\ f_{01}(n,\omega^{'}+\omega) \tag{4.27}$$

We may also combine these two equations into one as,

$$c_1(\omega^{'},n)f_{01}(n,\omega^{'}) = a_1(\omega^{'},n)f_{01}(n-1,\omega^{'}+\omega) + b_1(\omega^{'},n)f_{01}(n+1,\omega^{'}-\omega) \tag{4.28}$$

by defining,

$$c_1(\omega^{'},n) = (\omega^{'} - \frac{\epsilon^2}{\omega^{'}} - \frac{(n+1)|\lambda|^2}{\omega^{'}-\omega});$$
$$a_1(\omega^{'},n) = (\vec{\sigma}_{BA}\cdot\vec{\epsilon})\ \frac{\sqrt{n}\lambda^{*}}{\omega^{'}};$$
$$b_1(\omega^{'},n) = \sqrt{n+1}\lambda\ \frac{(\vec{\sigma}_{AB}\cdot\vec{\epsilon})}{(\omega^{'}-\omega)}.$$

Include up to the first harmonics in Eq. (4.28) put $\omega^{'}\rightarrow\omega^{'}+\omega$ we have,

$$f_{01}(\omega^{'}+\omega,n-1) = \frac{b_1(\omega^{'}+\omega,n-1)}{c_1(\omega^{'}+\omega,n-1)}\, f_{01}(\omega^{'},n),$$

and put $\omega^{'}\rightarrow\omega^{'}-\omega$ in same equation we gave,

$$f_{01}(\omega^{'}-\omega,n+1) = \frac{a_1(\omega^{'}-\omega,n+1)}{c_1(\omega^{'}-\omega,n+1)}\, f_{01}(\omega^{'},n),$$

back substitution in to Eq.(4.28) gives,

$$c_1(\omega^{'},n) - a_1(\omega^{'},n)\,\frac{b_1(\omega^{'}+\omega,n-1)}{c_1(\omega^{'}+\omega,n-1)} - b_1(\omega^{'},n)\,\frac{a_1(\omega^{'}-\omega,n+1)}{c_1(\omega^{'}-\omega,n+1)} = 0.$$

Since Eq.(4.28) is a homogeneous system of equations, it defines an eigenvalue problem. The eigenvalues are precisely the variable $\omega^{'}$. An iterative solution of this eigenvalue problem yields a continued fraction description of the eigenvalue equation. The continued fraction method of solution of the Rabi problem has been introduced in the context of the study of Bloch-Siegert shift[112] by Swain[135,136].

$$\begin{aligned}
c_{2^n}(\omega^{'},n)\,f_{01}(n,\omega^{'}) &= a_{2^n}(\omega^{'},n)\,f_{01}(n-2^n,\omega^{'}+2^n\omega) \\
&\quad + b_{2^n}(\omega^{'},n)\,f_{01}(n+2^n,\omega^{'}-2^n\omega) \\
\\
c_{2^n}(\omega^{'},n) &= c_{2^{n-1}}(\omega^{'},n) - \frac{a_{2^{n-1}}(\omega^{'},n)\,b_{2^{n-1}}(\omega^{'}+2^{n-1}\omega,n-2^{n-1})}{c_{2^{n-1}}(\omega^{'}+2^{n-1}\omega,n-2^{n-1})} \\
&\quad - \frac{b_{2^{n-1}}(\omega^{'},n)\,a_{2^{n-1}}(\omega^{'}-2^{n-1}\omega,n+2^{n-1})}{C_{2^{n-1}}(\omega^{'}-2^{n-1}\omega,n+2^{n-1})} \qquad (4.29) \\
\\
a_{2^n}(\omega^{'},n) &= \frac{a_{2^{n-1}}(\omega^{'},n)\,a_{2^{n-1}}(\omega^{'}+2^{n-1}\omega,n-2^{n-1})}{c_{2^{n-1}}(\omega^{'}+2^{n-1}\omega,n-2^{n-1})} \\
\\
b_{2^n}(\omega^{'},n) &= \frac{b_{2^{n-1}}(\omega^{'},n)\,b_{2^{n-1}}(\omega^{'}-2^{n-1}\omega,n+2^{n-1})}{c_{2^{n-1}}(\omega^{'}-2^{n-1}\omega,n+2^{n-1})}
\end{aligned}$$

The Rabi frequency $\omega^{'}$ is determined by the solution of

$$c_{2^n}(\omega^{'},n) = 0$$

where n is the level of iteration. We saw in our earlier work[53], that choosing $n = 0$ amounts to ignoring all harmonics (even the first harmonic). This leads to an erroneous result for the Rabi frequency when $\omega \sim 2\epsilon$ (the conventional RWA), but is quite adequate for obtaining the ARWA result when $\epsilon \to 0$. Here too we find that when $\epsilon = 0$, $c_1(\omega^{'},n) = 0$ gives,

$$c_1(\omega^{'},n) \approx (\omega^{'} - \frac{(n+1)|\lambda|^2}{-\omega}) = 0.$$

Thus the Rabi frequency associated with the probability amplitude comes out as $\frac{(n+1)|\lambda|^2}{\omega}$ which is $\frac{\omega_R^2}{\omega}$ for n large compared to unity. The Rabi frequency associated with polarization and current is twice this value - a result that matches with the one obtained in the earlier work[53]. We need to do better of course. We need one equation that correctly describes both the regimes - the RWA and the ARWA regimes. Again, the earlier work shows the way. Just iterating once more gets the job done.

$$c_2(\omega^{'},n) \equiv f_2(\omega^{'},\omega,\epsilon) = \omega^{'} - \frac{\epsilon^2}{\omega^{'}} - \frac{|\lambda|^2(1+n)}{(\omega^{'}-\omega)} \tag{4.30}$$
$$-\frac{(1+n)\epsilon^2|\lambda|^2}{(\omega^{'}-\omega)^2(\omega^{'}-\frac{|\lambda|^2(2+n)}{(\omega^{'}-2\omega)}-\frac{\epsilon^2}{(\omega^{'}-\omega)}-\omega)} - \frac{n\epsilon^2|\lambda|^2}{\omega^{'2}(-\frac{|\lambda|^2 n}{\omega^{'}}+\omega^{'}+\omega-\frac{\epsilon^2}{(\omega^{'}+\omega)})} = 0.$$

Consider the two regions separately - (i) RWA: $\Delta \equiv \omega - 2\epsilon \ll \omega$ and $\epsilon \gg \omega_R \equiv \sqrt{|\lambda|^2 n}$ and (ii) ARWA: $\omega \gg \epsilon, \omega_R$ but $\omega\epsilon = b^2 \sim \omega_R^2$. In order to investigate case (i) we have to examine the limit,

$$Lim_{\epsilon\to\infty}\ f_2(\epsilon+x, 2\epsilon+\Delta, \epsilon) = 2x - \frac{|\lambda|^2(n+1)}{2(x-\Delta)} + O(\frac{1}{\epsilon}) = 0 \tag{4.31}$$

The conventional Rabi frequency associated with the probability amplitude is $\psi_\pm \sim e^{i\Omega_{R,\pm}t}$,

$$\Omega_\pm(n) = \epsilon + \frac{1}{2}(\Delta \pm \sqrt{|\lambda|^2(1+n)+\Delta^2}) \tag{4.32}$$

Thus the conventional Rabi frequency associated with the current $j \sim \psi_+^\dagger\psi_-$ is therefore,

$$\Omega_R(n) = \sqrt{|\lambda|^2(1+n)+\Delta^2} \tag{4.33}$$

This result matches the ones obtained in our earlier work[53] when $n \gg 1$. In order to investigate case (ii) we have to examine the limit,

$$Lim_{\omega\to\infty}\ f_2(\frac{x}{\omega},\omega,\frac{r}{\omega}) = \frac{1}{\omega}(|\lambda|^2(n+1) + \frac{r^2}{|\lambda|^2 n - x} + x) + O(\frac{1}{\omega^2}) = 0$$

Therefore, the anomalous Rabi frequency associated with the probability amplitude is,

$$\Omega_\pm(n) = \frac{1}{2\omega}(-|\lambda|^2 \pm \sqrt{|\lambda|^4(1+2n)^2+4r^2}). \tag{4.34}$$

The anomalous Rabi frequency matches with the one obtained earlier - Eq.(4.7), by a series solution of the differential equation. The ARWA frequency for the current is,

$$\Omega_{AR}(n) = 2\frac{\sqrt{|\lambda|^4(n+\frac{1}{2})^2+\epsilon^2\omega^2}}{\omega}. \tag{4.35}$$

These results are identical to what we obtained earlier. It is now important to ascertain that these values are retained when we do a further iteration. We have remarked that iterating the recursion Eq.(4.29) once (i.e. set $n = 1$) is sufficient to reproduce both the RWA and ARWA frequencies correctly. Now we must make sure that these expectations continue to hold even at the next level of iteration, i.e. $n = 2$. This is indeed the case since,

$$\begin{aligned} Lim_{\epsilon\to\infty} \quad & (f_4(\epsilon+x, 2\epsilon+\Delta, \epsilon) - f_2(\epsilon+x, 2\epsilon+\Delta, \epsilon)) = \frac{|\lambda|^4(n+1)(n+2)}{96(x-\Delta)^2\epsilon} \\ & +O(\frac{1}{\epsilon^2}) + ... \end{aligned} \tag{4.36}$$

Therefore, differences show up only at strong enough fields. In the ARWA case, the agreement is even more striking.

$$Lim_{\omega\to\infty}\ (f_4(\frac{x}{\omega}, \omega, \frac{r}{\omega}) - f_2(\frac{x}{\omega}, \omega, \frac{r}{\omega})) = -\frac{|\lambda|^4(n-1)nr^4}{2(|\lambda|^2 n - x)^2\omega^7}. \tag{4.37}$$

4.6 Results and discussion

In this section, we plot the graphs obtained from above calculations. In Fig.(4.1), the real part of the polarization for graphene $p_+(t)$ is plotted versus $t\frac{|\lambda|^2}{\omega}$ with $\bar{n} = 15$. This figure depicts anomalous Rabi oscillations followed by collapse and revival with this sequence repeating indefinitely (in the saddle point scheme). In the left plot of the Fig.(4.2) we see the collapse time associated with both conventional and anomalous Rabi oscillations in arbitrary units with a choice $\omega = 100$ and $|\lambda| = 1$ versus $\bar{n}$. Whereas the other plot of Fig.(4.2) we see the corresponding plot for the revival times.

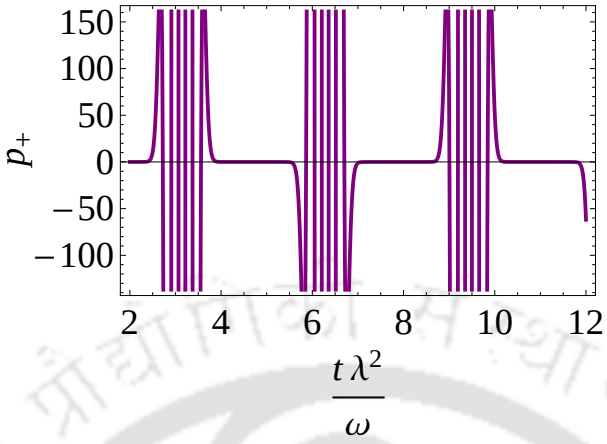

Figure 4.1: The figure depicts the collapse and revival phenomenon. The real part of the polarization is plotted versus time ($\frac{t|\lambda|^2}{\omega}$). To plot, we have taken $\bar{n} = 10$.

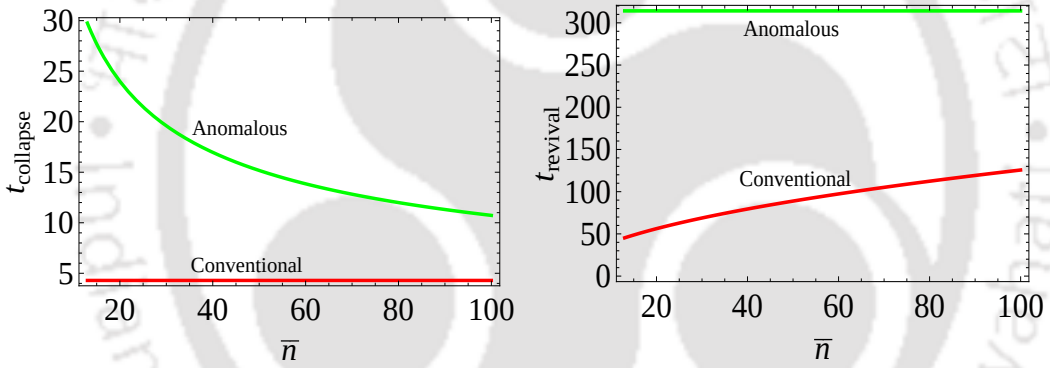

Figure 4.2: The above figures depicts the collapse times (left figure), revival time (right figure) versus the average number of photons $\bar{n}$.

4.7 Conclusions

In this chapter, we have conclusively established that the phenomenon of anomalous Rabi oscillations that occur far from resonance, shown to be unique to graphene-like systems in an earlier work and attributable to pseudospin, survive even when radiation is treated quantum mechanically. New phenomena such as zero-point or vacuum anomalous Rabi oscillations in graphene have now been predicted. In the presence of a coherent photon field, the phenomenon of collapse and revival is seen both in conventional and anomalous Rabi oscillations. The anomalous collapse and revival times of graphene are extracted and contrasted with the corresponding forms seen in the Jaynes

Cummings model.

Chapter 5

Summary, conclusions and future directions

In this thesis, we have investigated various coherent nonlinear phenomena that arise from an interaction of graphene with an electromagnetic field. The goal of the thesis is to study one of the well-known coherent optical effect viz. Rabi oscillations in graphene with the matter-field interaction treated both semiclassically as well as quantum mechanically. More specifically, it is the study of coherent Rabi oscillations in graphene in the presence of classical as well as quantum field in two different regimes namely close to conventional resonance and at far from resonance. Rabi oscillation is one of the well-studied optical phenomenon predicted theoretically a long time ago in case of two level systems. Conventionally, the phenomena of Rabi oscillations take place when the frequency of the incident optical field is nearly equal to the transition frequency of the two level systems, referred to as the resonance condition. This phenomenon is also seen in two-band systems such as semiconductors (with levels being replaced by bands) though this came a long time after its theoretical prediction in the 1980's. Far from resonance when the frequency of external radiation is large compared to the frequency corresponding to the energy of a particle-hole pair, the Rabi oscillations have not been observed in two level systems or in conventional semiconductors. In case of graphene, however, we predicted a second kind of Rabi oscillation that occur far-from resonance. Among all the peculiarities of graphene, pseudospin is one of the most striking which is not present in the conventional semiconductors. We have demonstrated in this thesis that the existence of anomalous Rabi oscillations is because of the pseudospin nature of graphene. Finally, we would like to present a brief summary of each of the chapters

in the following way.

chapter 1 is an introduction to the basic notions involved in this thesis. It includes a survey of relevant literature dating back to the work of Wallace on the electronic structure of graphite all the way to cutting edge applications of graphene being contemplated today.

In chapter 2, we proposed theoretically, a second kind of (anomalous) Rabi oscillations present in graphene. The main technical advancement reported here is the use of a new technique viz. an alternative to the well-known rotating wave approximation (which we have called 'asymptotic rotating wave approximation'). This alternative approach is applicable far from resonance, where it is able to show that for systems with pseudospin such as graphene, a second anomalous Rabi frequency is present, and the current density in the frequency domain exhibits a crossover from one kind of singular behavior close to the normal Rabi frequency to another kind of singular behavior close to the (typically smaller) anomalous Rabi frequency ($\frac{2\omega_R^2}{\omega}$). We have studied the phenomenon of crossover of Rabi oscillations as a function of detuning - the difference between the frequency of the incident wave and inter-band energy ($2v_F|k|$). It is shown by comparison with an exactly solved model with bands having linear dispersion but lacking pseudospin that this crossover is unique to graphene, attributable to the pseudospin character of the graphene Hamiltonian. This exactly solvable model also validates the asymptotic rotating wave approximation (this approximation on the solvable model agrees with the appropriate limit of the exact solution) which is the new technique introduced in this thesis. A group theoretic argument for why this model is solvable is given. We compute the nonlinear current using our formalism, the main prediction being the threshold behavior (with exponent equal to 1/2) of the slowly varying part of the current in the frequency domain with threshold frequency being $\frac{2\omega_R^2}{\omega}$ ('anomalous' Rabi frequency) where ω_R is the Rabi frequency for zero detuning. The novelty of our approach is the introduction of an alternative to the rotating wave approximation (RWA) (called asymptotic RWA here) which is argued to be important in demonstrating this crossover. We provide an interpolation method between these two regimes, that shows novel phenomena attributable to harmonic generation and also the new minima (resonances) in the effective Rabi frequency brought about by frequency doubling. A fully numerical solution to the Bloch equations verifies the analytical results and the various approximation schemes.

In chapter 3, we proposed an experimental technique - pump probe spectroscopy

that can detect anomalous Rabi oscillations in graphene. Pump-probe experiments are typically used to study relaxation phenomena in nonlinear optical systems, however, we use it as a tool to detect experimentally the phenomenon of anomalous Rabi oscillations in graphene which is a coherent phenomenon. Unlike, conventional Rabi oscillations, anomalous Rabi oscillations are unique to graphene (and possibly to surface states of topological insulators (TI)), attributable to the pseudospin (conventional spin for TI) degree of freedom and Dirac-fermion character of the graphene system. A pump pulse of a finite duration long enough to contain a large number of cycles induces a current density that oscillates with the frequency of the pump pulse. The amplitude associated with these fast oscillations is seen to exhibit much slower oscillations with a frequency equal to the anomalous Rabi frequency. This effect is easily probed by a probe pulse subsequent to the pump, where it manifests itself as periodic oscillations of the probe susceptibility as a function of pump duration at each probe frequency. Alternatively, it is also seen as an oscillatory function of the pump probe delay with other variables remaining fixed. This period corresponds to the anomalous Rabi frequency. An analysis of previously reported experimental data confirms the presence of anomalous Rabi oscillations in graphene.

In preceding two chapters, the study of anomalous Rabi oscillations has been reported in the presence of classical field. However, chapter 4 shows that both anomalous and conventional Rabi oscillations survive even with the radiation field treated quantum mechanically. New phenomena such as zero-point or vacuum anomalous Rabi oscillations in graphene have been predicted. This is to be expected for conventional Rabi oscillations, however, the prediction that anomalous Rabi oscillations also occur in the single-photon situation means that this notion of ARO is robust and not an artifact of approximations. We reported collapse and revival of both conventional and anomalous Rabi oscillations in response to a coherent radiation field. The anomalous collapse and revival times of graphene are extracted and contrasted with the corresponding forms seen in the Jaynes Cummings model.

In this thesis, we have discussed the coherent nonlinear optical response of graphene without taking into account the interaction between the charge carriers. Future research will be based upon the Coulomb interactions that are present between charge carriers in the system. The alternative to the rotating wave approximation namely, asymptotic RWA should pave the way for a detailed study of excitonic and other effects in graphene based systems and is hence likely to be of broad significance.

Appendix A

Detailed Calculations

In this appendix A, we present the detailed theoretical calculation of chapter 1 and chapter 2.

A.1 Derivation of low energy Hamiltonian in terms of creation(annihilation) operators

In order to derive the low energy Hamiltonian (2.1) in terms of the basis vectors $(c^{\dagger}_{p,A} \;\; c^{\dagger}_{p,B})$, rewrite the Hamiltonian (1.10) as (here 'q' is replaced by 'p'),

$$\hat{H} = \hbar v_F \begin{pmatrix} c^{\dagger}_{p,A} & c^{\dagger}_{p,B} \end{pmatrix} \begin{pmatrix} 0 & p_x + ip_y \\ p_x - ip_y & 0 \end{pmatrix} \begin{pmatrix} c_{p,A} \\ c_{p,B} \end{pmatrix}$$

After little simplification we have,

$$\hat{H} = \hbar v_F (p_x + ip_y)\, c^{\dagger}_{p,B} c_{p,A} + (p_x - ip_y)\, c^{\dagger}_{p,A} c_{p,B} = \hbar v_F \sum_{\alpha,\beta=A,B} (\vec{\sigma}\cdot\vec{p})_{\alpha,\beta}\, c^{\dagger}_{p,\alpha} c_{p,\beta}$$

A.2 Calculation for the value of population excess and polarization at time '$t = 0$'

In absence of field the Hamiltonian (2.1) can be written as,

$$\hat{H}_0 = \sum_{p,\alpha,\beta} c^{\dagger}_{p\alpha}\, (\vec{\sigma}.\vec{p})\, c_{p,\beta},$$

where, all parameters has been defined in chapter 1. The above Hamiltonian can be written in extended form as,

$$H_0 = \sum_p c^\dagger_{pA}\,(p_x - ip_y)\,c_{pB} + \sum_p c^\dagger_{pB}\,(p_x + ip_y)\,c_{pA}.$$

Expectation value of any operator can be written as,

$$\langle \hat{O} \rangle = \frac{Tr\left(e^{-\beta(H_0-\mu N)}\,\hat{O}\right)}{Z},$$

where, $Z = Tr(e^{-\beta(H_0-\mu N)})$ is the partition function, $\beta = \frac{1}{k\,T}$, k is the Boltazmaan constant, T is the temperature, μ is the chemical potential, $N = \sum_p (c^\dagger_{pA}\,c_{pA} + c^\dagger_{pB}\,c_{pB})$ is the number operator. We have to find out the expectation value polarization density defined as $p_0(k) = \langle c^\dagger_{kA}\,c_{kB}\rangle$,

$$\begin{aligned}\langle c^\dagger_{ps}\,c_{ps'}\rangle &= \frac{Tr\left(e^{-\beta(H_0-\mu N)}\,c^\dagger_{ps}\,c_{ps'}\right)}{Z} = \frac{Tr\left(c_{ps'}\,e^{-\beta(H_0-\mu N)}\,c^\dagger_{ps}\right)}{Z} \\ &= \frac{Tr\left(e^{-\beta(H_0-\mu N)}\,e^{\beta(H_0-\mu N)}\,c_{ps'}\,e^{-\beta(H_0-\mu N)}\,c^\dagger_{ps}\right)}{Z}.\end{aligned}$$

Define, $f(\beta, s') = e^{\beta(H_0-\mu N)}\,c_{ps'}\,e^{-\beta(H_0-\mu N)}$ differentiate w.r.t. β we have,

$$\frac{\partial}{\partial\beta} f(\beta, s') = e^{\beta(H_0-\mu N)}\,[(H_0 - \mu N), c_{ps'}]\,e^{-\beta(H_0-\mu N)}.$$

One can easily find the value of $[(H_0 - \mu N), c_{ps'}]$ using operator's commutation relation as,

$$\begin{aligned}[(H_0 - \mu N), c_{pA}] &= -v_F\,(p_x - ip_y)\,c_{pB} + \mu\,c_{pA}, \\ [(H_0 - \mu N), c_{pB}] &= -v_F\,(p_x + ip_y)\,c_{pA} + \mu\,c_{pB}.\end{aligned}$$

After substituting these values in to the above equation we have,

$$\frac{\partial}{\partial\beta} f(\beta, A) = e^{\beta(H_0-\mu N)}\;\left(-v_F\,(p_x - ip_y)\,c_{pB} + \mu\,c_{pA}\right)\;e^{-\beta(H_0-\mu N)}$$

and,

$$\frac{\partial}{\partial\beta} f(\beta, B) = e^{\beta(H_0-\mu N)}\;\left(-v_F\,(p_x + ip_y)\,c_{pA} + \mu\,c_{pB}\right)\;e^{-\beta(H_0-\mu N)}$$

After solving these coupled equations we have,

$$f(\beta, A) = e^{\beta\mu}\ \left(c_{pA}\cosh(pv_F\beta) - \frac{p_x - ip_y}{|p|}\ c_{pB}\sinh(pv_F\beta)\right),$$
$$f(\beta, B) = e^{\beta\mu}\ \left(c_{pB}\cosh(pv_F\beta) - \frac{p_x + ip_y}{|p|}\ c_{pA}\sinh(pv_F\beta)\right)$$

Hence the equation for $\langle c^\dagger_{ps}\ c_{pA}\rangle$,

$$\langle c^\dagger_{ps}\ c_{pA}\rangle = \frac{Tr\left(e^{-\beta(H_0-\mu N)}\ f(\beta, A)\ c^\dagger_{ps}\right)}{Z},$$
$$\langle c^\dagger_{ps}\ c_{pB}\rangle = \frac{Tr\left(e^{-\beta(H_0-\mu N)}\ f(\beta, B)\ c^\dagger_{ps}\right)}{Z}$$

Putting the value of $f(\beta, A)$ and $f(\beta, B)$ in to the above equations we have,

$$\langle c^\dagger_{ps}\ c_{pA}\rangle = \frac{Tr\left(e^{-\beta(H_0-\mu N)}\ e^{\beta\mu}\ \left(c_{pA}\cosh(pv_F\beta) - \frac{p_x-ip_y}{|p|}\ c_{pB}\sinh(pv_F\beta)\right)\ c^\dagger_{ps}\right)}{Z},$$
$$\langle c^\dagger_{ps}\ c_{pB}\rangle = \frac{Tr\left(e^{-\beta(H_0-\mu N)}\ e^{\beta\mu}\ \left(c_{pB}\cosh(pv_F\beta) - \frac{p_x+ip_y}{|p|}\ c_{pA}\sinh(pv_F\beta)\right)\ c^\dagger_{ps}\right)}{Z}$$

or,

$$\langle c^\dagger_{ps}\ c_{pA}\rangle = e^{\beta\mu}\ \left((\delta_{s,A} - \langle c^\dagger_{ps}\ c_{pA}\rangle\cosh(pv_F\beta) - \frac{p_x - ip_y}{|p|}\ (\delta_{s,B} - \langle c^\dagger_{ps}\ c_{pB}\rangle\ \sinh(pv_F\beta)\right),$$
$$\langle c^\dagger_{ps}\ c_{pB}\rangle = e^{\beta\mu}\ \left((\delta_{s,B} - \langle c^\dagger_{ps}\ c_{pB}\rangle\ \cosh(pv_F\beta) - \frac{p_x + ip_y}{|p|}\ (\delta_{s,A} - \langle c^\dagger_{ps}\ c_{pA}\rangle\ \sinh(pv_F\beta)\right)$$

Solving above coupled equations at temperature T=0 or $\beta \to \infty$ we get,

$$\langle c^\dagger_{ps}\ c_{pA}\rangle = \frac{\frac{1}{2}(\delta_{s,A} - \delta_{s,B}\frac{p_x-ip_y}{|p|})e^{\beta(pv_F-\mu)} + \delta_{s,A}}{e^{\beta(pv_F-\mu)}+1}.$$

Here we have two cases,

A.2.1 When $v_F|\mathbf{p}| > \mu$

$$\langle c^\dagger_{ps}\ c_{pA}\rangle = \frac{1}{2}\left(\delta_{s,A} - \delta_{s,B}\frac{p_x - ip_y}{|p|}\right)\ ;\ \langle c^\dagger_{ps}\ c_{pB}\rangle = \frac{1}{2}\left(\delta_{s,B} - \delta_{s,A}\frac{p_x + ip_y}{|p|}\right).$$

A.2.2 When $v_F|\mathbf{p}| < \mu$

$$\langle c_{ps}^{\dagger}\ c_{pA}\rangle = \delta_{s,A}\ ;\ \ \langle c_{ps}^{\dagger}\ c_{pB}\rangle = \delta_{s,B}.$$

Finally, the equilibrium zero temperature distributions are,

$$\langle c_{ps}^{\dagger}\ c_{pA}\rangle = \Theta(v_F|p| - \mu)\ \frac{1}{2}(\delta_{s,A} - \delta_{s,B}\frac{p_x - ip_y}{|p|}) + \Theta(\mu - v_F|p|)\ \delta_{s,A},$$
$$\langle c_{ps}^{\dagger}\ c_{pB}\rangle = \Theta(v_F|p| - \mu)\ \frac{1}{2}(\delta_{s,B} - \delta_{s,A}\frac{p_x + ip_y}{|p|}) + \Theta(\mu - v_F|p|)\ \delta_{s,B}$$

where, $\Theta(x)$ is the step function.

Thus we can write the value of population density and polarization density at t=0,

$$N_A = \langle c_{pA}^{\dagger}\ c_{pA}\rangle = \frac{1}{2}\Theta(v_F|p| - \mu) + \Theta(\mu - v_F|p|),$$
$$N_B = \langle c_{pB}^{\dagger}\ c_{pB}\rangle = \frac{1}{2}\Theta(v_F|p| - \mu) + \Theta(\mu - v_F|p|)$$

$$p_0 = \langle c_{pA}^{\dagger}\ c_{pB}\rangle = -\Theta(v_F|p| - \mu)\ \frac{p_x + ip_y}{2|p|},\quad p_0^{*} = \langle c_{pB}^{\dagger}\ c_{pA}\rangle = -\Theta(v_F|p| - \mu)\ \frac{p_x - ip_y}{2|p|}$$

which is the value of polarization density at t=0.

A.3 Current density calculations

In second quantization language, low energy hamiltonian for graphene (2.1) in absence of field can be expressed as,

$$\hat{H} = \int\ d^2r'\ v_F\ \left(c_A^{\dagger}(\vec{r'},t)(p_x^{'} - ip_y^{'})c_B(\vec{r'},t) + c_B^{\dagger}(\vec{r'},t)(p_x^{'} + ip_y^{'})c_A(\vec{r'},t)\right).$$

From Heisenberg equation of motion,

$$i\hbar\partial_t\ \hat{A} = [\hat{A}, \hat{H}].$$

To calculate the expression for current density we use the equation of continuity

$$\vec{\nabla}\cdot\hat{J}(\vec{r},t) + \partial_t\hat{\rho}(\vec{r},t) = 0,$$

where, $\hat{\rho}(\vec{r},t) = e\ c_A^\dagger(\vec{r},t)\ c_A(\vec{r},t) + e\ c_B^\dagger(\vec{r},t)\ c_B(\vec{r},t)$ defined as the charge density,

First we have to calculate the equation for charge density. With the help of above Heisenberg equation we can get the following result easily (To derive these equations we have used the property of Dirac delta function),

$$i\hbar\partial_t\ c_A(\vec{r},t) = v_F\ (p_x - ip_y)\ c_B(\vec{r},t), \quad i\hbar\partial_t\ c_B(\vec{r},t) = v_F\ (p_x + ip_y)\ c_A(\vec{r},t)$$
$$i\hbar\partial_t\ c_A^\dagger(\vec{r},t) = v_F\ (p_x + ip_y)\ c_B^\dagger(\vec{r},t), \quad i\hbar\partial_t\ c_B^\dagger(\vec{r},t) = v_F\ (p_x - ip_y)\ c_A(\vec{r},t)$$

Equation of motion for $\hat{\rho}(\vec{r},t)$ is given by,

$$i\hbar\partial_t\ \hat{\rho}(\vec{r},t) = e\ \left(i\hbar\partial_t\ c_A^\dagger(\vec{r},t)\right)\ c_A(\vec{r},t) + e\ c_A^\dagger(\vec{r},t)\ (i\hbar\partial_t\ c_A(\vec{r},t))$$
$$+e\ \left(i\hbar\partial_t\ c_B^\dagger(\vec{r},t)\right)\ c_B(\vec{r},t) + e\ c_B^\dagger(\vec{r},t)\ (i\hbar\partial_t\ c_B(\vec{r},t))\,,$$

after putting the values the above equation becomes,

$$\begin{aligned} i\hbar\partial_t\ \hat{\rho}(\vec{r},t) \ &= \ (e\ v_F\ (p_x + ip_y)\ c_B^\dagger(\vec{r},t))\ c_A(\vec{r},t) + c_A^\dagger(\vec{r},t)\ (e\ v_F\ (p_x - ip_y)\ c_B(\vec{r},t)) \\ &\quad +(e\ v_F\ (p_x - ip_y)\ c_A^\dagger(\vec{r},t))\ c_B(\vec{r},t) + c_B^\dagger(\vec{r},t)\ (e\ v_F\ (p_x + ip_y)\ c_A(\vec{r},t)), \end{aligned}$$

since $p_x = i\hbar\frac{\partial}{\partial x}$ and $p_y = i\hbar\frac{\partial}{\partial y}$ are operators, using these properties we have,

$$i\hbar\partial_t\ \hat{\rho}(\vec{r},t) = e\ v_F\ (p_x + ip_y)\ (c_B^\dagger(\vec{r},t)\ c_A(\vec{r},t)) + e\ v_F\ (p_x - ip_y)\ (c_A^\dagger(\vec{r},t)\ c_B(\vec{r},t)),$$

or,

$$\partial_t\hat{\rho}(\vec{r},t) = \frac{1}{i\hbar}\ e\ v_F\ \left((p_x + ip_y)\ P^\dagger(\vec{r},t) + (p_x - ip_y)\ P(\vec{r},t)\right),$$

where, $P(\vec{r},t) = c_A^\dagger(\vec{r},t)\ c_B(\vec{r},t)$ is defined as polarization density and $P^\dagger(\vec{r},t) = c_B^\dagger(\vec{r},t)\ c_A(\vec{r},t)$ as hermitian conjugate of $P(\vec{r},t)$.

Using equation of continuity we have,

$$j_x = e\ v_F\ (P^\dagger(\vec{r},t) + P(\vec{r},t)), \quad j_y = i\ e\ v_F\ (P^\dagger(\vec{r},t) - P(\vec{r},t))$$

or,

$$J(\vec{r},t) = j_x\ \hat{x} + j_y\ \hat{y} = e\ v_F\ P^\dagger(\vec{r},t)(\hat{x} + i\hat{y}) + e\ v_F\ P(\vec{r},t)(\hat{x} - i\hat{y})$$

Using Pauli's matrices, the expression for current density,

$$J(\vec{r},t) = e\ v_F\ P^{\dagger}(\vec{r},t)\ \vec{\sigma}_{BA} + e\ v_F\ P(\vec{r},t)\ \vec{\sigma}_{AB}$$

A.4 Analysis of Bloch equation in RWA regime

Bloch equation (2.2) and (2.3) can be written in matrix form as (including complex conjugate of Eq. (2.3)),

$$i\ \partial_t \begin{pmatrix} n_{diff}(\vec{k},t) \\ p(\vec{k},t) \\ p^*(\vec{k},t) \end{pmatrix} = \begin{pmatrix} 0 & 2z_k & -2z_k^* \\ z_k^* & 0 & 0 \\ -z_k & 0 & 0 \end{pmatrix} \begin{pmatrix} n_{diff}(\vec{k},t) \\ p(\vec{k},t) \\ p^*(\vec{k},t) \end{pmatrix}$$
$$+ \begin{pmatrix} 0 & -2z_A^* & 2z_A \\ -z_A & 0 & 0 \\ z_A^* & 0 & 0 \end{pmatrix} \begin{pmatrix} n_{diff}(\vec{k},t) \\ p(\vec{k},t) \\ p^*(\vec{k},t) \end{pmatrix} \tag{A.1}$$

where, $z_k = v_F\ (\vec{\sigma}_{AB} \cdot \vec{k})$ and $z_A = v_F\ (\vec{\sigma}_{BA} \cdot \frac{e}{c}\vec{A}(t))$.

Diagonalize the first matrix of Eqn (A.1) (matrix corresponding to unperturbed hamiltonian) than after make the following substitutions,

$$\begin{pmatrix} n_{diff}(\vec{k},t) \\ p(\vec{k},t) \\ p^*(\vec{k},t) \end{pmatrix} = \begin{pmatrix} 0 & 2\sqrt{\frac{z_k^*}{z_k}} & -2\sqrt{\frac{z_k^*}{z_k}} \\ \frac{z_k^*}{z_k} & -\frac{z_k^*}{z_k} & -\frac{z_k^*}{z_k} \\ 1 & 1 & 1 \end{pmatrix} \begin{pmatrix} \tilde{n}_{diff}(\vec{k},t) \\ \tilde{p}(\vec{k},t) \\ \tilde{p}'(\vec{k},t) \end{pmatrix}$$

After substitution, Eqn (A.1) becomes,

$$i\ \partial_t \begin{pmatrix} \tilde{n}_{diff}(\vec{k},t) \\ \tilde{p}(\vec{k},t) \\ \tilde{p}'(\vec{k},t) \end{pmatrix} = \begin{pmatrix} 0 & 0 & 0 \\ 0 & -2v_F|k| & 0 \\ 0 & 0 & 2v_F|k| \end{pmatrix} \begin{pmatrix} \tilde{n}_{diff}(\vec{k},t) \\ \tilde{p}(\vec{k},t) \\ \tilde{p}'(\vec{k},t) \end{pmatrix}$$
$$+ \begin{pmatrix} 0 & \frac{-z_A z_k + z_A^* z_k^*}{v_F|k|} & \frac{z_A z_k - z_A^* z_k^*}{v_F|k|} \\ \frac{z_A z_k - z_A^* z_k^*}{2v_F|k|} & \frac{z_A z_k + z_A^* z_k^*}{v_F|k|} & 0 \\ \frac{-z_A z_k + z_A^* z_k^*}{2v_F|k|} & 0 & -\frac{z_A z_k + z_A^* z_k^*}{v_F|k|} \end{pmatrix} \begin{pmatrix} \tilde{n}_{diff}(\vec{k},t) \\ \tilde{p}(\vec{k},t) \\ \tilde{p}'(\vec{k},t) \end{pmatrix}$$

Applying RWA after making the substitutions, $\tilde{p}'(\vec{k},t) = e^{-2iv_F|k|t}P'(\vec{k},t)$, $\tilde{p}(\vec{k},t) =$

$e^{2iv_F|k|t}P(\vec{k},t)$ we have,

$$i\partial_t\tilde{n}_{diff}(\vec{k},t) = -e^{-i\Delta t}\frac{z_R z_k}{v_F|k|}P(\vec{k},t) - \frac{z_R^* z_k^*}{v_F|k|}e^{i\Delta t}P^{'}(\vec{k},t)$$

$$i\partial_t P(\vec{k},t) = -e^{i\Delta t}\frac{z_R^* z_k^*}{2v_F|k|}\tilde{n}_{diff}(\vec{k},t)$$

$$i\partial_t P^{'}(\vec{k},t) = -e^{-i\Delta t}\frac{z_R z_k}{2v_F|k|}\tilde{n}_{diff}(\vec{k},t)$$

where, $\Delta = \omega - 2v_F|k|$. Further substitution $P^{'}(\vec{k},t) = e^{-i\Delta t}\ u^{'}(\vec{k},t)$, $P(\vec{k},t) = e^{i\Delta t}\ u(\vec{k},t)$ gives the above equations in to the following form,

$$i\partial_t\tilde{n}_{diff}(\vec{k},t) = -\frac{z_R z_k}{v_F|k|}\ u(\vec{k},t) - \frac{z_R^* z_k^*}{v_F|k|}\ u^{'}(\vec{k},t)$$

$$i\partial_t u(\vec{k},t) - \Delta\ u(\vec{k},t) = -\frac{z_R^* z_k^*}{2v_F|k|}\tilde{n}_{diff}(\vec{k},t)$$

$$i\partial_t u^{'}(\vec{k},t) + \Delta\ u^{'}(\vec{k},t) = -\frac{z_R z_k}{2v_F|k|}\tilde{n}_{diff}(\vec{k},t)$$

After solving these coupled equations we have,

$$u(\vec{k},t) = A(\vec{k})\ \sin(\sqrt{\Delta^2+\omega_R^2}\ t) + B(\vec{k})\ (1-\cos(\sqrt{\Delta^2+\omega_R^2}\ t))$$

$$u^{'}(\vec{k},t) = A^{'}(\vec{k})\ \sin(\sqrt{\Delta^2+\omega_R^2}\ t) + B^{'}(\vec{k})\ (1-\cos(\sqrt{\Delta^2+\omega_R^2}\ t))$$

where, A($\vec{k}$), B($\vec{k}$), A$^{'}$($\vec{k}$), and B$^{'}$($\vec{k}$) are the 'k' dependent coefficients. Back substitution gives the following set of equations for $\tilde{n}_{diff}(\vec{k},t)$,

$$-\Delta\ B(\vec{k}) + A(\vec{k})\ i\ \sqrt{\Delta^2+\omega_R^2}\ \cos(\sqrt{\Delta^2+\omega_R^2}\ t) + \Delta\ B(\vec{k})\ \cos(\sqrt{\Delta^2+\omega_R^2}\ t)$$

$$+B(\vec{k})\ i\ \sqrt{\Delta^2+\omega_R^2}\ \sin(\sqrt{\Delta^2+\omega_R^2}\ t) - \Delta\ A(\vec{k})\ \sin(\sqrt{\Delta^2+\omega_R^2}\ t)$$

$$= -\frac{z_R^* z_k^*}{2v_F|k|}\tilde{n}_{diff}(\vec{k},t)$$

and,

$$\Delta\ B^{'}(\vec{k}) + A^{'}(\vec{k})\ i\ \sqrt{\Delta^2+\omega_R^2}\ \cos(\sqrt{\Delta^2+\omega_R^2}\ t) - \Delta\ B^{'}(\vec{k})\ \cos(\sqrt{\Delta^2+\omega_R^2}\ t)$$

$$+B^{'}(\vec{k})\ i\ \sqrt{\Delta^2+\omega_R^2}\ \sin(\sqrt{\Delta^2+\omega_R^2}\ t)+\Delta\ A^{'}(\vec{k})\ \sin(\sqrt{\Delta^2+\omega_R^2}\ t)$$
$$=-\frac{z_R z_k}{2v_F|k|}\tilde{n}_{diff}(\vec{k},t)$$

The value of the coefficients at t=0 (since we know that $n_{diff}(\vec{k},0)=0$ and $p(\vec{k},0)=-\theta(v_F|k|-\mu)\frac{z_k^*}{2v_F|k|}$),

$$A(\vec{k})=\frac{z_R^*}{4i\ \sqrt{\Delta^2+\omega_R^2}}\theta(v_F|k|-\mu),\quad B(\vec{k})=-\frac{z_R^*\ \Delta}{4\ (\Delta^2+\omega_R^2)}\theta(v_F|k|-\mu)$$

$$A^{'}(\vec{k})=\frac{z_R z_k}{z_k^*}\ \frac{1}{4i\ \sqrt{\Delta^2+\omega_R^2}}\theta(v_F|k|-\mu),\quad B^{'}(\vec{k})=\frac{z_R z_k}{z_k^*}\ \frac{\Delta}{4\ (\Delta^2+\omega_R^2)}\theta(v_F|k|-\mu)$$

Hence the solution for $\tilde{n}_{diff}(\vec{k},t)$, $u(\vec{k},t)$ and $u^{'}(\vec{k},t)$ is given by,

$$\tilde{n}_{diff}(\vec{k},t)=-\frac{v_F|k|}{z_k^*}\ \frac{\Delta^2\ \theta(v_F|k|-\mu)}{2\ (\Delta^2+\omega_R^2)}-\frac{v_F|k|}{2z_k^*}\ \frac{\omega_R^2\ \theta(v_F|k|-\mu)}{(\Delta^2+\omega_R^2)}\ \cos(\sqrt{\Delta^2+\omega_R^2}\ t)$$

$$u(\vec{k},t)=\frac{z_R^*\ \theta(v_F|k|-\mu)}{4i\ \sqrt{\Delta^2+\omega_R^2}}\ \sin(\sqrt{\Delta^2+\omega_R^2}\ t)-\frac{z_R^*\ \Delta\ \theta(v_F|k|-\mu)}{4\ (\Delta^2+\omega_R^2)}\ (1-\cos(\sqrt{\Delta^2+\omega_R^2}\ t))$$

$$u^{'}(\vec{k},t)=\frac{z_R z_k}{z_k^*}\ \frac{\theta(v_F|k|-\mu)}{4i\ \sqrt{\Delta^2+\omega_R^2}}\ \sin(\sqrt{\Delta^2+\omega_R^2}\ t)+\frac{z_R z_k}{z_k^*}\ \frac{\Delta\ \theta(v_F|k|-\mu)}{4\ (\Delta^2+\omega_R^2)}\ (1-\cos(\sqrt{\Delta^2+\omega_R^2}\ t))$$

Back substitution gives the solution for $n_{diff}(\vec{k},t)$, $p(\vec{k},t)$ as,

$$n_{diff}(\vec{k},t)=\frac{\theta(v_F|k|-\mu)}{2i\ (v_F|k|)\ \sqrt{\Delta^2+\omega_R^2}}(z_k^* z_R^*\ e^{i\omega t}-z_k z_R\ e^{-i\omega t})\ \sin(\sqrt{\Delta^2+\omega_R^2}\ t)$$

$$-\frac{\Delta\ \theta(v_F|k|-\mu)}{2(v_F|k|)\ (\Delta^2+\omega_R^2)}(z_k^* z_R^*\ e^{i\omega t}+z_k z_R\ e^{-i\omega t})\ (1-\cos(\sqrt{\Delta^2+\omega_R^2}\ t))$$

and,

$$p(\vec{k},t)=\left(\frac{-(v_F|k|)\ \Delta^2\ \theta(v_F|k|-\mu)}{2z_k\ (\Delta^2+\omega_R^2)}+\frac{z_k^* z_R^*\ \Delta\ \theta(v_F|k|-\mu)}{4z_k\ (\Delta^2+\omega_R^2)}\ e^{i\omega t}-\frac{z_R\ \Delta\ \theta(v_F|k|-\mu)}{4(\Delta^2+\omega_R^2)}e^{-i\omega t}\right)$$

$$-\left(\frac{z_k^* z_R^*\ \theta(v_F|k|-\mu)}{4iz_k(\sqrt{\Delta^2+\omega_R^2})}e^{i\omega t}+\frac{z_R\ \theta(v_F|k|-\mu)}{4i\ (\sqrt{\Delta^2+\omega_R^2})}e^{-i\omega t}\right)\sin(\sqrt{\Delta^2+\omega_R^2}\ t)$$

$$-\left(\frac{(v_F|k|){\omega_R}^2\,\theta(v_F|k|-\mu)}{2z_k\,(\Delta^2+\omega_R^2)}+\frac{z_k^* z_R^*\,\Delta\,\theta(v_F|k|-\mu)}{4z_k\,(\Delta^2+\omega_R^2)}e^{i\omega t}-\frac{z_R\,\Delta\,\theta(v_F|k|-\mu)}{4(\Delta^2+\omega_R^2)}e^{-i\omega t}\right)\cos(\sqrt{\Delta^2+\omega_R^2}\,t)$$

Appendix B

Detailed Calculations

In this appendix we present the detail calculations of chapter 3.

B.1 Probe equations

The pump equations,

$$i\partial_t\, n_{diff}(\vec{k},t) = 2(z_k - z_A^*(t))\, p(\vec{k},t) - 2(z_k^* - z_A(t))\, p^*(\vec{k},t)$$

$$i\partial_t\, p(\vec{k},t) = (z_k^* - z_A(t))\, n_{diff}(\vec{k},t)$$

To get the probe response make the following substitutions in to above equations,

$$n_{diff}(\vec{k},t) \to n_{diff}(\vec{k},t) + \delta n_{diff}(\vec{k},t), p(\vec{k},t) \to p(\vec{k},t) + \delta p(\vec{k},t),$$
$$z_A(t) \to z_A(t) + \delta z_A(t)$$

$$\begin{aligned} i\partial_t\, (n_{diff}(\vec{k},t) + \delta n_{diff}(\vec{k},t)) &= 2(z_k - z_A^*(t) - \delta z_A^*(t))\, (p(\vec{k},t) + \delta p(\vec{k},t)) \\ &\quad -2(z_k^* - z_A(t) - \delta z_A(t))\, (p^*(\vec{k},t) + \delta p^*(\vec{k},t)) \end{aligned}$$

$$i\partial_t\, (p(\vec{k},t) + \delta p(\vec{k},t)) = (z_k^* - z_A(t) - \delta z_A(t))\, (n_{diff}(\vec{k},t) + \delta n_{diff}(\vec{k},t))$$

or,

$$\begin{aligned} i\partial_t\ \delta n_{diff}(\vec{k},t) &= 2(z_k - z_A^*(t))\ \delta p(\vec{k},t) - 2\delta z_A^*(t))\ (p(\vec{k},t) + \delta p(\vec{k},t)) \\ &\quad -2(z_k^* - z_A(t))\ \delta p^*(\vec{k},t) + 2\delta z_A(t)\ (p^*(\vec{k},t) + \delta p^*(\vec{k},t)) \end{aligned}$$

$$i\partial_t\ \delta p(\vec{k},t) = (z_k^* - z_A(t))\ \delta n_{diff}(\vec{k},t) - \delta z_A(t))\ (n_{diff}(\vec{k},t) + \delta n_{diff}(\vec{k},t))$$

while deriving the Linearized Bloch equations we have taken the non-overlapping case i.e. there is finite time duration between the pump and probe field. keeping this assumption in mind we can ignore the terms; $z_A^*(t)\ \delta p(\vec{k},t), z_A(t)\ \delta p^*(\vec{k},t), z_A(t)\ \delta n_{diff}(\vec{k},t)$, and we can neglect the terms $\delta z_A^*(t)\ \delta p(\vec{k},t), \delta z_A(t)\ \delta p^*(\vec{k},t)$, since it is the product of probe field and probe response.

Hence the linearized Bloch equations,

$$i\partial_t\ \delta n_{diff}(\vec{k},t) = 2z_k\ \delta p(\vec{k},t) - 2\delta z_A^*(t)\ p(\vec{k},t) - 2z_k^*\ \delta p^*(\vec{k},t) + 2\delta z_A(t)\ p^*(\vec{k},t)$$

$$i\partial_t\ \delta p(\vec{k},t) = z_k^*\ \delta n_{diff}(\vec{k},t) - \delta z_A(t)\ n_{diff}(\vec{k},t)$$

Appendix C

Detailed Calculations

In this appendix we present the detail calculations of chapter 4.

C.1 Probability amplitude equation for graphene

The objective is to find the probability amplitude equation for the state $\langle 0,1,n|\phi(t)\rangle_{in}$ and $\langle 1,0,n|\phi(t)\rangle_{in}$. Initially let us find the general probability amplitude equation for $\langle n_A, n_B, n_\nu|\phi(t)\rangle_{in}$ using the Hamiltonian (4.1) and with the following Schodinger/Dirac equation,

$$i\hbar\, \partial_t|\phi(t)\rangle = \hat{H}\, |\phi(t)\rangle$$

From the completeness condition (taking $\hbar = 1$) ,

$$i\, \partial_t|\phi(t)\rangle = \sum_{n'_A,n'_B,n'_\nu} \hat{H}\, (|n'_A, n'_B, n'_\nu\rangle\langle n'_A, n'_B, n'_\nu|)\, |\phi(t)\rangle$$

using the following relations,

$$\hat{c}\, |n\rangle = \sqrt{n}\, |n-1\rangle, \quad \hat{c}^\dagger\, |n\rangle = \sqrt{n+1}\, |n+1\rangle$$

After some straight forward calculation, the equation of motion becomes,

$$
\begin{aligned}
i\,\partial_t|\phi(t)\rangle = &\sum_{n'_A,n'_B,n'_\nu} (\vec{\sigma}_{AB}\cdot\vec{\epsilon})\ \sqrt{(n'_A+1)n'_B}\ |n'_A+1,n'_B-1,n'_\nu\rangle\langle n'_A,n'_B,n'_\nu|\phi(t)\rangle\\
&+\sum_{n'_A,n'_B,n'_\nu} (\vec{\sigma}_{BA}\cdot\vec{\epsilon})\ \sqrt{n'_A(n'_B+1)}\ |n'_A-1,n'_B+1,n'_\nu\rangle\langle n'_A,n'_B,n'_\nu|\phi(t)\rangle\\
&+\sum_{n'_A,n'_B,n'_\nu} \lambda^*\sqrt{(n'_A+1)n'_B(n'_\nu+1)}\ |n'_A+1,n'_B-1,n'_\nu+1\rangle\langle n'_A,n'_B,n'_\nu|\phi(t)\rangle\\
&+\sum_{n'_A,n'_B,n'_\nu} \lambda\sqrt{n'_A(n'_B+1)n'_\nu}\ |n'_A-1,n'_B+1,n'_\nu-1\rangle\langle n'_A,n'_B,n'_\nu|\phi(t)\rangle\\
&+\sum_{n'_A,n'_B,n'_\nu} \omega\ n'_\nu|n'_A,n'_B,n'_\nu\rangle\langle n'_A,n'_B,n'_\nu|\phi(t)\rangle
\end{aligned}
$$

or,

$$
\begin{aligned}
i\,\partial_t\langle n_A,n_B,n_\nu|\phi(t)\rangle = &\sum_{n'_A,n'_B,n'_\nu} (\vec{\sigma}_{AB}\cdot\vec{\epsilon})\ \sqrt{(n'_A+1)n'_B}\ \delta_{n_A,n'_A+1}\delta_{n_B,n'_B-1}\delta_{n_\nu,n'_\nu}\langle n'_A,n'_B,n'_\nu|\phi(t)\rangle\\
&+\sum_{n'_A,n'_B,n'_\nu} (\vec{\sigma}_{BA}\cdot\vec{\epsilon})\ \sqrt{n'_A(n'_B+1)}\ \delta_{n_A,n'_A-1}\delta_{n_B,n'_B+1}\delta_{n_\nu,n'_\nu}\langle n'_A,n'_B,n'_\nu|\phi(t)\rangle\\
&+\sum_{n'_A,n'_B,n'_\nu} \lambda^*\sqrt{(n'_A+1)n'_B(n'_\nu+1)}\ \delta_{n_A,n'_A+1}\delta_{n_B,n'_B-1}\delta_{n_\nu,n'_\nu+1}\langle n'_A,n'_B,n'_\nu|\phi(t)\rangle\\
&+\sum_{n'_A,n'_B,n'_\nu} \lambda\sqrt{n'_A(n'_B+1)n'_\nu}\ \delta_{n_A,n'_A-1}\delta_{n_B,n'_B+1}\delta_{n_\nu,n'_\nu-1}\langle n'_A,n'_B,n'_\nu|\phi(t)\rangle\\
&+\sum_{n'_A,n'_B,n'_\nu} \omega\ n'_\nu\ \delta_{n_A,n'_A}\delta_{n_B,n'_B}\delta_{n_\nu,n'_\nu}\ \langle n'_A,n'_B,n'_\nu|\phi(t)\rangle
\end{aligned}
$$

Hence the equation of motion for the $\langle n_A,n_B,n_\nu|\phi(t)\rangle$ is given by,

$$
\begin{aligned}
&i\,\partial_t\langle n_A,n_B,n_\nu|\phi(t)\rangle = (\vec{\sigma}_{AB}\cdot\vec{\epsilon})\ \sqrt{n_A(n_B+1)}\ \langle n_A-1,n_B+1,n_\nu|\phi(t)\rangle\\
&+(\vec{\sigma}_{BA}\cdot\vec{\epsilon})\ \sqrt{(n_A+1)n_B}\ \langle n_A+1,n_B-1,n_\nu|\phi(t)\rangle\\
&+\lambda^*\sqrt{n_A(n_B+1)n_\nu}\ \langle n_A-1,n_B+1,n_\nu-1|\phi(t)\rangle\\
&+\lambda\sqrt{(n_A+1)n_B(n_\nu+1)}\ \langle n_A+1,n_B-1,n_\nu+1|\phi(t)\rangle+\omega\ n_\nu\ \langle n_A,n_B,n_\nu|\phi(t)\rangle
\end{aligned}
$$

To find the equation of motion for $\langle 0,1,N|\phi(t)\rangle_{in}$, put $n_A = 0,\ n_B = 1,\ n_\nu = N$ we have,

$$\begin{aligned} i\,\partial_t\langle 0,1,N|\phi(t)\rangle_{in} &= (\vec{\sigma}_{BA}\cdot\vec{\epsilon})\ \langle 1,0,N|\phi(t)\rangle_{in} + \lambda\,\sqrt{N+1}\,\langle 1,0,N+1|\phi(t)\rangle_{in} \\ &\quad +\omega\ N\ \langle 0,1,N|\phi(t)\rangle_{in} \end{aligned}$$

Again to find the equation of motion for $\langle 1,0,N+1|\phi(t)\rangle_{in}$, put $n_A = 1,\ n_B = 0,\ n_\nu = N+1$,

$$\begin{aligned} i\,\partial_t\langle 1,0,N+1|\phi(t)\rangle_{in} &= (\vec{\sigma}_{AB}\cdot\vec{\epsilon})\ \langle 0,1,N+1|\phi(t)\rangle_{in} + \lambda^*\,\sqrt{N+1}\,\langle 0,1,N|\phi(t)\rangle_{in} \\ &\quad +\omega\ N\ \langle 1,0,N|\phi(t)\rangle_{in} \end{aligned}$$

Make the following unitary transformation,

$$\langle 0,1,N|\phi(t)\rangle_{in} = \langle 0,1,N|\phi(t)\rangle\ e^{-i\omega nt},\quad \langle 1,0,N|\phi(t)\rangle_{in} = \langle 1,0,N|\phi(t)\rangle\ e^{-i\omega nt}$$

Hence the equation of motion for $\langle 0,1,N|\phi(t)\rangle$ and $\langle 1,0,N|\phi(t)\rangle$ are given by,

$$i\,\partial_t\langle 0,1,N|\phi(t)\rangle = (\vec{\sigma}_{BA}\cdot\vec{\epsilon})\ \langle 1,0,N|\phi(t)\rangle + \lambda\,\sqrt{N+1}\,e^{-i\omega t}\,\langle 1,0,N+1|\phi(t)\rangle$$

and,

$$i\,\partial_t\langle 1,0,N+1|\phi(t)\rangle = (\vec{\sigma}_{AB}\cdot\vec{\epsilon})\ \langle 0,1,N+1|\phi(t)\rangle + \lambda^*\,\sqrt{N+1}\,e^{i\omega t}\,\langle 0,1,N|\phi(t)\rangle$$

C.2 Probability amplitude equation for "pseudospinless" graphene

The general equation for the probability amplitude $\langle n_c,n_d,n_\nu|\phi(t)\rangle$ using the "pseudospinless" graphene Hamiltonian (4.17) is given by,

$$i\partial_t\ \langle n_c,n_d,n_\nu|\phi(t)\rangle = \langle n_c,n_d,n_\nu|\hat{H}_{PSL}|\phi(t)\rangle$$

using the similar derivation from the earlier section one can easily find the following equation of motion,

$$i\partial_t \langle n_c, n_d, n_\nu|\phi(t)\rangle = \epsilon\,(n_c+n_d)\,\langle n_c, n_d, n_\nu|\phi(t)\rangle + \lambda\,\sqrt{n_c n_d(n_\nu+1)}$$
$$\langle n_c-1, n_d-1, n_\nu+1|\phi(t)\rangle + \lambda^*\,\sqrt{(n_c+1)(n_d+1)n_\nu}\,\langle n_c+1, n_d+1, n_\nu-1|\phi(t)\rangle$$
$$+\omega n_\nu\,\langle n_c, n_d, n_\nu|\phi(t)\rangle$$

To find the equation of motion for $\langle 0,0,n|\phi(t)\rangle_{PSL,in}$ and $\langle n_c, n_d, n_\nu|\phi(t)\rangle_{PSL,in}$ put $n_c=0, n_d=0, n_\nu=n$ and $n_c=1, n_d=1, n_\nu=n-1$ respectively, we get,

$$i\partial_t\,\langle 0,0,n|\phi(t)\rangle_{PSL,in} = \lambda^*\,\sqrt{n}\,\langle 1,1,n-1|\phi(t)\rangle_{PSL,in} + \omega n\,\langle 0,0,n|\phi(t)\rangle_{PSL,in}$$

and,

$$\begin{aligned} i\partial_t\,\langle 1,1,n-1|\phi(t)\rangle_{PSL,in} &= 2\epsilon\,\langle 1,1,n-1|\phi(t)\rangle_{PSL,in} + \lambda\,\sqrt{n}\,\langle 0,0,n|\phi(t)\rangle \\ &\quad +\omega(n-1)\,\langle 1,1,n-1|\phi(t)\rangle_{PSL,in} \end{aligned}$$

using the unitary transformation $\langle 0,0,n|\phi(t)\rangle_{PSL,in} = \langle 0,0,n|\phi(t)\rangle_{PSL}\,e^{-i\omega nt}$ and $\langle 1,1,n-1|\phi(t)\rangle_{PSL,in} = \langle 1,1,n-1|\phi(t)\rangle_{PSL}\,e^{-i\omega(n-1)t}$ we get the desired equation of motion,

$$i\partial_t\,\langle 0,0,n|\phi(t)\rangle_{PSL} = \lambda^*\,\sqrt{n}\,\langle 1,1,n-1|\phi(t)\rangle_{PSL}$$

and,

$$i\partial_t\,\langle 1,1,n-1|\phi(t)\rangle_{PSL} = 2\epsilon\,\langle 1,1,n-1|\phi(t)\rangle_{PSL} + \lambda\,\sqrt{n}\,e^{-i\omega t}\,\langle 0,0,n|\phi(t)\rangle_{PSL}$$

Bibliography

[1] S. Iijima, J. Cryst. Growth **50**, 675 (1980).

[2] S. Iijima, Nature **354**, 56 (1991).

[3] K. S. Novoselov, A. K. Geim, S. V. Morozov, D. Jiang, Y. Zhang, and S. V. Dubonos et al., Science **306**, 666 (2004).

[4] A. H. C. Neto, F. Guinea, N. M. R. Peres, K. S. Novoselov, and A. K. Geim, Rev. Mod. Phys. **81**, 109 (2008).

[5] A. J. van Bommel, J. E. Crombeen, and A. van Tooren, Surf. Sci. **48**, 463 (1975).

[6] H. P. Boehm et al., Z. Naturforschung **17b**, 150 (1962).

[7] X. Lu, M. Yu, H. Huang, and R. S. Ruoff, Nanotechnology **10**, 269 (1999).

[8] R. B. Little, J. Cluster Sci. **14**, 135 (2003).

[9] C. Berger et al., J. Phys. Chem. B **108**, 19912 (2004).

[10] M. I. Katsnelson and K. S. Novoselov, Solid State Commun. **143**, 3 (2007).

[11] A. M. J. Schakel, Phys. Rev. D **43**, 1428 (1991).

[12] J. Gonzalez, F. Guinea, and M. A. H. Vozmediano, Phys. Rev. Lett. **77**, 3589 (1996).

[13] E. V. Gorbar, V. P. Gusynin, V. A. Miransky, and I. A. Shovkovy, Phys. Rev. B **66**, 045108 (2002).

[14] M. I. Katsnelson, Euro. Phys. J. B **51**, 157 (2006).

[15] M. I. Katsnelson, K. S. Novoselov, and A. K. Geim, Nat. Phys. **2**, 620 (2006).

[16] J. Tworzydlo, B. Trauzettel, M. Titov, A. Rycerz, and C. W. J. Beenakker, Phys. Rev. Lett. **96**, 246802 (2006).

[17] N. D. Mermin, Phys. Rev. **176**, 250 (1967).

[18] J. C. Semenoff, Phys. Rev. Lett. **53**, 2449 (1984).

[19] E. Fradkin, Phys. Rev. B **33**, 3263 (1986).

[20] F. D. M. Haldane, Phys. Rev. Lett. **61**, 2015 (1988).

[21] P. M. Ostrovsky and I. V. Gornyi, Phys. Rev. B **74**, 235443 (2006).

[22] Y. Y. Wang, Z. H. Ni, Z. X. Shen, H. M. Wang, and Y. H. Wu, Appl. Phys. Lett. **92**, 043121 (2008).

[23] J. S. Park, A. Reina, R. Saito, J. Kong, G. Dresselhaus, and M. S. Dresselhaus, Carbon **47**, 1303 (2009).
[24] D. Graf, The Eur. Phys. J. Spl. Top. **148**, 171 (2007).
[25] Y. y. Wang et al., J. Phys. Chem. C **112**, 10637 (2008).
[26] Z. H. Ni et al., Phys. Rev. B **77**, 115416 (2008).
[27] A. C. Ferrari et al., Phys. Rev. Lett. **97**, 187401 (2006).
[28] W. S. Boyle and P. Nozieres, Phys. Rev. **111**, 782 (1958).
[29] F. Bassani and E. Tosatti, Phys. Lett. **27**, 446 (1968).
[30] A. B. Djurisic and E. H. Li, J. Appl. Phys. **85**, 7404 (1999).
[31] I. Ohlidal and F. Vizda, J. Mod. Opt. **46**, 2043 (1999).
[32] R. Saito, G. Dresselhaus, and M. S. Dresselhaus, *Physical Properties of carbon Nanotubes*, Imperial College Press, 1998.
[33] C. Kittel, *Introduction to Solid State Physics, 7th edition*, John Wiley and Sons, Singapur, 1996.
[34] N. W. Ashcroft and N. D. Mermin, *Solid State Physics*, Harcourt Brace, Fort Worth, 1976.
[35] P. R. Wallace, Phys. Rev. **71**, 622 (1947).
[36] S. Reich, J. Maultzsch, and C. Thomsen, Phys. Rev. B **66**, 035412 (2002).
[37] C. Bena and G. Montambaux, New J. Phys. **11**, 095003 (2009).
[38] Y. Hasegawa, R. Konno, H. Nakano, and M. Kohmoto, Phys. Rev. B **74**, 033413 (2006).
[39] A. J. Legget, **(Lecture notes 21)**, Physics Department, University of Illinois, Urbana (Fall 2009, url-http://online.physics.uiuc.edu/courses/phys598PTD//fall09/L21.pdf).
[40] I. K. Piyush Pushkar, *Graphene: Band Structure (Video)*, url-http://www.youtube.com/watch?v=FGJ5bynuzSA, March, 2011.
[41] K. S. Novoselov et al., Proc. Natl Acad. Sci. USA **102**, 10451 (2005).
[42] K. S. Novoselov et al., Nature **438**, 197 (2005).
[43] Y. Zhang, Y.-W. Tan, H. L. Stormer, and P. Kim, Nature **438**, 201 (2005).
[44] J. Baringhaus et.al., Nature **http://www.nature.com/nature/journal/vaop/ncurrent/full/nature12952.html** (2014).
[45] L. Allen and J. H. Eberly, *Optical Resonances and Two-Level Atoms*, Wiley and Sons, 1975.
[46] H. Haug and S. W. Koch, *Quantum Theory of Optical and Electronic Properties of Semiconductors*, World Scientific, 2004.
[47] C. Gerry and P. Knight, *Introductory Quantum Optical*, Cambridge University

Press, 2005.
[48] L. Mandel and E. Wolf, *Optical Coherence and Quantum Optics*, Cambridge University Press, 1995.
[49] R. W. Boyd, *Nonlinear Optics*, Academic Press, 2008.
[50] P. A. Lee, Phys. Rev. Lett. **71**, 1887 (1993).
[51] A. W. W. Ludwig, M. P. A. Fisher, R. Shankar, and G. Grinstein, Phys. Rev. B **50**, 7426 (1994).
[52] K. Ziegler, Phys. Rev. Lett. **80**, 3113 (1998).
[53] Enamullah, V. Kumar, and G. S. Setlur, Physica B **407**, 4600 (2012).
[54] E. G. Mishchenko, Phys. Rev. Lett. **103**, 246802 (2009).
[55] K. L. Ishikawa, Phys. Rev. B **82**, 201402 (2010).
[56] Enamullah, V. Kumar, U. Kumar, and G. S. Setlur, J. Opt. Soc. Am. B **31**, 484 (2014).
[57] S. Kumar, M. Anija, N. Kamaraju, K. S. Vasu, K. S. Subrahmanyam, A. K. Sood, and C. N. R. Rao, Appl. Phys. Lett. **95**, 191911 (2009).
[58] M. Breusing et al., Phys. Rev. B **83**, 153410 (2011).
[59] P. Blake et al., Appl. Phys. Lett. **91**, 063124 (2007).
[60] Z. H. Ni et al., Nano Lett. **7**, 2758 (2007).
[61] R. R. Nair et al., Science **320**, 1308 (2008).
[62] J. M. Dawlaty, S. Shivaramam, M. Chandrashekhar, F. Rana, and M. G. Spencer, Appl. Phys. Lett. **92**, 042116 (2008).
[63] J. Shang, Z. Luo, C. Cong, J. Lin, T. Yu, and G. G. Gurzadyan, Appl. Phys. Lett. **97**, 163103 (2010).
[64] P. A. George, J. Strait, J. M. Dawlaty, S. Shivaraman, M. Chandrashekhar, F. Rana, and M. G. Spencer, Nano Lett. **8**, 4248 (2008).
[65] B. A. Ruzicka, L. K. Werake, H. Zhao, S. Wang, and K. P. Loh, Appl. Phys. Lett. **96**, 173106 (2010).
[66] H. Wang, J. H. Strait, P. A. George, S. Shivaraman, and V. B. Shields et al., Appl. Phys. Lett. **96**, 081917 (2010).
[67] T. M. Rusin and W. Zawadzki, Phys. Rev. B **80**, 045416 (2009).
[68] N. Stander, B. Huard, and D. G. Gorden, Phys. Rev. Lett. **102**, 026807 (2009).
[69] V. Lukose, R. Shankar, and G. Baskaran, Phys. Rev. Lett. **98**, 116802 (2007).
[70] P. Recher et al., Phys. Rev. B **76**, 235404 (2007).
[71] S. Russo, J. B. Oostinga, D. Wehenkel, H. B. Heersche, and S. S. Sobhani, Phys. Rev. B **77**, 085413 (2008).
[72] K. S. Novoselov et al., Nat. Phys. **2**, 177 (2006).
[73] V. P. Gusynin and S. G. Sharapov, Phys. Rev. Lett. **95**, 146801 (2005).

[74] X. Du, I. Skachko, F. Duerr, A. Luican, and E. Y. Andrei, Nature **462**, 192 (2009).
[75] K. I. Bolotin, F. Ghahari, M. D. Shulman, H. L. Stormer, and P. Kim, Nature **462**, 196 (2009).
[76] V. Singh and M. M. Deshmukh, Phys. Rev. B **80**, 081404(R) (2009).
[77] A. B. Kuzmenko, E. van Heumen, F. Carbone, and D. van der Marel, Phys. Rev. B **77**, 085413 (2008).
[78] V. P. Gusynin, S. G. Sharapov, and J. P. Carbotte, New J. Phys. **11**, 095013 (2009).
[79] Y. W. Tan et al., Phys. Rev. Lett. **99**, 245803 (2007).
[80] C. Beneventano, P. Giacconi, E. Santangelo, and R. Soldati, J. Phys. A: Math. Theor. **42**, 275401 (2009).
[81] A. K. Geim and K. S. Novoselov, Nature Mat. **6**, 183 (2007).
[82] W. A. de Heer et.al, Solid State Commun. **143**, 92 (2007).
[83] P. W. Sutter, J.-I. Flege, and E. A. Sutter, Nature Mat. **7**, 406 (2008).
[84] S. Bae et al., Nature Nanotechnology **5**, 574 (2010).
[85] K. S. Kim et al., Nature **457**, 706 (2009).
[86] J. Yan et al., Nature Nanotechnology **7**, 472 (2012).
[87] A. V. Fedorov et. al., Nature Communications **5**, 3257 (2014).
[88] G. Profeta, M. Calandra, and F. Mauri, Nat. Phys. **8**, 131 (2012).
[89] L. Gengchiau, S. B. Kumar, M. B. A. Jalil, and S. G. Tan, Appl. Phys. Lett. **99(8)**, 083107 (2011).
[90] F. Schedin, A. K. Geim, S. V. Morozov, E. W. Hill, P. Blake, M. I. Katsnelson, and K. S. Novoselov, Nature Mat. **6**, 652 (2007).
[91] Z. H. Ni, T. Yu, Y. H. Lu, Y. Y. Wang, Y. P. Feng, and Z. X. Shen, ACS Nano **2(11)**, 2301 (2008).
[92] E. W. Hill, A. K. Geim, F. Schedin, and P. Blake, IEEE Trans. Magn. **42**, 2694 (2006).
[93] H. B. Heersche, P. Jarillo-Herrero, J. B. Oostinga, L. M. K. Vandersypen, and A. F. Morpurgo, Nature **446**, 56 (2007).
[94] I. I. Rabi, Phys. Rev. **51**, 652 (1937).
[95] M. Lindberg and S. W. Koch, Phys. Rev. B **38**, 3342 (1988).
[96] R. Binder, S. W. Koch, M. Lindberg, N. Peyghambarian, and W. Schafer, Phys. Rev. Lett. **65**, 899 (1990).
[97] M. Welkowsky and R. Braunstein, Phys. Rev. B **5**, 497 (1972).
[98] L. Banyai, I. Galbraith, C. Ell, and H. Haug, Phys. Rev. B **36**, 6099 (1987).
[99] M. Sinada and S. Sigano, J. Phys. Soc. Jpn. **21**, 1936 (1966).

[100] S. Schmitt-Rink, D. Chemla, and H. Haug, Phys. Rev. B **37**, 941 (1988).
[101] N. Kosugi, S. Matsuo, K. Konno, and N. Hatakenaka, Phys. Rev. B **72**, 172509 (2005).
[102] A. Schulzgen, R. Binder, M. E. Donovan, M. Lindberg, K. Wundke, and H. M. Gibbs et al., Phys. Rev. Lett. **82**, 2346 (1999).
[103] M. Brune, F. Schmidt-Kaler, A. Maali, J. Dreyer, E. Hagley, and J. M. Raimond et al., Phys. Rev. Lett. **76**, 1800 (1996).
[104] M. Hirtschulz, F. Milde, E. Malic, S. Butscher, C. Thomsen, and S. Reich et al., Phys. Rev. B **77**, 035403 (2008).
[105] E. Hendry, P. J. Hale, J. Moger, A. K. Savchenko, and S. A. Mikhailov, Phys. Rev. Lett. **105**, 097401 (2010).
[106] S. A. Mikhailov, Microelectronics J. **40**, 712 (2009).
[107] S. A. Mikhailov and K. Ziegler, J. of Phys.: Condens. Matter **20**, 384204 (2008).
[108] S. A. Mikhailov, **40**, 2626 (2008).
[109] H. K. Avetissian, A. K. Avetissian, G. F. Mkrtchain, and K. V. Sedrakian, Phys. Rev. B **85**, 115443(1) (2012).
[110] P. N. Romanets and F. T. Vasko, Phys. Rev. B **81**, 241411 (2010).
[111] B. Dora, K. Ziegler, P. Thalmeier, and M. Nakamura, Phys. Rev. Lett. **102**, 036803 (2009).
[112] F. Bloch and A. Siegert, Phys. Rev. **57**, 522 (1940).
[113] Y.-C. Han and L. B. Madsen, Phys. Rev. A **81**, 063420(1) (2010).
[114] S. Kumar, N. Kamaraju, K. S. Vasu, A. Nag, A. K. Sood, and C. N. R. Rao, Chem. Phys. Lett. **499**, 152 (2010).
[115] Enamullah, V. Kumar, U. Kumar, and G. S. Setlur, PRAMANA J. of Phys. **Accepted for publication** (2014).
[116] D. Frohlich, A. Nothe, and K. Reimann, Phys. Rev. Lett. **55**, 1335 (1985).
[117] S. Schmitt-Rink, D. S. Chemla, and H. Haug, Phys. Rev. B **37**, 941 (1988).
[118] C. Ell, J. F. Muller, K. E. Sayed, and H. Haug, Phys. Rev. Lett. **62**, 304 (1989).
[119] D. Sun et al., Phys. Rev. Lett. **101**, 157402 (2008).
[120] E. H. Hwang, B. Y. Hu, and S. D. Sarma, Phys. Rev. B **76**, 115434 (2007).
[121] R. Ulbricht, E. Hendry, J. Shan, T. F. Heinz, and M. Bonn, Rev. Mod. Phys. **83**, 543 (2011).
[122] C. Q. et al., Scientific Reports **3**, No. 2315 (doi:10.1038/srep02315) (2013).
[123] D. A., Nature Nanotechnology **3**, 210 (2008).
[124] M. Farkas, *Applied Mathematical Science 104: Periodic Motions*, Springer, 2010.
[125] S. R. Barone and M. A. Narcowich, Phys. Rev. A **15**, 1109 (1977).
[126] L. Tarruell, D. Greif, T. Uehlinger, G. Jotzu, and T. Esslinger, Nature **483**, 302

(2012).
[127] D. Hsieh, D. Qian, L. Wray, Y. Xia, Y. S. Hor, R. J. Cava, and M. Z. Hasan, Nature **452**, 970 (2008).
[128] D. Hsieh et al., Science **323**, 919 (2009).
[129] F. W. Cummings, Phys. Rev. **140**, A1051 (1965).
[130] E. T. Jaynes and F. W. Cummings, Proc. IEEE **51**, 89 (1982).
[131] J. H. Eberly, N. B. Narozhny, and J. J. Sanchez-Mondragon, Phys. Rev. Lett. **44**, 1323 (1980).
[132] N. B. Narozhny, J. J. Sanchez-Mondragon, and J. H. Eberly, Phys. Rev. A **23**, 236 (1981).
[133] H. I. Yoo, J. J. Sanchez-Mondragon, and J. H. Eberly, J. Phys. A **14**, 1383 (1981).
[134] G. S. Setlur, *Dynamics of Classical and Quantum Fields- An Introduction*, Taylor and Francis Group, 2013.
[135] S. Swain, Phys. Lett. A **46**, 435 (1974).
[136] S. Swain, J. Phys. B: Atom. Molec. Phys. **7**, 2363 (1974).

List of publications

Journal:

1. *Cross-over of coherent Rabi oscillations in graphene.*
   Enamullah, Vipin Kumar and Girish S. Setlur, **Physica B 407, 4600-4609 (2012)**.

2. *Nonlinear optical response of asymmetric monolayer graphene.*
   Vipin Kumar, **Enamullah** and Girish S. Setlur, **Phys. Express 4, 4 (2013)**.

3. *A theoretical study of pump-probe experiment in single layer, bilayer and multilayer graphene.*
   Enamullah, Vipin Kumar, Upendra Kumar and Girish S. Setlur, **Pramana (Indian Academy of Sciences) 82(6), 1085-1101 (2014)**.

4. *Quantum Rabi oscillations in graphene.*
   Enamullah, Vipin Kumar, Upendra Kumar and Girish S. Setlur, **J. Opt. Soc. Am. B 31, 484-493 (2014)**.

5. *Coherent nonlinear optical response in SU(2) symmetry broken in single and bilayer graphene.*
   Vipin Kumar, **Enamullah**, Upendra Kumar and Girish S. Setlur, **Physica B 436, 140-148 (2014)**.

6. *Linear optical response of highly nonequilibrium graphene.*
   Enamullah, Vipin Kumar, Upendra Kumar and Girish S. Setlur, **J. Nanosci. Lett. 4, 33 (2014)** .

7. *Anomalous Rabi oscillations of AB and ABC- stacked graphene.*
   Vipin Kumar, **Enamullah**, Upendra Kumar and Girish S. Setlur, **J. Nanosci. Lett. 4, 32 (2014)**.

8. *Anomalous Bloch-Siegert effect in graphene.*
   Upendra Kumar, **Enamullah**, Vipin Kumar and Girish S. Setlur, **J. Nanosci. Lett. 4, 30 (2014)**.

9. *Band structure effect on the nonlinear optical response of bilayer graphene.*
   Vipin Kumar, **Enamullah**, Upendra Kumar and Girish S. Setlur, **Eur. Phys. J. B 87, 70 (2014)**.

10. *Coherent nonlinear electromagnetic response in twisted bilayer and few-layer graphene.*
    Vipin Kumar, **Enamullah**, Upendra Kumar and Girish S. Setlur, **Accepted** for publication in **Pramana (Indian Academy of Sciences)** Journal of Physics.

11. *Strain effect on the nonlinear electromagnetic response of 2D carbon based material.*
    Enamullah, Vipin Kumar, Upendra Kumar and Girish S. Setlur, manuscript **Accepted** for the publication in **Advanced Science Letters (Adv. Sci. Lett.)**.

12. *Bloch-Siegert effect in asymmetric monolayer graphene.*
    Upendra Kumar, Vipin Kumar, **Enamullah** and Girish S. Setlur, Manuscript **Under Review** in **J. Opt. Soc. Am. B (JOSAB)**.

Conference Publications:

1. *Rabi oscillations in graphene.*
   Enamullah and Girish S. Setlur, AIP Conf. Proc. **1447**, 235 (2012).

2. *Rabi oscillations in gapped bilayer graphene.*
   Vipin Kumar, **Enamullah**, Upendra Kumar and Girish S. Setlur, AIP Conf. Proc. **1536**, 266 (2012).

3. *Rabi oscillations in trilayer graphene.*
   Enamullah , Vipin Kumar and Girish S. Setlur, AIP Conf. Proc. **1536**, 315 (2013).

4. *Bilayer graphene in optical regime.*
   Vipin Kuamr, **Enamullah** and Girish S. Setlur, AIP Conf. Proc. **1536**, 351 (2013).

5. *Conventional and anomalous quantum Rabi oscillations in graphene.*
   Enamullah, Vipin Kumar, Upendra Kumar and Girish S Setlur, AIP Conf. Proc. **1591**, 318 (2014).

6. *Effect of trigonal warping on anomalous Rabi oscillations in graphene bilayer.*
   Vipin Kumar, **Enamullah**, Upendra Kumar and Girish S Setlur, AIP Conf. Proc. **1591**, 1406 (2014).

7. *Nonlinear electromagnetic response of strained 2D carbon based material.*
   Enamullah, Vipin Kumar, Upendra Kumar and Girish S Setlur, **Published** in **'Advances in Nanotechnology and Renewable Energy'** conference proceedings with **ISBN: 978-93-81212-65-3 page no 46**.

8. *Anomalous behavior of Hg Te clean quantum well.*
   Upendra Kumar, **Enamullah**, Vipin Kumar, and Girish S Setlur, **Published** in **'Advances in Nanotechnology and Renewable Energy'** conference proceedings with **ISBN: 978-93-81212-65-3 page no 46**.

Vitae

Mr. Enamullah, born at Nautanwa in Uttar Pradesh, India, did his B.Sc. with Physics and Mathematics in 2005 from St. Andrew's College, Gorakhpur, Uttar Pradesh and M.Sc. in Physics in 2007 from Deen Dayal Upadhyay Gorakhpur University Gorakhpur, Uttar Pradesh, India. He joined IIT Guwahati for Ph.D. in 2009. He was awarded Junior Research Fellowship in 2009 and Senior Research Fellowship in 2011 by MHRD, India.